Developing proxies to constrain redox gradients in terminal Ediacaran oceans

Rosalie Tostevin

A dissertation submitted to University College London in accordance with the requirements for award of the degree of Doctor of Philosophy in the Faculty of Science

Department of Earth Sciences

Date of submission: December 19, 2014 Viva: 12th February 2015
Examiners: Dr R Newton and Prof E Oelkers

Word Count:

~65,150

Author's Declaration

I, Rosalie Tostevin, confirm that the work presented in this thesis is my own. Where information has been derived from other sources, I confirm that this has been indicated in the thesis.

Rosalie Tostevin
December 19, 2014

Abstract

There is a long-standing interest in the relationship between the rise of early Metazoans and changes in the redox structure of the oceans. As such, there is a need for reliable geochemical proxy archives that record palaeo-redox. Before we can use proxies in deep time we must understand their application in modern environments, and ensure pristine seawater signals can be extracted effectively. We investigate the sulfur cycle in the modern ocean, using new data from minor sulfur isotopes to constrain the proportional pyrite burial flux - a key control on atmospheric oxygen regulation through time - to between 20 and 35%. Ce anomalies in rare earth element patterns record redox information, and we develop the leaching methods for extracting pristine signals from carbonates. We suggest that a partial leach in nitric acid reduces the risk of contamination.

We apply multiple redox proxies (Fe-speciation, TOC, carbon isotopes, CAS-pyr paired sulfur isotopes and Ce anomalies) to terminal Ediacaran carbonates from the Nama Group, Namibia, to reconstruct the redox structure of the Nama Group and its relationship to the distribution of biomineralising Metazoans. We generate a holistic redox model that distinguishes between anoxic, intermediate and fully oxygenated waters, including identification of manganous conditions using novel observations of positive Ce anomalies. We distinguish between spatial and temporal variability in redox using nine sections from variable relative water depths. Dynamic redox conditions are associated with small, monospecific communities of Metazoans in short-lived horizons. Metazoans are largely absent from low oxygen manganous waters, whereas fully oxic waters host large, complex Metazoan communities. We suggest that redox exerted an important control on the ecological structure of terminal Ediacaran Metazoan communities.

Acknowledgements

I'm very thankful to have been given the opportunity to study something that fascinates me for three years. The work of many dedicated scientists before me has helped to create a magical image of life on early Earth that I've very much enjoyed learning about. I hope I've helped to move the field forward, in some small way, and that in the future my work may interest others.

First and foremost, I would like to thank my supervisors: Professor Graham Shields and Professor Rachel Wood. I hope this PhD is the start of lifelong academic research, and I would very much like the chance to work with you both throughout. Graham - I appreciate the freedom you have given me to make my own decisions and to follow my developing interests. I've run many different research ideas past you, some better than others, and I hope that you're happy with the eventual outcome. You're calm approach has been an antidote to my occasional stress and impatience. Rachel - working with you is a lot of fun. Thanks for taking me along to Namibia. You were a fantastic guide, to both the ecology and the country. I've really enjoyed my trips up to beautiful Edinburgh and working with you and your students.

Being part of NERC's Life and the Planet project has given me the chance to work with some top scientists from across the UK, and I'm very grateful to them all. Simon Poulton, in particular, thanks for the use of your labs, the gossip, the karaoke and the red wine. And Ying, you have brightened up all of our meetings.

Sasha Turchyn, you are a fantastic supervisor, and I'm very grateful that you continued to work with me well beyond my Master's deadline.

My PhD would not have been possible without the technical assistance from Gary Tarbuck. Thank you for your tireless daily efforts to solve my lab woes, keeping my spirits up when I was pipetting and being a good sport when you lost the premier league to City. Thanks also to Jim Davy for all your help in rock prep and for your unwavering cheery greetings.

Some of the best times over the last few years have been working in the field in Namibia, and that wouldn't be so without such good company. Thank you to Fred Bowyer and Amelia Penny for tolerating my music and my driving; Gerd Winterleitner for changing tyres and protecting me from baboons; Andrew Curtis for starting fires and fixing bonnets; and Rachel Wood for your infectious enthusiasm about unequivocal

insitu *Cloudina*.

Tianchen He, my friend since the very beginning, thank you for helping me to navigate vegetarian Chinese cuisine and for answering my increasingly frequent questions as thesis submission drew near.

Romain and Richard,'team cream', for all the good times (of which I won't go into details!), but I hope you'll both be lifelong friends.

Joel Gill, working with you has shown me that there is much more to being a geologist than looking at rocks. I am grateful to have been a small part of what I'm sure is just the beginning of something big for Geology for Global Development.

Amy Edgington, you were a wonderful flat mate, thanks for the cups of tea, rescuing me from cockroaches and spiders, and sharing the department gossip (of which, I admit, I may have been an occasional star of).

Robin Wylie, thank you for tolerating my constant whining, abuse and tea-demands. You've made me laugh. A lot.

'UCL lunch crew' you've created some of my favourite memories of UCL, thanks for the good times in Paolinas, Carousel, Wedstock, and the steps.

The Stott-Parsons, my surrogate family in London, thanks for the many long meals and even longer debates. I've learnt a lot from you all.

To my four bright little sisters, I hope you all too find something that you love and take the opportunity to do it.

And of course, thank you to my mum, for the advice on everything bar the science.

I dedicate this thesis to my dad, a brilliant scientist.

Glossary of common abbreviations

AVG	Average
BIF	Banded Iron formations
BSI	Bell shaped index (with respect to REY patterns)
BSD	Bacterial sulfur disproportionation
BSR	Bacterial sulfate reduction
DIC	Dissolved inorganic carbon
CAS	Carbonate associated sulfate
Ce/Ce*	Cerium anomaly
$\delta^{13}C$	Ratio of heavy (^{13}C) to light (^{12}C) stable carbon isotope
$\delta^{34}S$	Ratio of heavy (^{34}S) to light (^{32}S)stable sulfur isotope
$\Delta^{34}S_{SO4-pyr}$	Difference in isotope composition of sulfate and coeval pyrite
Eu/Eu*	Europium anomaly
FeHR	Highly reactive iron pool
FeT	Total iron content (wt%)
fpyr	Fractional pyrite burial flux
Ga	Billion years ago
GOE	Great Oxidation Event
HREE	Heavy rare earth elements
HST	Highstand systems tract
ICP-MS	Inductively coupled plasma mass spectrometry
ICP-OES	Inductively coupled optical emission spectrometry
LREE	Light rare earth elements
Ma	Million years ago
MIF	Mass independent fractionation
MFS	Maximum flooding surface
mM	millimolar
MREE	Middle rare earth elements
Myrs	Millions of years
NOE	Neoproterozoic oxygenation event
OM	Organic matter
OMZ	Oxygen minimum zones
OS1	Lower Omkyk member
OS2	Upper Omkyk member
PAL	Present atmospheric levels
REY	Rare Earth elements and yttrium
SAS	Secondary atmospheric sulfate
TST	Transgressive systems tract

Contents

List of Figures

List of Tables

Chapter 1

Introduction: the history of oxygen and life on Earth

Author Contributions: This chapter benefitted from discussions with Graham Shields, Rachel Wood and Romain Guilbaud.

The abrupt appearance in the rock record of complex life forms has motivated some of the biggest unanswered questions in Earth science. Early thinking speculated that the fossil record was 'woefully incomplete' (Darwin, 1859), or that conditions were hostile to life before the Cambrian (Daly, 1907). The apparent association between fossil appearances and geochemical changes in the rock record has fueled speculation that early biological evolution was directed by environmental change, with a commonly proposed trigger being oxygenation (see figure 1.1 for summary of early evolutionary events and the rise of oxygen in the atmosphere and oceans). As a result, there has been considerable interest in reconstructing redox gradients in ancient oceans.

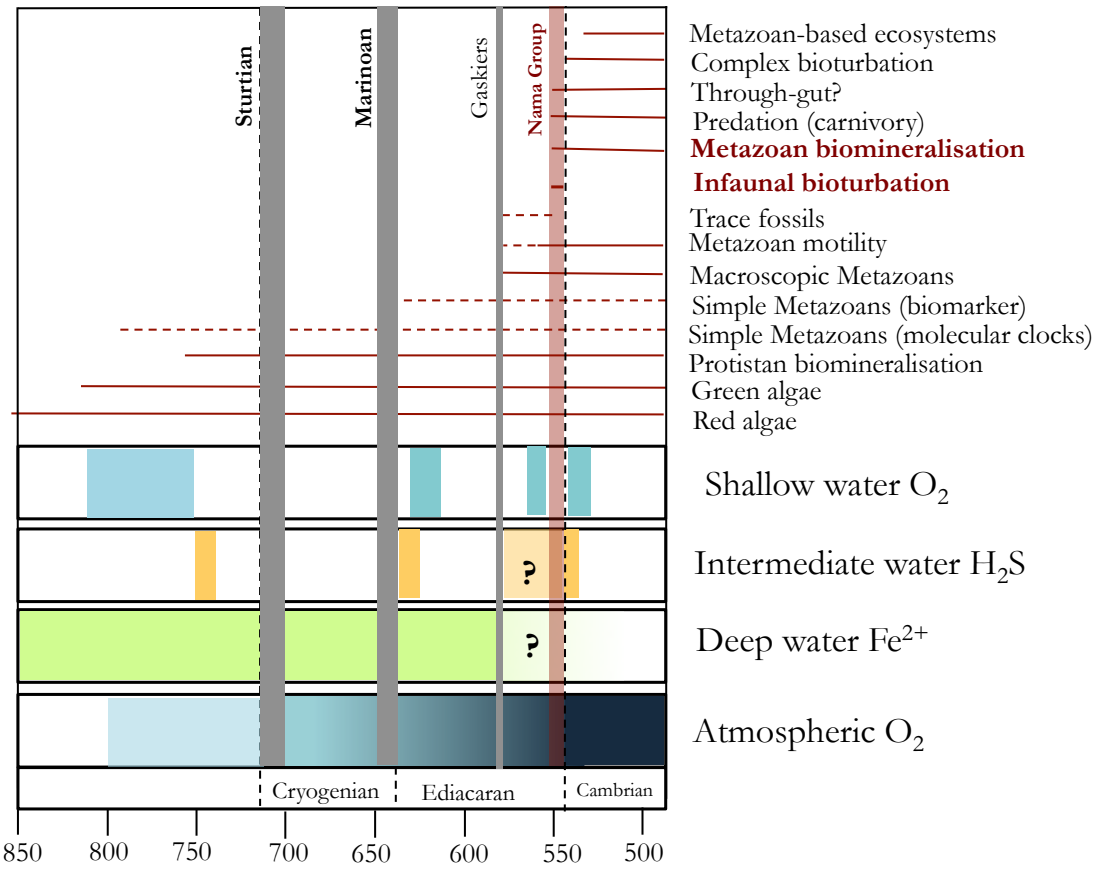

Figure 1.1: Major evolutionary events and the rise of oxygen in the atmosphere and oceans. The focus of this study is on 550-541 Ma, coincident with the first biomineralising Metazoans and infaunal bioturbation. The study area, the Nama Group, is highlighted by the red bar. Adapted after Canfield et al. (2008).

It is widely assumed that low oxygen conditions are unfavourable, and sulfidic conditions lethal, to the existence of large, complex animal life, although some exceptions are beginning to come to light (Danovaro et al., 2010; Mills et al., 2014). Animals demand oxygen to sustain active lifestyles and build hard body parts. Nursall (1959) postulated that the first Metazoan fossils

should be found above geochemical evidence for a rise in atmospheric oxygen, but we have not yet been able to fully constrain the timing of either.

The rise of complex animal life was not as abrupt as early fossil hunters had been led to believe; some Precambrian life forms existed but were rarely preserved. The precise timing for the emergence of complex multicellular animals is contentious, but they appear as the Earth was emerging from a series of severe glaciations, around a billion years after the evolution of the eukaryotic cell. It was not until the twilight years of the Ediacaran that Metazoa began to move, hunt and produce energy-intensive hard body parts (~551 Ma), and it was not until later, in the Cambrian (~530 Ma), that most familiar animal phyla appeared and radiated.

This emanation of animal life was accompanied and possibly driven by major environmental changes. The conventional view is that atmospheric oxygen rose in two major steps. An early modest rise occurred ~2.3 Ga, during the Great Oxidation Event (Farquhar et al., 2000), followed by a second rise in the Neoproterozoic, which was accompanied by the ventilation of the oceans (Canfield et al., 2007; Och and Shields-Zhou, 2012; Sahoo et al., 2012). The Neoproterozoic Oxygenation Event (NOE) was complex and occurred in stages between 750 and 520 Ma. The oxygenation of the atmosphere may ultimately have been driven by increased productivity, influenced by weathering processes, nutrient recycling and respiration. But the relationship is not so straightforward - the evolution of animals, particularly filter-feeders and those with guts, will have affected the geochemical cycles in the ocean and in turn produced feedbacks on atmospheric oxygen. Controversies persist on this issue, with biologists challenging the geochemists that simply assume rising oxygen permitted evolutionary advances. Ecological escalations may have been the true driver, and the coincidence in the rock record of rising oxygen may be simply that - a coincidence (Butterfield, 2009). Others have argued the inverse, that it was the evolution of more complex animals that drove the oxygenation of the oceans (e.g. Boyle et al. 2014 or Lenton et al. 2014).

Previous work has made broad characterisations on the redox state of the oceans during the NOE; usually low-resolution studies spanning long timescales and relying on data from a single section that may vary in lithology and relative water depth. The relationship with animal evolution has also been only broadly characterised, usually with general statements about significant global first appearance datums and their rough correspondence to a geochemical change in that section. What has been lacking is a study that considers spatial as well as temporal change in high-resolution, and relates the geochemistry directly to accompanying observations of fossil

distributions. Here, we explore in detail the relationship between the ecological distribution of biominerals and motile animals and the oxygenation of the ocean using a combination of carbon isotopes, Fe-speciation, TOC, cerium anomalies and sulfur isotopes across nine sections from the Nama Basin, Namibia.

The progressive oxygenation of the ocean is recorded by a series of geochemical proxies. As oxygen becomes depleted in the water column, the conditions transition through a large spectrum of intermediate redox states (Canfield and Thamdrup, 2009). Each proxy has a unique response to rising oxygen, and the combination of multiple redox proxies can provide a more detailed picture of the progressive oxygenation of the Ediacaran ocean. Here, we use sulfidic-sensitive sulfur isotopes, sulfidic and ferruginous-sensitive Fe-speciation and manganous-sensitive cerium anomalies to provide a holistic view of redox across the Nama Basin, and improve our understanding of how these proxies differ and overlap.

Reconstructing ocean chemistry around half a billion years ago based on the sediments that remain preserved at the Earth surface is not without its difficulties. We explore the methods used to extract chemical signals from rocks to identify optimal methods for isolating a seawater rare earth elements signal. Development of proxies is essential before we can confidently apply them in deep time.

We also look at biogeochemical cycles in the modern ocean, and use novel methods to constrain global fluxes in the sulfur cycle. Pyrite burial represents an important source of oxygen to the atmosphere over Earth history (Berner, 1987), but the proportional burial flux in modern marine sediments has been a subject of recent debate (Canfield, 2013; Halevy et al., 2012). We use a novel approach, based on box models of multiple sulfur isotopes and constraints from experimental work on sulfate reducing bacteria, to place new limits on the modern pyrite burial flux. Using geochemical proxies to understand modern day cycles is an essential precedent to applying these proxies in deep time.

1.1 The emergence of complex life

Life probably originated around 3.7-3.5 Ga (Buick et al., 1981; Orgel, 1998; Schidlowski, 1988), and for billions of years was limited to a simple bacterial slime that lived in anoxic oceans. Anoxygenic photosynthetic organisms populated the surface ocean, and the organic carbon pump was based on the cycling of iron and sulfur. Estimates of the timing of the first appearance of oxygen producing cyanobacteria range over a billion years: from 2.3 Ga (Kirschvink and Kopp, 2008; Kopp et al., 2005), to 3.7 Ga (Rosing and Frei, 2004), but more recent estimates suggest an origin closer to 3 Ga (Planavsky et al., 2014a). Oxygenic cyanobacteria, coupling abundant water to carbon dioxide, were able to produce oxygen in significant quantities for the first time. More controversially, it has been proposed that multicellularity was present from as early as 2.1 Ga (El Albani et al., 2010), but the oceans were likely devoid of complex life at this time.

The appearance of the first life into the oceans was followed by a long period of little innovation, dubbed the 'boring billion' (Holland, 2006). During this period, stretching from the GOE (~2.3 Ga) through to the Cryogenian glaciations (~800 Ma), oxygen levels remained low, the climate was relatively stable (no large global glaciations) and there was little evolutionary innovation (Johnston et al., 2009; Kasting and Ono, 2006). This long stretch of Earth history has been largely overlooked, but the discovery of large algae (Shixing and Huineng, 1995) and the early diversification of eukaryotes (Javaux et al., 2013; Knoll, 1992; Knoll et al., 2006) suggest the 'boring billion' may deserve a re-evaluation.

The time period between the global glaciations and the Cambrian explosion (~500 Ma) witnessed the evolution of complex body plans and Metazoans, accompanied by an increase in the diversity of acritarchs and protistan morphotypes. Eukaryote diversification is pinned to shortly before the global glaciations, after which eukaryotes supplanted cyanobacteria to dominate the biological pump (Butterfield, 2000; Parfrey et al., 2011). Crown group members of some algae, heterokonts and testate amoebae had all appeared by 750 Ma (Knoll et al., 2006), and must have survived the subsequent global glaciations. It has long been assumed that global glaciations and the shut down of the active hydrological cycle would have imposed a serious hurdle to life, particularly eukaryotes. But life has been found to persist in harsh natural environments, including under sea ice and at hydrothermal vents (Kashefi and Lovley, 2003). Some have proposed that life sheltered in small melt water ponds within the glaciers (Hoffman and Schrag, 2002), or that the glaciations were not as harsh, or global, as first assumed. More controversially, some recent studies have argued that animal life evolved prior to the Cryogenian and withstood the glaciations

to persist into the Ediacaran where they began to thrive (Erwin et al., 2011). Molecular clock evidence places the divergence of animals from sister groups at 800 Ma, and biomarker evidence for sponges has been identified prior to the end of the Marinoan low latitude glaciation (Love et al., 2009), but there is no convincing animal body fossil record prior to the glaciations.

Early animal evolution is thought to have occurred in two discrete steps, set apart by tens of millions of years. In the Ediacaran simple, mostly soft-bodied cnidaria-grade organisms, bilaterians and problematica (collectively referred to as the Ediacaran biota) first appeared, followed by a second phase in the early Cambrian in which small shelly fossil invertebrates appeared in the Fortunian stage and rapidly diversified during Stages II, III and IV (the Cambrian explosion) (Grotzinger et al., 1995). A summary of the first appearances and forms of some of the Ediacaran biota are shown in figure 1.2. Fossilized cnidarians, possible bilaterian eggs and embyros preceding the Ediacaran radiation and other enigmatic macrofossils suggest that the classic 'Ediacaran biota' does not represent the first appearance of animals but merely the emergence of large and architecturally more complex organisms (Narbonne, 2005).

Body fossils of the Ediacaran biota are known from 575 Ma, found initially in deeper waters and later in shallow marine settings (Martin et al., 2000; Narbonne and Gehling, 2003). The Ediacaran soft-bodied organisms were composed of soft, flexible tissue and were most likely immobile animals or animal grade organisms. The earliest Ediacaran communities exhibited vertical and lateral subdivisions, similar to Phanerozoic and modern communities. Later innovations include mobility (>555 Ma, Grazhdankin 2004; Liu et al. 2010; Martin et al. 2000) and predation (>549 Ma, Bengtson and Morris 1992; Hua et al. 2003). The assessment of the temporal distribution and range of the Ediacaran biota at a global scale has been aided by the use of correlations between oscillations in the carbon isotope curve (Grotzinger et al., 1995).

Metazoan calcium carbonate biomineralisation appears in the fossil record for the first time in the terminal Neoproterozoic, marking the beginning of a step-change in the carbon cycle. Although some of these early tentative animals may have been biomineralising passively, biomineralisation became fully established in the subsequent Cambrian Period. Biologically controlled carbonate formation is a significant ecological innovation that demands large amounts of energy. The trigger for its abrupt and global appearance in the fossil record at 553-550 Ma is not yet fully understood. This innovation occurs against a backdrop of major perturbations to the iron and sulfur cycles, suggesting an environmental change, such as a rise in oxygen concentrations or a change in carbonate saturation, permitted the production of energy-intensive biominerals.

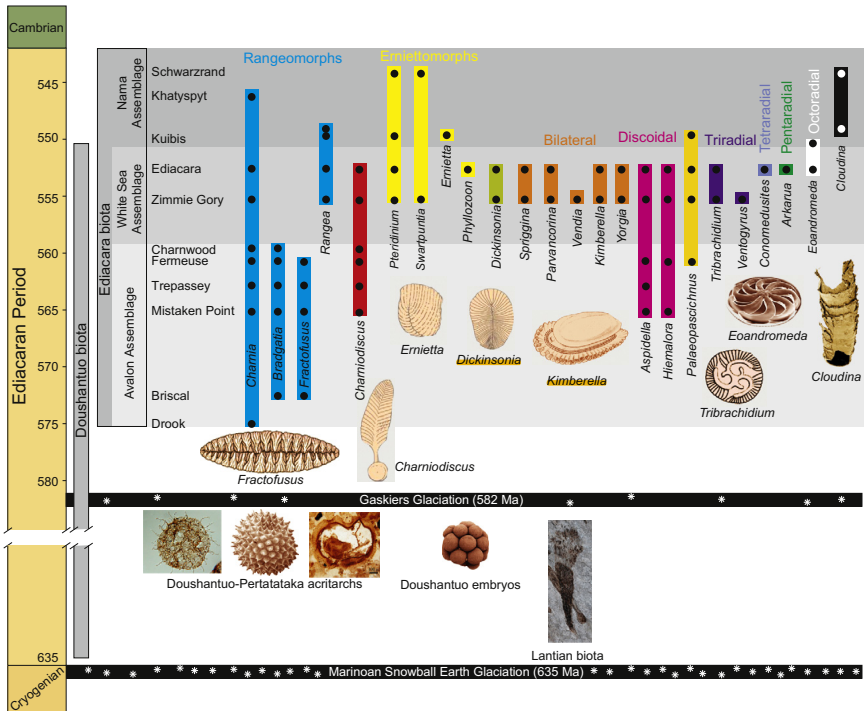

Figure 1.2: Ediacaran megafossil zonation. After Xiao and Laflamme (2009).

Degens et al. (1985) proposed that the ability to control Ca^{2+} levels first evolved in order to avoid the precipitation of calcium carbonate as oceans became oversaturated, with the ability later adapted to encourage calcification when intracellular calcium levels became high enough to require a metabolic detoxification process (Kirschvink and Hagadorn, 2000; Marin et al., 1996; Simkiss, 1977). Calcium saturation itself may in part be controlled by rising oxygen (Higgins et al., 2009). But the consequences of oxygenation may have been more direct; building biominerals is energy intensive (Palmer, 1992), and a rise in oxygen levels may have permitted this innovation around 550 Ma.

Alternately, there may have been an ecological trigger for the emergence of biomineralisation. Control of buoyancy allowed access to the nutrient rich Proterozoic benthic zone and hence new ecological opportunities (Cohen, 2005). The introduction of biomineralisation is also coincident with the rise of motile predators, which suggests that biominerals are an armoured response to predation. Recent work by Penny et al. (2014) (presented here as appendix A) shows reef building activity and mutual cementation in *Cloudina* samples from the Nama Group, consistent with more efficient feeding, competitive substrate strategies and anti-predation. These observations support the view that early skeletonisation was promoted in carbonate environments by the rise of substrate competitors and bilaterian predators (Bengston, 2004; Hua et al., 2003;

Knoll, 2003a; Wood, 2011). Apparent predatory boreholes in some specimens support this view (Bengtson and Morris, 1992; Hua et al., 2003).

Towards the end of the Ediacaran and into the Cambrian bioturbation became increasingly prevalent. Bioturbation is a sign of motility and more complex active feeding structures, and would have altered the dynamics of the sediment-water interface. Although simple trace fossils may have appeared with the ~579–559 Ma Avalon Assemblage (Liu et al., 2010), and were certainly preserved in the ~558–550 Ma White Sea Assemblage (Jensen et al., 2006), more complex feeding patterns emerged during the terminal Ediacaran, as highlighted by the spreiten forms reported in the Nama assemblage (Macdonald et al., 2014) and in the Khatyspyt Formation of Siberia (Rogov et al., 2012). Recent reports of bioturbation in late Ediacaran strata (e.g. Carbone and Narbonne 2014; Rogov et al. 2012) suggest that extensive infaunal activity preceded the 'Cambrian Explosion' but post-dated the Shuram carbon isotope excursion (Grotzinger et al., 2011). Bioturbation is likely to have become more intensive, and penetrated deeper into the sediments, in the Cambrian Period.

The Ediacaran biota, including skeletal forms, undergo extinction at the Precambrian/Cambrian boundary, which is defined by the appearance of the complex trace fossil *Treptichnus pedum* (Narbonne et al., 1987) at 541±1 Ma (Amthor et al., 2003; Gradstein et al., 2004; Grotzinger et al., 1995; Maloof et al., 2010). It remains unclear whether the end-Ediacaran extinction was a global event or a step-wise replacement of an old biota with a new one, but the Ediacaran forms disappear from the fossil record (Amthor et al., 2003). Several possible triggers have been proposed for the extinction, including a salinity crisis or the upward expansion of anoxic water masses (Kimura and Watanabe, 2001). Methane release has also been invoked, supported by a large, sharp, negative carbon isotope excursion, coincident with the boundary (Amthor et al., 2003). However, because microbial mats, critical for the preservation of Ediacaran type biota (Gehling, 1999), decreased in abundance due to the rapid evolution of grazing and burrowing organisms during the Cambrian explosion, the scarcity of Ediacaran survivors in the Cambrian could be taphonomic rather than evolutionary (Jensen et al., 1998). Because the affinities of the Ediacaran biota are debated, the apparent wide separation in time of the Ediacaran biota from the Cambrian evolutionary pulse has long been used to support phylogenetic arguments that these creatures are not simple precursors to later forms, but instead represent a failed lineage, perhaps unrelated to the animal kingdom (Grotzinger et al., 1995; Seilacher, 2007).

A wide range of plausible triggers have been proposed as the cause of both the Ediacaran

radiation and the subsequent Cambrian explosion. These include developmental explanations, such as the evolution of Hox genes, and ecological explanations concerning new trophic capacities such as a predation arms race or new ecological niches (e.g. Boyle et al. 2007; Butterfield 2009). Environmental explanations, based on the concept of 'permissive evolution', include, among others, the extreme greenhouse conditions following 'Snowball Earth' (Hoffman et al., 1998), the Acraman meteorite impact, repeated methane release, a dramatic shift in terrestrial weathering processes (Kennedy et al., 2006) and changes in continental sedimentation during supercontinent amalgamation. The environmental explanation that has received the most attention, however, is a rise in atmospheric oxygen.

1.2 Redox state of the Earth through time

1.2.1 Redox transitions and respiration

The oxidation state describes the charge that an element would have in a compound if all bonds with other atoms were 100% ionic. Reactions involving the transfer of electrons between elements can result in loss of electrons, known as oxidation, or the gain of electrons, known as reduction. Most elements have more than one possible oxidation state. Carbon, for example, can bond with four hydrogen atoms to form methane, where it resides in the -4 oxidation state, or two oxygen atoms to form carbon dioxide, where it resides in the +4 oxidation state.

A change in oxidation state is accompanied by a change in Gibbs free energy, ΔG, which can be exploited by living organisms. During aerobic respiration, oxygen gas acts as an electron acceptor to oxidize organic matter, producing carbon dioxide and water vapour. This reaction is accompanied by the release of a large amount of energy, explaining why aerobic respiration is used exclusively among active, energy-sapping animals and by some microorganisms. Eukaryotes are mostly dependent on oxygen, but archaea and bacteria show a wide range of anaerobic metabolic states, and in some cases multiple metabolic states can be expressed in a single organism. As a result, microorganisms are found living in almost all environments at the Earth surface and are able to break down organic matter to extract energy even in the absence of oxygen.

Electron acceptors other than oxygen, such as sulfate, iron, manganese or nitrate, can be respired in anaerobic conditions. The order in which these anions will be respired depends on the Gibbs free energy released. In general, more favourable electron acceptors will be respired in preference to subsequent alternative electron acceptors. But an electron acceptor does not have to be depleted to exhaustion before the onset of the subsequent metabolic pathway. Many metabolic pathways may be operating in tandem, but with different rates that result in different geochemical signatures which reflect the dominant pathway. For example, Canfield et al. (2010) identify active sulfur cycling in modern oxygen minimum zones, but the turnover is minimal and does not result in measureable sulfur isotope variability (Johnston et al., 2014). Anaerobic respiration is principally used by prokaryotes, most of which are obligate anaerobes that would die in the presence of oxygen.

The redox state of the ocean refers to the dominant metabolism operating in the water column,

but does not necessarily require that the electron acceptor is present in high concentrations. These zones can overlap and sometimes co-occur with low levels of dissolved oxygen. Studies of anoxia have tended to focus on the extreme case of euxinia (anoxic and sulfidic) where sulfate reduction occurs and free sulfide builds up in the water column. However, the redox state of the ocean can vary widely, both spatially and temporally, from oxic, to low levels of oxygen, through anoxic and non-sulfidic, to the extreme state of euxinia (figure 1.3). Intermediate redox states include ferruginous conditions, where ferrous iron builds up in the water column, and less commonly manganous or nitrogenous conditions. In or below the nitrogenous zone, dissolved Mn typically accumulates as a product of Mn reduction. The upper bound of the manganous zone is defined by removal of Mn by O_2 or possibly nitrite, and the manganous zone can extend deep into anoxic environments, where its removal is governed mostly by carbonate saturation and precipitation (Canfield and Thamdrup, 2009). Dissolved Fe^{2+} accumulates as a result of biological and abiological iron oxide reduction. In nature, Fe^{2+} accumulate in the absence of oxygen and typically below the zones of nitrate and Mn reduction. The term 'suboxic' is often used in the literature to describe the manganous and nitrogenous zones as well as oxygen minimum zones. Ferruginous and sulfidic conditions are often described as 'anoxic', but manganous and nitrogenous zones may also occur in the absence of oxygen. Each of these zones may also overlap in the upper and lower bounds. Variability in redox state is complex, and the broad categories or 'anoxic', 'suboxic' are misleading and confusing; redox should really be described using the chemical zone based on the dominant electron acceptor (Canfield and Thamdrup, 2009).

Natural anoxic systems are often poised close to a switching point between ferruginous and euxinic conditions. On a geological timescale, the nature of anoxia is controlled by the relative budgets of sulfate and reactive iron (Poulton and Canfield, 2011). If the sulfide flux exceeds the highly reactive iron flux by a factor of 2 (the stoichiometric ratio of pyrite, FeS_2), then sulfide should accumulate, resulting in anoxic and sulfidic conditions (Raiswell and Canfield, 2012). Low sulfate concentrations, common in lakes but also in Precambrian oceans, limit the biological production of sulfide, and so encourage ferruginous conditions. The delivery of sulfate to the oceans depends on the inventory of sulfur in continental rocks and volcanic outgassing, as well as oxidative pyrite weathering. The availability of highly reactive iron in the oceans depends on the flux of iron from riverine and hydrothermal sources, the magnitude of which have changed significantly through time. The delivery of sulfate to the oceans scales with atmospheric oxygen concentrations, but only at the low end of the oxygen concentration range. Oxidative weathering

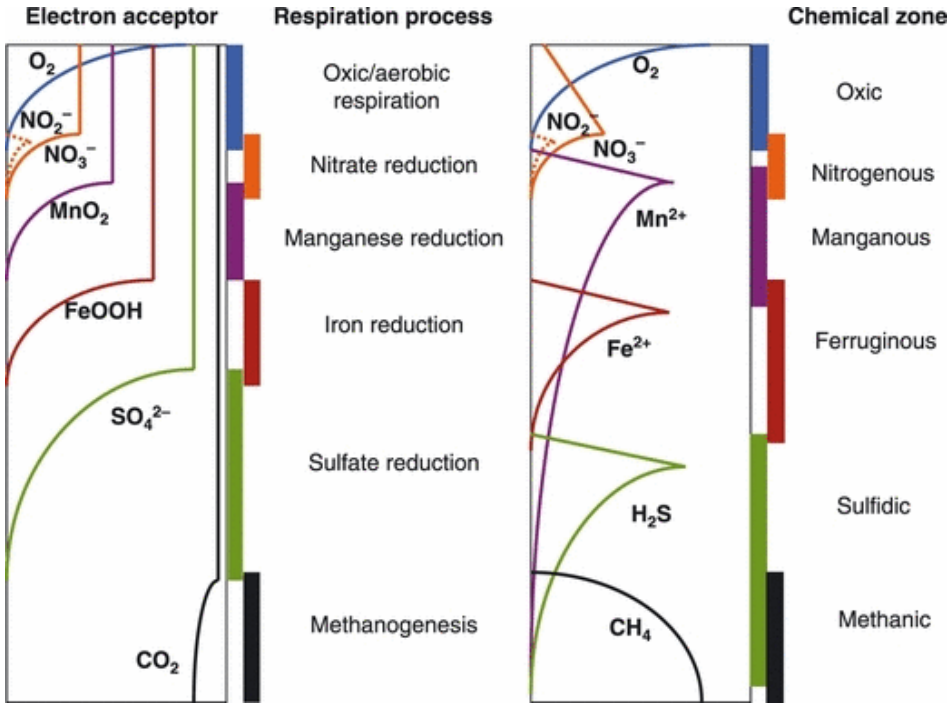

Figure 1.3: On the left, a cartoon representing the depth distribution of common electron acceptors in the environment and the names used to represent the zones where these different electron acceptors are used. This is an abstraction of the real system and not necessarily an accurate representation of how these profiles would look in nature. On the right, a cartoon reflecting the chemical zonations, which typically accompany the respiration processes on the left. Note that there is considerable overlap between some of these chemical zones and that they do not necessarily reflect the depth distribution of the accompanying respiration process. From Canfield and Thamdrup (2009).

of pyrite is complete at oxygen levels as low as 10^{-5} to 10^{-3} PAL. This means that counter intuitively, higher atmospheric oxygen concentrations are required to drive anoxic oceans into the more extreme euxinic state. Although the oceans have become locally sulfidic throughout Earth history, ferruginous conditions are thought to have dominated Precambrian oceans (Poulton and Canfield, 2011).

1.2.2 Redox in modern environments

The modern atmosphere is oxygen-rich, at 21%, and the Earth surface environment is broadly oxidized. The ocean is well oxygenated, with oxic conditions persisting to depth. Surface ocean waters generally have oxygen concentrations close to equilibrium with the Earth's atmosphere (20mg/L). As this water moves out of the mixed layer into the thermocline it is exposed to a

rain of organic matter from the productive photic zone above. Aerobic bacteria feed on this organic matter, progressively lowering the oxygen concentration. The downward flux of organic matter decreases sharply with depth, with 80-90% being consumed in the top 1000m. Oxygen minimum zones (OMZs), where oxygen saturation in seawater is at its lowest, occur between 200m and 1000m, depending on local circumstances. Oxygen is replenished in the deep ocean from the supply of cold, oxygen-rich deep waters from the polar regions.

OMZs, where the oxygen concentration can reach zero, occur in coastal upwelling zones, such as off the coast of Peru and Namibia. Within OMZs anaerobic respiration may be occurring in the open ocean; predominantly nitrate reduction, but sulfur cycling may also occur (Canfield et al. 2010, but see Johnston et al. 2014 for a contrasting view). High productivity off the coast of Namibia today results in oxygen depletion and the production of sulfide, and when this anoxic water body upwells it can result in widespread death of larger animals (fish stocks).

Anoxic conditions occur beneath the sediment water interface when the rate of oxidation of organic matter overwhelms the supply of dissolved oxygen. In lakes and coastal marine sediments, oxygen can drop to zero a few millimeters beneath the surface. Organic matter then continues to be broken down via other metabolic pathways. Nitrate respiration follows oxygen as the next largest energy yield, but nitrate is in short supply and so this zone can be short-lived, and similarly with manganous conditions. Iron reduction follows, and eventually sulfate reduction and methanogenesis. Sulfate is the second most abundant ion in modern seawater and so bacterial sulfate reduction is a major pathway of respiration in marine sediments. Sulfate reduction produces sulfide, which may react with iron to form pyrite. This is a major flux of sulfur removal in the modern ocean (Canfield, 2013; Garrels and Lerman, 1984; Tostevin et al., 2014). Some organic matter may be buried in the sediments if organic matter supply is particularly high, or organic matter is in a biologically unavailable form.

Rare isolated lakes and basins show anoxic conditions in modern environments. The Black Sea is anoxic due to density stratification, and is often used as an analog for Precambrian conditions when anoxia was widespread. In the Black Sea, strict zonations occur within the water column as each electron acceptor is sequentially depleted in order of reactivity, terminating in sulfidic deep waters (Lewis and Landing, 1991). The manganous zone in the Black Sea is distinct from the ferruginous zone and persists from 70 to 90m depth. Lake Vanda (Antarctica) and the Cariaco trench also show distinct anoxic zones at depth, including manganous, ferruginous and sulfidic zones. The Golfo Dulce, near the coast of Costa Rica, is a modern nitrogenous setting (den

Camp et al., 2006). Acton Lake and Lake Matano are some of the few modern environments where ferruginous conditions can be observed. The large flux of highly reactive iron overwhelms the small freshwater sulfate reservoir, preventing ferrous iron from being titrated out by sulfide accumulation. Many redox proxies that are applied in deep time have been calibrated in modern sediments to define the thresholds and values that characterize oxic and anoxic environments.

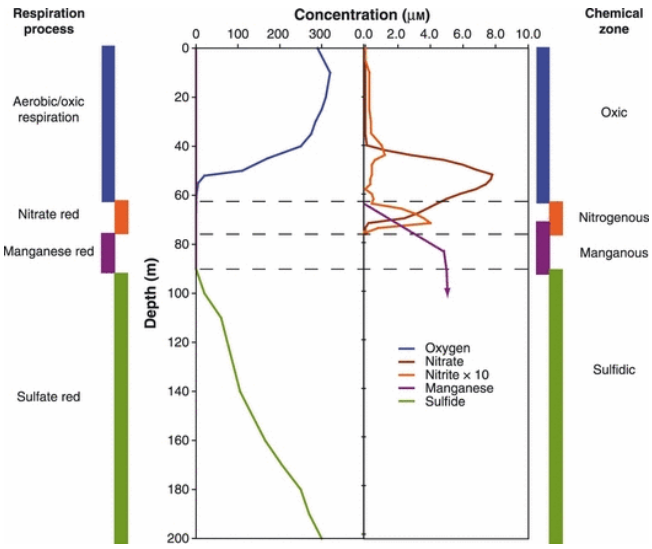

Figure 1.4: Chemical data and redox zones from the Black Sea. Listed are the depth distribution of chemical zones and respiration processes deduced from the chemical data, from Canfield and Thamdrup (2009). Colour scheme consistent with cartoon depiction in figure 1.3

Research in modern ocean systems has focussed on constraining the major fluxes and controls on the biogeochemical cycles of C, Fe and S, as well as the behaviour or trace nutrients in the marine system. Despite over fifty years of research on the subject, the magnitude of some major fluxes is still disputed. One of the major pathways of sulfur removal from the ocean, as buried pyrite, ranges in estimates from 10 to 90% of the total sulfur removal flux from the oceans (Canfield, 2013; Halevy et al., 2012).

The anaerobic microorganisms that thrived in Precambrian oceans still play a critical role in modern ecosystems, but they have retreated from the oceans into the sediments and locally anoxic water bodies. The microorganisms that use or tolerate oxygen, alongside larger complex Metazoa, have come to dominate the oxygenated open ocean. Life has also migrated out of the oceans onto dry land, altering weathering patterns and nutrient delivery to the ocean (e.g. Lenton et al. 2012).

Although our understanding of conditions and the response of redox proxies is founded on

modern studies, using them to understand the past requires a major assumption that the processes that we observe happening today have operated in the same manner throughout Earth history. There are major differences in the geochemical cycles of the surface environment between the modern day and the Precambrian. The unidirectional and escalating evolution of life over the past 580 Ma has altered the surface of the planet. Major innovations include the evolution of marine calcifying plankton in the Jurassic, which shifted the locus of carbonate precipitation from shallow shelves to the deep ocean. The introduction of biominerals to the carbonate record in the terminal Ediacaran coupled the inorganic and organic carbon pumps for the first time. The evolution of land plants changed continental weathering patterns, and bioturbation altered the dynamics of the sediment water interface. The evolution of guts produced fast sinking fecal pellets that changed the dynamics of geochemical recycling in the water column. The modern ocean does not operate within the same system bounds as in the geological past - and our assumptions face greater challenges the older the sediments.

1.2.3 A history of oxygen on Earth

Oxygenation of the Earth's surface environment probably occurred in two major episodes, the first; the Great Oxidation Event (~2400-2200 Ma) (Bekker et al., 2004), and the second; the Neoproterozoic Oxygenation Event (~800-540 Ma) (Och and Shields-Zhou, 2012). The latter event is implicated in the evolution of animals and other complex organisms during the Neoproterozoic (Canfield et al., 2007). However, oxygenation was not a simple one-way process (e.g. Lenton et al. 2014) and the details of the timing and mechanism of marine oxygenation remain poorly understood.

The surface of the early Earth was reducing, with no or little oxygen in the atmosphere or oceans. Following the evolution of oxygenic photosynthesis, around 3 Ga (Planavsky et al., 2014a), oxygen production began in small environmental pockets, but photosynthesis is tightly coupled with respiration, and early oxygen production was closely matched by consumption. Although a small amount of organic matter escaped unoxidised to the sediments, liberating some of the photosynthetic oxygen, excess oxygen was likely removed through reaction with reduced gases from volcanoes or existing pools of reduced chemical species on the Earth's surface. Crowe et al. (2013) suggest that some oxidative weathering was occurring as early as 3 Ga, but it is thought that oxygen began to build up in the atmosphere around half a billion years after the beginning of oxygenic photosynthesis, during the Great Oxidation Event (GOE) (figure 1.5). Oxygen build-up

may finally have been permitted by a global reduction in the production of volcanic gases as the Earth's interior cooled (Dobson and Brodholt, 2005; Holland, 2002). Alternately, the abundant Archean atmospheric methane may have been destroyed by UV, generating light hydrogen that could escape the Earth's atmosphere, clearing the way for oxygen build-up (Catling et al., 2001). The GOE (2.4 Ga) played out over hundreds of millions of years, gradually crossing the threshold for pyrite oxidation by 2.5 Ga, and resulting in the cessation of mass-independent fractionation of multiple sulfur isotopes 2.4 Ga (Farquhar et al., 2000) – potentially reaching 1% PAL by 2 Ga. However, recent work by Planavsky et al. (2014b), suggests atmospheric oxygen remained low (<0.1%PAL) until as late as 800 Ma.

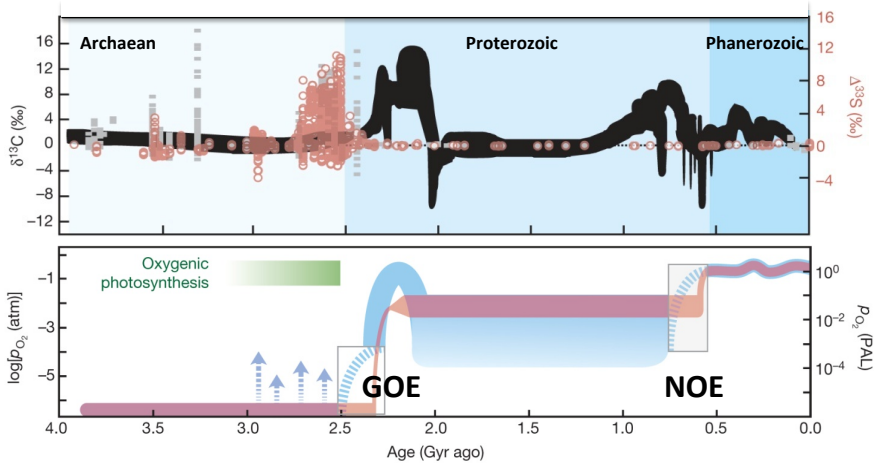

Figure 1.5: Bottom: Evolution of Earth's atmospheric oxygen content through time. The faded red curve shows a 'classical, two-step' view of atmospheric evolution, while the blue curve shows the emerging model. Arrows denote possible 'whiffs' of O_2 late in the Archaean; their duration and magnitude are poorly understood. Data are from Berner and Canfield (1989) and Bergman et al. (2004). Top: summary of carbon (black) and multiple sulphur (red and grey) isotope data through Earth's history. Multiple sulfur isotopes provided the original clinching evidence for early atmospheric oxygenation (Farquhar et al., 2000). Notable features include the large range of $\Delta^{33}S$ values during Archaean time, the large $\delta^{13}C$ excursion during the early Proterozoic, relative stasis in $\delta^{13}C$ during the mid-Proterozoic, and the large negative $\delta^{13}C$ excursions during the late Proterozoic. Data compiled from references within Reinhard et al. (2013) and Planavsky et al. (2012). Figure compiled from Lyons et al. (2014).

Despite the build up of oxygen in the atmosphere, there is a long delay before evidence of oxygen is observed in marine sediments. The rarity of significant deviation from trivalent Ce behaviour in Archean carbonates indicates that Ce oxidation was not prevalent, even on shallow water carbonate platforms (Planavsky et al., 2010a), suggesting oxygen was not consistently present in the oceans even at low ($<5\mu$M) levels. However, negative cerium anomalies in some Archean carbonates suggest oxygen may have persisted in small oases in protected shallow water

environments (Riding et al., 2014), but the oceans remained largely anoxic and dominated by Fe cycling until much later (Canfield, 1998; Poulton and Canfield, 2011). Oxygen could not build up in the oceans while they still contained a high concentration of reducing elements (such as Fe). The link between rising atmospheric oxygen levels and the ventilation of the ocean is not solely dependent on thermohaline circulation and diffusion, but depends partly on the strength of the biological pump and the ventilating actions of eukaryotes and animals. Under modern conditions, box models suggest that atmospheric oxygen levels would need to drop to as low as 0.5-0.7 PAL (Canfield, 1998) to induce widespread anoxic conditions in the oceans. However, if the supply of phosphorous (the limiting nutrient in modern oceans) was present in higher concentrations and less severely restrictive of primary production in the Precambrian, then widespread anoxia could be maintained at higher atmospheric oxygen concentrations.

Banded iron formations deposited throughout the Archean and late Palaeoproterozoic hint at dominantly anoxic and ferruginous conditions with low sulfate concentrations. BIF deposition occurred in pulses, and evidence for ferruginous conditions in the gaping time gaps between these pulses is sparse. BIF deposition, save some extreme climatic events later in the Neoproterozoic, ceased completely 1.8 Ga. Positive cerium anomalies preserved in iron formations in the late Palaeoproterozoic ($<$1.8 Ga) preserve evidence of a manganese shuttle between shallow oxic and deeper anoxic waters (Planavsky et al., 2010a).

As oxygen levels built up in the atmosphere, oxidative weathering began to increase sulfate supply to the ocean, encouraging sulfate reduction to occur in the open ocean. One suggestion for the termination of BIF deposition is the spread of sulfidic conditions, as free sulfide would titrate dissolved iron out of the water column (as pyrite). Sulfidic conditions create a strong sink for Fe(II), resulting in a crash in Fe(II) concentrations in the ocean. Sulfidic oceans were once thought to be widespread. An increase in the sulfur isotope fractionation between sulfate and sulfide (preserved as pyrite) was attributed to an increase in bacterial sulfate reduction, reducing the fresh influx of riverine sulfate to produce sulfide in marine environments (Canfield, 1998). The termination of BIF deposition, around 1.8 Ga, has been studied in detail by Poulton et al. (2004, 2010), where they showed that sulfidic conditions were restricted to continental margins at the time of the last BIF deposition. More recent evidence suggests that the deep oceans remained dominantly ferruginous throughout most of the Neoproterozoic, with sulfidic conditions restricted to a wedge on the outer shelf, comparable to modern day oxygen minimum zones (Li et al., 2010; Poulton and Canfield, 2011). Sulfidic conditions would have been concentrated near shore, where higher organic carbon fluxes drove sulfate reduction to exceed

the delivery flux of highly reactive iron phases (FeHR) from settling particles and upwelling deeper waters. Models of molybdenum isotopes suggest that sulfidic waters may have made up between 2 to 4 % of the Proterozoic seafloor (Dahl et al., 2011), in contrast to today where sulfidic waters do not occur in the open ocean save for extreme circumstances (Schunck et al., 2013).

The increased weathering of the land surface that is postulated to have cooled the climate into the Cryogenian glaciations should be accompanied by increased phosphorous delivery to the oceans and associated rise in productivity and atmospheric oxygen (Lenton and Watson, 2004) (figure 1.5). The weathering of large igneous provinces would have produced phosphorous pulses to the oceans, driving intermediate waters euxinic. The Chuar Group preserves evidence for a short lived flip from ferruginous to euxinic conditions, and enhanced Mo drawdown suggests there was some, albeit restricted, sulfidic waters (Dahl et al., 2011). Euxinic continental margins appear to be very sparse in the Neoproterozoic, in contrast to the Mesoproterozoic (Raiswell and Canfield, 2012). Neoproterozoic seawater is characterized by unusually high δ^{13}C, averaging +5‰ before the glaciations, indicating that the proportion of carbon buried as organic matter was elevated from 850 Ma until 720 Ma. This has been linked to a general diversification of eukaryotic plankton, which altered the dynamics of organic matter production and decomposition (Knoll, 2003b), alongside enhanced OM burial on the margins of a rupturing supercontinent. Because organic matter burial allows oxygen produced during photosynthesis to collect in the atmosphere, this has been used to argue for an early rise in oxygen before the first known animal fossils. However, the strontium isotope record suggests much lower rates of continental erosion at this time (Derry et al., 1992), so although the proportion of organic carbon burial was higher, the absolute burial flux would have been lower. Instead, the elevated carbon isotope values may result from the burial of inorganic light authigenic carbonate (Schrag et al., 2013). As such, there is no clear driver for rising atmospheric oxygen in the early Neoproterozoic.

The second oxygenation event, in the Neoproterozoic (NOE), occurred in several stages between the end of the global glaciations and the Cambrian explosion. The progressive oxygenation of the ocean has been reconstructed using a combination of different geochemical systems, including the Fe, C and S cycles, rare earth elements and redox sensitive trace elements. Each proxy provides a unique perspective on the NOE, and in combination they show that oxygenation was incremental and spatially heterogeneous.

The ocean became increasingly oxygenated following the Marinoan glaciation (Sahoo et al.,

2012). The melt back of the global glaciers left behind a land surface coated in fine powder, which was swept into the ocean in the warm wet environment following the end of the glaciations (Lenton et al., 2014; Planavsky et al., 2010b). On short timescales ($<10^4$years), the increased phosphorous delivery would have simulated production and increased oxygen demand, spreading ocean anoxia, but over longer timescales ($>10^6$ years) the burst in productivity would have led to higher OM burial rates and oxygen production. In the ~25 Myr following the Marinoan global glaciation the sulfate concentration of the ocean rose, inferred from an increase in the isotopic difference between sulfate and pyrite (Canfield, 1998). Increased [SO_4] probably correlates with increased oxygen availability in the oceans. But the signal of ocean oxygenation from Mo, V and U analyses is short-lived, at least in the restricted basin studied by Sahoo et al. (2012), suggesting the ocean was briefly oxygenated before returning to pre-glacial conditions. Global compilations of Fe-speciation data suggest that although surface waters were well oxygenated, bottom waters remained anoxic and ferruginous at least until the Gaskiers glaciation (580 Ma) (Canfield et al., 2007) (figure 1.6).

The first compelling evidence for the oxygenation of the deep ocean coincides with the Gaskiers glaciation (635-580Ma), but this oxygenation was not global in extent. Parts of the ocean may have remained anoxic and ferruginous until as late as the Palaeozoic. Similar explanations to the Cryogenian glacially-driven phosphorous burst and subsequent productivity induced oxygenation have been invoked for the Gaskiers glaciation, but unlike the Sturtian and Marinoan, the Gaskiers is not thought to have been global in extent. The glacial grinding and weathering would have been reduced, and the meltback would not have been followed by a wet warm period of high nutrient delivery to the oceans. Some have suggested that a shift in terrestrial weathering due to the colonisation of land could instead be responsible for a phosphorous pulse (Shields-Zhou and Och, 2011). Although this idea is supported by increased $^{87}Sr/^{86}Sr$, there is no direct evidence for colonisation of land at this time. Instead, the ocean may have been oxygenated by a shift in ocean ecology, with the rise to dominance of filter feeders and eukaryotes clearing the water column of organic carbon, and drawing the focus of oxygen demand deeper into the water column (Lenton et al., 2014).

The carbon isotope record has also been interpreted as evidence for changing redox conditions across the Neoproterozoic. Where organic carbon (Corg) oxidation rates are exceptionally low, due to the absence of free O_2 and inhibited bacterial sulfate reduction, and the lack of an effective ballasting mechanism, it is feasible that a large dissolved organic carbon pool might have accumulated over tens of millions of years prior to the NOE (Och and Shields-Zhou,

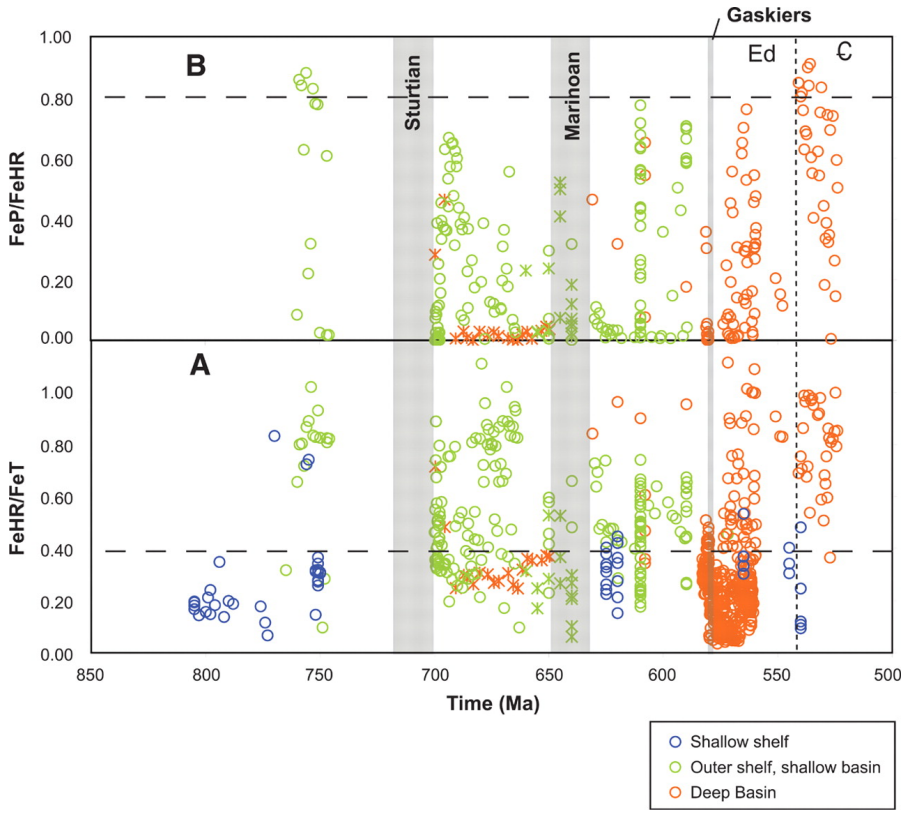

Figure 1.6: Fe-speciation compilation shows that ferruginous conditions dominated Neoproterozoic oceans (A) FeHR/FeT is shown. FeHR/FeT>0.38 (dashed line) indicated anoxic conditions. The proportion of FeHR bound as FeS_2, FeP/FeHR, is shown in (B). Only samples deposited below the mean storm wave base where anoxic deposition is indicated are plotted. Fepy/FeHR >0.8 (dashed line) indicates deposition from a sulfidic water body, and ratios <0.7 are consistent with deposition from ferruginous waters. Sulfidic conditions are restricted to the Chuar group and the Cambrian-Ediacaran boundary (vertical dotted line) on the Yangtze Platform. Figure taken from Canfield et al. (2008), data included within supplementary information of Canfield et al. (2008).

2012; Logan et al., 1995). This is supported by the carbon isotope record, where invariant δ^{13}C in organic carbon occurs alongside large changes in the δ^{13}C of carbonate minerals, suggesting the organic and inorganic carbon pools were decoupled. This could result from a large, isotopically light organic carbon pool that overwhelmed changes in $\delta^{13}C_{org}$ resulting from biological fractionation. In contrast, the small inorganic carbon pool would have been susceptible to large swings associated with organic carbon remineralization (Rothman et al., 2003).

The Neoproterozoic inorganic carbon isotope record is punctuated with negative excursions (Burns and Matter, 1993; Halverson et al., 2005), the largest of which reached values as low as -12‰ (considerably lighter than the input and output fluxes commonly used to constrain

isotope mass balance) (figure 1.7). This excursion, dubbed the Shuram/Wonoka anomaly, began 580 Ma, and was followed by a recovery period lasting 50Myr (Le Guerroué, 2010). The Shuram/Wonoka excursion has been identified globally (Calver, 2000; Condon et al., 2005; Fike et al., 2006; Grotzinger et al., 1995; Kaufman et al., 1991; Narbonne et al., 1994), suggesting it records a primary oceanic event (figure 1.8). If primary, the excursion is extraordinary because its magnitude and duration require explanations that differ from the modern carbon cycle, and it indicates a major perturbation to the carbon cycle and an increase in the redox potential of the ocean during the evolution of early macroscopic animal life.

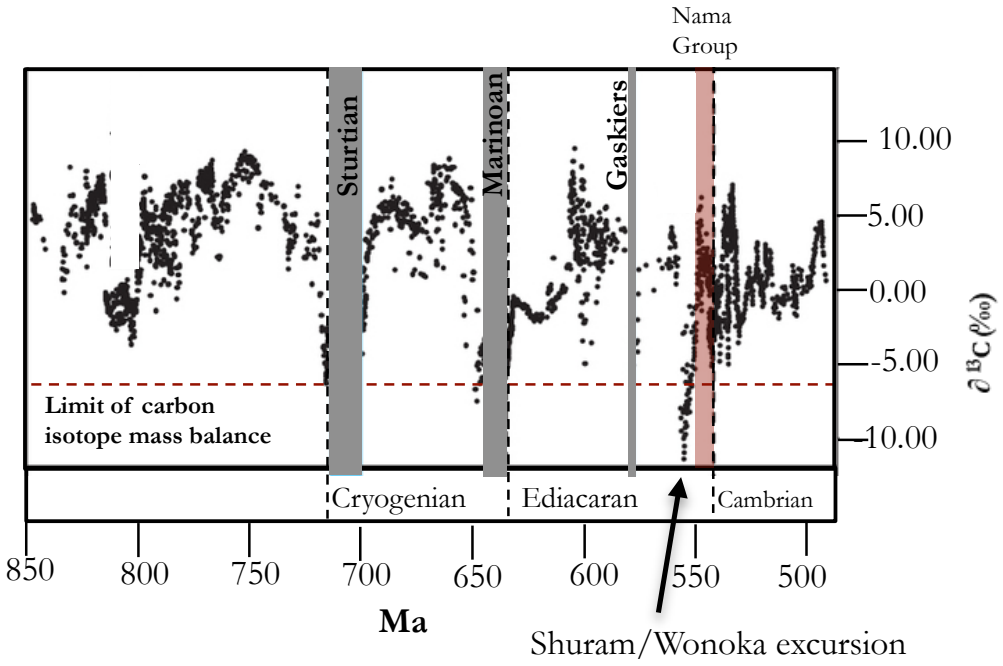

Figure 1.7: Summary of secular variation in the carbon isotope composition of marine carbonates through the Neoproterozoic. Note the Shuram/Wonoka negative excursion in the Ediacaran, where values are more negative than can be constrained by standard carbon isotope mass balance. Red box highlights this study area (Nama Group). Data taken from Lenton et al. (2014).

Reducing the fraction of organic carbon burial to zero can reduce carbon isotope values to as low as -6‰ (mantle values); to reach below this requires input of a light source of carbon. It is possible that the Shuram/Wonoka anomaly resulted from a global oxidation event that remineralised part of a proposed large organic matter pool (Fike et al., 2006; Rothman et al., 2003). The exhaustion of the organic matter pool may have been driven by an oxidising source, such as increased riverine sulfate delivery. Although at first this oxidant would work to remove the accumulated organic carbon pool, resulting in the negative excursion, as the pool became

depleted this oxidising source could drive an oxygenation event culminating at ~550 Ma. But it is unclear how this oxidation event would be triggered, and the large isotope excursions seemingly require more oxidant than can be supplied by the atmosphere and ocean system (Bristow and Kennedy, 2008), and thus the excursion may not represent a global oxygenation event. Bjerrum and Canfield (2011) propose that the Shuram-Wonoka anomaly, and the associated isotopic signatures, were generated by the massive release of methane from clathrate hydrates. Alternately the phenomena could be a result of meteoric diagenesis (Knauth and Kennedy, 2009) or contamination by detrital organic carbon (Derry, 2010). $\delta^{13}C_{org}$ invariance stopped at the Shuram-Wonoka anomaly; possibly as the large organic carbon pool was removed by the radiation of benthic suspension feeders.

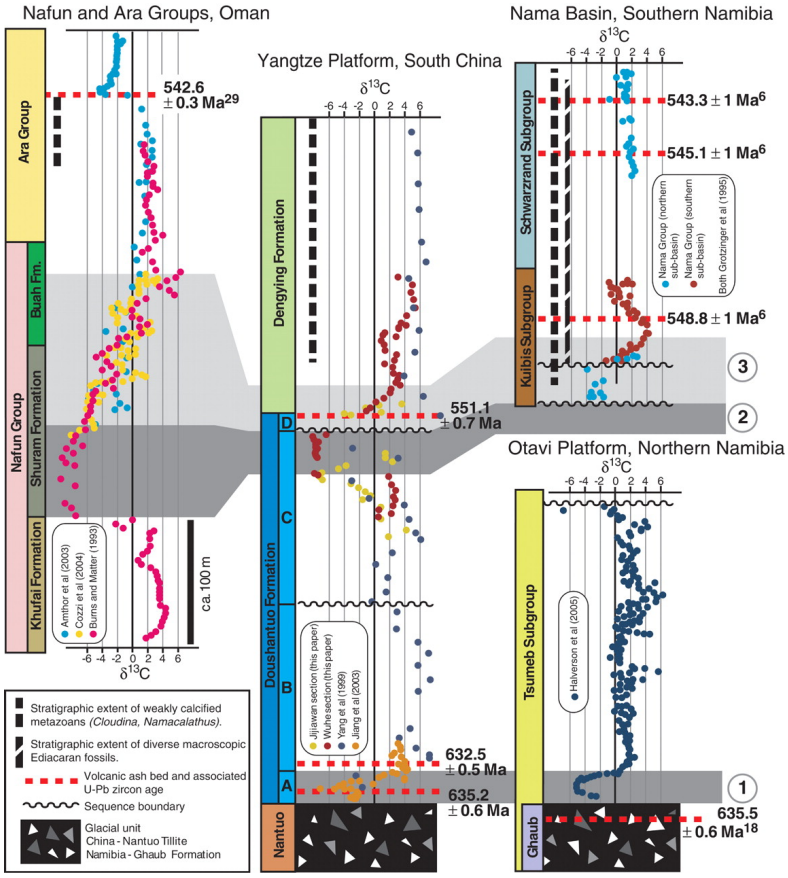

Figure 1.8: Correlation of Doushantuo Formation (Yangtze Platform) with the Nama Group (Nama Basin) and Nafun/Ara Groups (Oman) successions, showing the global nature of the Shuram/Wonoka negative carbon isotope excursion. Figure from Condon et al. (2005)

The constancy of $\Delta^{34}S_{SO4-pyr}$ during the Shuram/Wonoka excursion indicates that, despite these changes, bacterial sulfate reduction under sulfate replete condition remained the dominant pathway for sulfur cycling in the ocean. However, towards the tail end of the Shuram excursion,

close to 550 Ma, an increase in $\Delta^{34}S_{SO4-pyr}$ to ~50‰ indicates a change in metabolisms involved in marine sulfur cycling (Fike et al., 2006). The maximum fractionation observed in both laboratory and field studies during bacterial sulfate reduction is 46‰, with typical fractionations much smaller (Detmers et al., 2001). However, when BSR is combined with bacterial sulfur disproportionation (BSD), a pathway which utilises intermediate valence sulfur species, fractionations can approach ~70‰. Multiple sulfur isotope data suggests that BSD evolved as early as the Mesoproterozoic (Zerkle et al., 2009), but there are no reports of $\Delta^{34}S_{SO4-pyr}$ of more than 46‰ prior to the terminal Ediacaran. The expansion in $\Delta^{34}S_{SO4-pyr}$ following recovery from the Shuram/Wonoka excursion indicates that the oxidative side of the sulfur cycle must have been active, and demonstrates additional oxidation of the Ediacaran ocean and the third and final stage of the Neoproterozoic oxygenation event. Total sulfur and S/Corg ratios support an increase in S burial in the terminal Ediacaran and suggests rising oxygen levels at the Earth surface (Och et al., 2011; Och and Shields-Zhou, 2012). Alternately, this increase in $\Delta^{34}S_{SO4-pyr}$ may reflect an increase in the complexity of the sedimentary sulfur cycle caused by bioturbating animals (Canfield and Farquhar, 2009). Paradoxically, several studies have found superheavy pyrite in terminal Proterozoic sections (Bottomley et al., 1992; Ries et al., 2009; Strauss et al., 1992; Liu et al., 2006), where the sulfur isotope composition of pyrite approached, or even exceeded, coeval sulfate. This indicates, at least locally, a return to low sulfate concentrations and the reappearance of ferruginous conditions in the Late Neoproterozoic ocean (Canfield et al., 2008), and intense aerobic oxidation.

Ling et al. (2013) identify increasingly negative cerium anomalies towards the Cambrian boundary, which they interpret as evidence for localised progressive oxygenation on the South China Craton. Further evidence for rising atmospheric oxygen levels comes from positive $\delta^{53}Cr$ values up to 4.9‰, indicating a rise to modern atmospheric oxygen levels at the Precambrian/Cambrian boundary (Frei et al., 2011) (but see Planavsky et al. 2014b, suggesting that chromium isotopes identify an earlier rise in atmospheric oxygen, 800 Ma). Enrichment of Mo and V in black shales between 663 and 551 Ma further supports a rise in atmospheric oxygen (Och et al., 2011).

In the final few million years of the Ediacaran Period, fossil evidence suggests that motility and bioturbation began to influence the sediment-water interface (Jensen et al., 2006; Liu et al., 2010; Macdonald et al., 2014; Rogov et al., 2012). Oxygenation of the upper sediments through bioturbation would have added sulfate to the ocean, lessening the role of methanogensis in OM respiration, and additionally, would have removed phosphorous. The

resulting reduction in phosphate concentrations and organic carbon burial would ultimately have decreased atmospheric oxygen (Boyle et al., 2014). This may explain the widespread return to ferruginous conditions in the early Palaeozoic, when bioturbation became widespread.

Extremely negative carbon isotope values and large amplitude swings ceased once the modern marine ecosystem became established 520 Ma. A negative excursion of 6-7‰ in δ^{13}C of carbonates occurs coincident with the Ediacaran-Cambrian boundary, where there is evidence for an anoxic event and accompanying extinction horizon (Amthor et al., 2003). Once the deep ocean had undergone its irreversible oxygenation (except for episodic ocean anoxic events), the build up of sulfate levels ensured that the effects of future carbon cycle perturbations on atmospheric oxygen could be buffered by an ocean sulfate capacitor.

The Neoproterozoic oxygenation event may represent a significant rise in atmospheric oxygen levels, but it is likely they remained lower than the present day, perhaps as low as 20% PAL, and may not have reached comparable levels to the present day until the mid-Palaeozoic (Berry and Wilde, 1978; Dahl et al., 2010). There are even reports of widespread sulfidic conditions during the Late Cambrian SPICE event (Gill et al., 2011). Although Phanerozoic oceans were broadly oxygenated, there has been some considerable variation in atmospheric oxygen concentrations. Oxygen concentrations as high as 150% PAL in the late Carboniferous coincide with gigantism in the fossil record, and oxygen concentrations reached as low as 60% PAL in the early Jurassic. Oceanographic processes have occasionally produced widespread marine anoxia during the Phanerozoic, such as the Cretaceous ocean anoxic events (Jenkyns, 2010), which may have contributed to episodes of mass extinctions of marine animals.

1.3 Life and oxygen

Life and the planet have coevolved through Earth history, with changes in the environment permitting and restricting evolution, and novel evolutionary traits altering the environment. Of these complex relationships, few are more durable, or more complex, than that between life and oxygen. Most fundamentally, oxygen levels of at least 0.002 bar are necessary to form an ozone layer capable of absorbing UV radiation that is potentially harmful to life – a threshold that was surpassed during the Great Oxidation Event. Low levels of oxygen are required for biosynthetic reactions in all eukaryotes; without it complex life on Earth would likely be impossible. Complex animals rely on the high energy yield of aerobic metabolisms to support energetic lifestyles. For physiologically simple aerobic organisms, the diffusion of oxygen into the body limits their size. More advanced organisms that are motile or produce biominerals demand even higher oxygen concentrations, and their evolution throughout the Ediacaran and Phanerozoic shows broad correlations with rising atmospheric oxygen concentrations.

Oxygen is produced by cyanobacteria in the surface ocean, and is depleted during respiration of organic matter throughout the water column and sediments. In this regard, oxygen distribution is fundamentally controlled by the biological pump. In the modern ocean, oxygen minimum zones occur at mid-depths where oxygen demand from sinking organic matter is highest. The euxinic wedge postulated for much of the Neoproterozoic oceans occurred in a similar position, where sinking cyanobacteria created the highest oxygen demand. High latitude deep waters would have been relatively easy to oxygenate, with the most stubbornly anoxic zones occurring in areas of upwelling where high nutrient supply resulted in rain down of organic matter and high oxygen demand at mid-depths.

In Palaeo- and Meso- Proterozoic oceans, where cyanobacteria dominated the biological pump, the slow movement of organic matter may have allowed oxygen to build up in the deep ocean, but these zones would been biological deserts due to the absence of metabolisable organic matter (Raiswell and Canfield, 2012). The diversification of eukaryotes prior to the global glaciations was accompanied by their coup of cyanobacteria as they came to dominate the biological pump. The larger cell size, along with ballasting from tests and scales and a tendency to form particulate aggregates, means eukaryotes sink faster through the water column. Eukaryotes accelerated the biological pump, spreading oxygen demand into deeper waters. Lenton et al. (2014) suggest that this transfer of oxygen demand to the deep ocean would have increased the efficiency of phosphate removal into the sediments, further limiting nutrient supply and causing a drop in

global productivity which in turn would lower oxygen demand. All eukaryotes require oxygen at some stage in their life cycle, even if only to build the membrane-stiffening sterols found in all eukaryote membranes. Metazoans additionally require oxygen to build collagen proteins.

The earliest stages of Metazoan evolution are constrained to an early period of global cold, with tentative pre-glacial evidence for animals, but no hard body fossil evidence until shortly after the final glaciation, 575 Ma. Planavsky et al. (2014b) suggest that a rise in atmospheric oxygen 800 Ma can be linked directly to the first appearance of animals. There is limited evidence for increased organic carbon burial (and therefore preglacial marine oxygenation), but the return to ferruginous conditions by 750 Ma suggests that any oxygenation was reversible. Spiny acritarchs, found only prior to the Shuram/Wonaka anomaly, are interpreted by some as the diapause egg cysts of primitive Metazoans (Yin et al., 2007), creating the possibility that Metazoans evolved in the presence of oxygen stress. The enzymes used in the facultatively anaerobic mitochondria of Metazoans are nearly identical across all animal lineages, indicating a common and early origin. The ability to withstand anoxia, whilst still benefiting from the energy yield of an aerobic metabolism, is hardwired into all 6 major eukaryote lineages and may have existed near the base of the Metazoan family tree (Müller et al., 2012). It is possible the first animals emerged into spreading anoxia rather than an abundance of oxygen, raising the question of whether early animals were, like their modern counterparts, obligate anaerobes.

These early animals were likely sponge-grade organisms; sponges are the sister group to all other animals and so may provide our closest living analog to ancestral life. Modern sponges grown in laboratory conditions are able to tolerate oxygen levels as low as 0.5% PAL, a condition likely to have characterized surface oceans long before the Ediacaran (Mills et al., 2014). Sponges have no special adaptations to low oxygen conditions, but can survive by virtue of their simple body plan, whereby every cell is in contact with surrounding seawater (Knoll and Sperling, 2014). Sponges can actively generate a water current through their aquiferous system, a mechanism adapted for both feeding and breathing. And so the modest oxygen requirements of sponges suggest that low oxygen concentrations would not have presented an impediment to the origin of multicellularity.

High oxygen levels are demonstrably important in maintaining high levels of Metazoan diversity and ecosystem complexity, but the mere existence of simple Metazoans does not necessarily require high oxygen levels. The oxygen levels below which Metazoans are unsupported remain unquantified. Until this threshold is defined, it is difficult to fully determine whether the ancient

Earth was capable of supporting Metazoans. It is possible that there has been sufficient oxygen to meet the requirements of simple Metazoans in local surface environments in direct contact with the atmosphere since the GOE.

In contrast, larger, more complex organisms have higher energy demands, and likely require oxygen to meet this demand. The lower energy yield of anaerobic reactions means that when compared with an aerobic organism of similar size, an anaerobic organism would require high concentrations of the electron acceptor, exhibit a much lower metabolic rate, or have a lower volume:area ratio (Payne et al., 2011). Depending on an organisms size, shape and physiology, minimum requirements for oxygen can be inferred for aerobic organisms. The transport of electron acceptors into the body can present a severe limitation, and so maintaining the flux of oxygen to the mitochondria, the cell organelle carrying out aerobic respiration, limits the size of an organism according to the ambient oxygen availability. A disk is the most efficient shape for maximising diffusion, a shape employed by the Ediacaran biota *Dickinsonia* (Runnegar, 1991) and *Aspidella* (Gehling et al., 2000). Rising oxygen can raise the maximum size of a ball of cells that lack a circulatory system (i.e. stop the diffusion-limited cells in the interior from becoming oxygen starved).

Larger Cambrian animals used respiratory and circulatory systems, making quantification of the relationship between pO_2 and maximum size more challenging. Experimental work has shown that reduced body size under hypoxia results from developmental plasticity, whereas size increase following hyperoxia is evolutionary and only appears after multiple generations (Klok and Harrison, 2009). However, Butterfield (2009) suggests that it may in fact have been rapidly metabolising small animals that are most challenged by low O_2, and that body size divergence is likely forced by evolutionary interactions and evolutionary wedging than 'permissive' conditions. Oxygen requirements reflect size, transport mechanisms within tissues, and metabolic demand. A rise in oxygen may be necessary, but is not necassarily sufficient, to explain increased complexity of animals.

Some natural environments in the modern ocean mimic Precambrian conditions. Oxygen minimum zones provide a natural environmental oxygen gradient that has proven to be a useful natural laboratory, but difficulties in isolating the effect of decreasing oxygen from increasing food supply have not been resolved (Levin and Whitfield, 1994). Animals in modern dysoxic waters tend to be tiny (Gibson and Atkinson, 2003). Megafauna such as echinoids and large gastropods are reported from OMZs down to low oxygen concentrations ($<$0.25ml/l), but are

typically absent from the most oxygen starved settings (<0.1ml/l), which tend to be dominated by protists and invertebrate animals <1mm (Payne et al., 2011). But many extant animals are facultative anaerobes and are not wholly dependent on oxygen (Budd, 2008); parasite worms and the common mussel can live without oxygen. Some Loriciferans can even withstand free sulfide (Danovaro et al., 2010), which is toxic to all other known Metazoans. If modern Metazoans can exist in anoxic or very low oxygen conditions, this challenges the widespread assumption that oxygenation led directly to the evolution of animals.

Metazoans demand oxygen to support aerobic metabolisms and build hard body parts, and so it has been presumed that a rise in oxygen, perhaps incrementally, facilitated this evolution of complexity (Fike et al., 2006; Canfield et al., 2007; McFadden et al., 2008; Scott et al., 2008). A broad correlation between rising atmospheric oxygen levels and animal evolution has been observed in the rock record (Knoll and Sperling, 2014). The evolution of animals occurred in a three-stage process whereby metabolically versatile, multicellular heterotrophs initially evolved during a period of climatic and environmental extremes as part of a wide diversification of eukaryotes, that may have followed a modest rise in atmospheric oxygen (Planavsky et al., 2014b). Mobility and macroscopic size were attained in a second stage during ocean ventilation in the Ediacaran period. Irreversible, stable atmospheric oxygenation by the end of the Precambrian may have paved the way for the emergence of modern animal phyla. Periods of anoxia in the Phanerozoic have been implicated in prominent episodes of mass extinction (Meyer et al., 2008), and Mesozoic ocean anoxic events have been linked to rapid radiation and turnover of marine phytoplankton (Leckie et al., 2002).

If the Shuram/Wonoka anomaly does represent the exhaustion of a vast organic carbon pool, its culmination ~551 Ma could correspond to a rise in atmospheric oxygen just prior to the late Ediacaran-Cambrian emergence of modern animal phyla. Although the Cambrian explosion was undoubtedly escalated through an ecological arms race to evolve predatory and protective features, it seems likely that oxygenation permitted additional opportunities to evolve energy-sapping musculature and biominerals. Furthermore, rising oxygen levels in the atmosphere could have had an indirect effect on the course of evolution by increasing the availability of bioessential trace elements (Anbar and Knoll, 2002) and altering alkalinity (Higgins et al., 2009).

Early thinking on the coevolution of animals and the oxygenation of the planet was based on limited knowledge of animal physiology and the fossil record, as well as a broad-brush approach to oxygenation. We now know that oxygenation was not a simple step change, but protracted and

complex. The oxygen distribution in the ocean does not relate simply to atmospheric oxygen, but will vary locally depending on nutrient supply and productivity. Experiments on animals in low oxygen environments in both the laboratory and modern natural environments show that multicellular animal life does not necessarily demand high oxygen concentrations (Knoll and Sperling, 2014; Mills et al., 2014), but this does not undermine the close relationship between animals and oxygen. Although simple animals such as sponges may be able to tolerate low oxygen conditions, they may be sensitive to fluctuating anoxia, and smaller forms may tolerate low oxygen more easily than larger forms. So instead of a search for the first complex animal above evidence for an oxygenated ocean, we need to redirect our search to look for evidence of larger, more complex animals under more stable oxygenated conditions.

The relationship between animals and oxygen is not necessarily one way. Although modestly rising oxygen levels may have facilitated the evolution of animals in the Ediacaran and Cambrian, oxygenation may in part have been a consequence of animal evolution. In this view, filter-feeding animals cleared surface oceans of dense bacterial populations, while planktonic bilaterians accelerated export from surface waters via rapidly sinking fecal pellets, shifting oxygen demand from the surface ocean to the deep ocean and promoting oxygen enrichment (Lenton et al., 2014). The filter feeding of basal Metazoa such as sponges clear the water of dissolved organic carbon and picoplankton, reducing turbidity and shifting oxygen demand deeper into the sediments. Sponges would also have removed phosphorous into the sediments, easing oxygen demand in shallow waters and further promoting oxygenation. The evolution of more complex feeding patterns and associated bioturbation likely had an impact on remineralization rates in marine sediments (e.g., Boyle et al. 2014; Canfield and Farquhar 2009), releasing sulfate and phosphorous. Sediment mixing by Metazoan infaunal activity can affect both redox zonation in the sediment column and the cycling of organic matter by supplying oxidants to otherwise anoxic pore waters (Aller, 1990). The burgeoning record of complex Ediacaran trace fossils has important implications for mixing at the sediment-water interface prior to the Cambrian Period (Chen et al., 2014). For example, in modern settings, bioturbation can affect sediment column redox zonation and the localized recycling of organic matter (Aller, 1994; Meysman et al., 2006). It has long been recognized that the transition from firm-ground substrates of the Proterozoic to the more soupy, well-mixed upper sedimentary layers of the Phanerozoic had critical biogeochemical and ecological impacts (Canfield and Farquhar 2009; Droser et al. 2002; McIlroy and Logan 1999, but see Mángano and Buatois 2014 and Tarhan and Droser 2014 for a contrasting view).

The timespan from the late Mesoproterozoic to the Cambrian witnessed major clade divergence within the eukaryotes and an overall increase in organism size and complexity. How these events precisely relate to the NOE is currently still under debate and is most probably a result of combined feedback mechanisms and direct and indirect environmental triggers involving both climatic and tectonic changes.

1.4 Redox proxies

Our understanding of the history of oxygen through time (section 1.2.3) comes from geochemical proxies that record changing ocean redox conditions. There are a multitude of different proxies, some more traditional and robust, others new and still being tested. Each proxy has a unique response to anoxia, determined by its biogeochemical behaviour, reduction potential and ocean residence time. The signal of rising oxygen should be detected first in the most redox-sensitive elements. Some proxies record global conditions (e.g. Mo isotopes), whereas others are sensitive to local conditions (e.g. cerium anomalies). Our understanding of palaeo-redox is built up of information from multiple different proxies.

The 'redox state' of the ocean cannot be categorised as simply anoxic or oxic, but is a continuous progression under oxygen deplete conditions through the redox potentials of different redox sensitive elements, and each proxy will be sensitive to different stages in this transition. Sulfur isotopes respond to sulfide production through bacterial sulfate reduction, and so are sensitive to euxinic conditions (Canfield, 1998; Chambers and Trudinger, 1979), whereas Fe-speciation allows the differentiation between euxinia and the less extreme ferruginous anoxic state. Cerium anomalies may respond to the even milder manganese redox boundary. Carbon isotopes and TOC are controlled by the other side of the respiration equation, the supply and demand of organic matter, and provide a broad indicator of redox conditions.

Neoproterozoic ocean redox has so far been predominantly constrained through shale geochemistry using Fe-speciation, trace metals, rare earth element and several isotope systems. However, using shales to reconstruct redox presents a number of complications (Hood and Wallace, 2014). It is often difficult to distinguish between water-mass chemistry and pore-water chemistry, and even more difficult to constrain chemical depth gradients (Piper and Calvert, 2009). Furthermore, deciphering seawater signatures from detrital contamination is problematic (Hood and Wallace, 2014). Marine carbonates, which record the chemistry of the parent seawater via trace element incorporation during precipitation, offer a potentially more direct way of determining ancient ocean chemistry (Kamber and Webb, 2001, 2007; Nothdurft et al., 2004; Webb and Kamber, 2000). Carbonates represent shallow marine environments and often host biomineral fossils. Here, we introduce a range of redox proxies and their application in carbonate settings.

1.4.1 Total organic carbon

Marine sediments are the primary long-term repository for organic matter. Because roughly one mole of molecular oxygen is generated for every mole of carbon fixed during photosynthesis, burial of organic matter (OM) can maintain high atmospheric oxygen concentrations. In a perfect balance between respiration and photosynthesis, no oxygen would accumulate. However, the burial of organic carbon in sediments allows oxygen to accumulate in the atmosphere. The preservation of OM is controlled by the productivity of photosynthesizers in the photic zone, and the availability of electron acceptors to break down matter in the water column and the sediment, such as O_2 and $SO_4{}^{2-}$. On short time-scales, the burial of OM may serve as an indicator of palaeo-oceanographic conditions.

Organic matter in marine sediments may be of either terrestrial or marine origin. Terrestrial OM that enters the oceans through rivers is dominated by OM from eroded shales, as well as recent plant debris and older soil humus. Most riverine OM is deposited near shore (Degens, 1969). Coastal regions have higher rates of photosynthesis than offshore regions, but most photosynthetic production ($50x10^{15}$ g C yr^{-1}) occurs in the open ocean. A fraction of this organic carbon is then released in dissolved form, and consumed by bacteria and protozoans. The remainder is eaten by zooplankton and transferred up the food chain, or settles intact through the water column. The vertical flux of particulate organic carbon is predominantly in the form of large fecal pellets and amorphous aggregates (marine snow). Because of regenerative mechanisms in the surface ocean, the global flux of particulate organic carbon that escapes the surface ocean ($<$100m) is estimated to be around 10-20% of total production (Bishop, 2009; Martin et al., 1987). The OM that escapes the surface is subject to further degradation in the deep ocean and at the sediment-water interface. As a result, the proportion of organic carbon that reaches the sediments is around, on average, 1% of total primary production, but can reach as high as 50% in some near shore environments. Romankevich (1984) demonstrated that 80-90% of global organic carbon burial ($0.06*10^{15}$ g C yr^{-1}) occurs within the continental margin, because of the relatively high carbon contents and high sedimentation rates characteristic of this zone, and lower rates of remineralisation in the surface ocean (Platt and Harrison, 1985).

The distribution of organic carbon that is preserved in sediments is controlled by two things: the availability of electron donors and subsequent transport processes (Canfield, 1994). The amount of OM in the mixed layer should be linearly proportional to the particulate flux of OM to the sediments. Different forms of organic carbon will be reoxidised at differing rates. OM

degradation may precede faster in the presence of oxygen, than via denitrification or Mn, Fe or SO_4 reduction, and indeed particular biomolecules cannot be broken down in the absence of oxygen. A correlation has been shown between OM content of the sediment and oxygen concentration where oxygen levels in bottom waters become low (Richards and Redfield, 1954). We would expect, therefore, that in times of widespread bottom water anoxia, the proportion of OM that is preserved in the sedimentary record will increase.

The concentration of OM in sediments has been used to infer changes in productivity of the ocean through time (e.g. Sarnthein et al. 1987). This is complicated by the variety of outside factors that can enrich or dilute the localised concentration of OM. TOC may also vary with redox changes. Although not sufficient as a redox proxy alone, TOC can provide supporting and complementary data to redox studies. TOC is also helpful in interpretation of Fe-speciation data, discussed in 1.4.3. Here, we measure TOC on carbonates from nine sections across the Nama Basin to provide supporting redox information where FeT is too low for effective Fe-speciation analyses.

1.4.2 Carbon isotopes

On geological timescales, the CO_2 emitted from volcanoes and the weathering of sedimentary rocks departs the fluid Earth in two primary sinks – carbonate minerals, and organic carbon; the burial of organic carbon can be linked stoichiometrically to fluxes of O_2 to the atmosphere (Grotzinger et al., 2011). Owing to biases intrinsic to the sedimentary record, direct measurements of the amount of organic carbon buried as a function of time provide ambiguous information. Instead, we use carbon isotope ratios in carbonate rocks to constrain the proportional organic carbon burial flux.

The ratio of the two stable isotopes of carbon in seawater (^{12}C and ^{13}C) varies as a function of changes in the input flux of carbon and subsequent partitioning between organic and inorganic carbon. The fractionation is reported in delta notation (equation 1.1), and using units of part per thousand (permil, ‰). The following notation is standard for reporting stable isotope ratios, as demonstrated here for δ^{13}C:

$$\delta^{13}C = \left[\frac{(^{13}C/^{12}C_{sample})}{(^{13}C/^{12}C_{standard})} - 1 \right] * 1000 \tag{1.1}$$

Preferential uptake of the lighter isotope during CO_2 fixation by autotrophic organisms enriches dissolved inorganic carbon in ^{13}C. Carbon fixation during oxygenic photosynthesis uses the RuBisCo enzyme, and produces a δ^{13}C fractionation of around -28‰. Larger fractionations occur during methanogenesis, up to -78‰ (Botz et al., 1996). This photosynthetic isotope effect drives δ^{13}C depth gradients in the modern ocean. Shallower water is depleted in the lighter isotope, and deeper waters, where organic carbon is released via respiration, are enriched in ^{12}C.

The majority of organic carbon produced in the surface ocean is reoxidised in the water column or within the sediment pile – larger isotope fractionations can only occur when organic carbon is removed more permanently through burial. Burial of organic carbon occurs when the flux of organic carbon overwhelms the oxidising capacity of electron donors, or when organic carbon is in a form that is inaccessible to microbes. Organic carbon burial, and enrichment of the carbon isotope composition of dissolved inorganic carbon ($\delta^{13}C_{SW}$), is therefore increased during times of excess productivity, perhaps driven by an increased nutrient flux, or during periods of widespread anoxia. High carbon isotope values indicate that the rate of organic matter burial exceeds that of oxidative weathering, reflecting high rates of net oxygen production. Swings to lower carbon isotope values indicate excess oxidation over burial and atmospheric oxygen depletion. However, the carbon isotope composition of the oceans can also be influenced by anomalous input fluxes, such as methane release, the oxidation of a large organic matter pool or weathering perturbations (Kasemann et al., 2010; Lenton et al., 2012). Over long timescales, the input flux is controlled by volcanic carbon input, with a value of -6‰ (figure 1.9). This standard approach to carbon isotopes may be challenged when reconstructing peculiar events in Earth history, but it has been widely applied to carbon isotope interpretation through Earth history.

Inorganic calcium carbonate acquires the $\delta^{13}C$ of the coeval dissolved inorganic carbon pool. Thus, the carbon isotopic ratio of ancient seawater can be reconstructed using the δ^{13}C of limestones, provided they have not experienced alteration through extensive dolomitisation or deep burial recrystallisation. Limestones may record an integrated signal that partly reflects inorganic authigenic carbonate, precipitated in situ (Schrag et al., 2013). Diagenetic reactions, such as pyrite precipitation, are a source of alkalinity that encourages the precipitation of authigenic carbonate, and so authigenic carbonate may have had a significant influence on the carbon isotope record derived from limestones when O_2 is low. This complicates the relationship between carbon isotopes and the redox budget of the Earth surface. $\delta^{13}C_{SW}$ varies through Earth history, and has been widely be used to reconstruct the global carbon cycle. $\delta^{13}C_{SW}$ should be globally homogeneous, and so large carbon isotope excursions have been used for

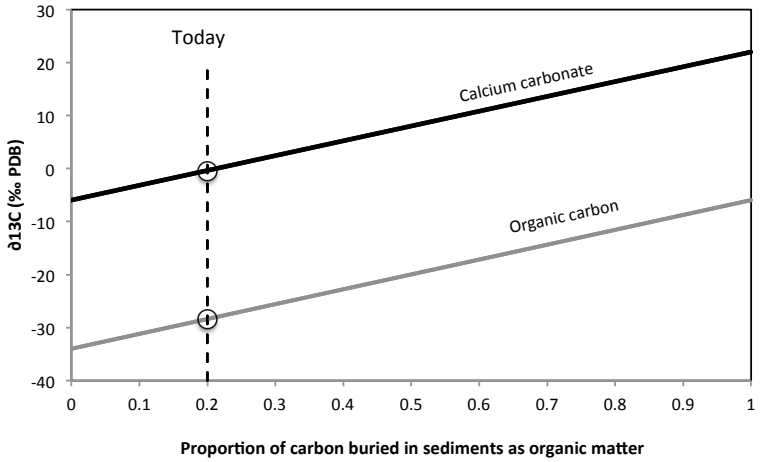

Figure 1.9: Variability in carbon isotopes is controlled by the input flux of carbon and the fraction of organic matter burial. Larger fractional burial rates of organic carbon drive higher $\delta^{13}C$ in carbonates. The mantle input value of carbon is -6‰. The fractionation associated with carbon fixation by autotrophic bacteria (shown here) is 28‰ – this fractionation is larger for methanotrophic reduction. Today the fraction of carbon buried as organic matter, as opposed to in limestones, is around 20%, and so carbon isotope values in limestones are elevated compared with mantle input.

chemostratigraphic correlation between sections. Here, we measure $\delta^{13}C$ on carbonates from Zebra River, the Nama Group, to identify recovery from the Shuram-Wonoka excursion and explore its relationship to other redox information.

1.4.3 Iron redox proxies

Iron can reside in multiple oxidation states under ambient conditions, with the reduction of ferric (III) iron to ferrous (II) iron occurring with an E° = +0.77V. Ferruginous conditions occur when Fe reduction is active and Fe(II) has titrated all H_2S available, enabling Fe to build up in the water column. Anoxic sediments become enriched in Fe through the addition of shelf sources of highly reactive Fe that are decoupled from siliciclastic sources. Where Fe is transported into anoxic sulfidic waters and precipitated as sulfide minerals, sediments will contain enrichments in the proportion of Fe deposited as pyrite (e.g. Canfield et al. 1996). Under anoxic ferruginous conditions, other highly reactive Fe minerals (FeHR) may also form, resulting in FeHR and FeT enrichments (e.g. Zegeye et al. 2012). Precambrian ferruginous sediments can result from Fe added by hydrothermal activity, upwelling of deep Fe rich waters or Fe released from sediment porewaters. The FeT/Al and Fe-speciation proxies have been developed over several decades to detect ferruginous and euxinic conditions in ancient siliciclastic, and more recently carbonate

rich, sediments (Clarkson et al., 2014; Poulton and Canfield, 2005; Raiswell et al., 1988).

Iron speciation

Iron speciation is a widely utilized proxy for determining palaeo-redox conditions. It can clearly distinguish oxic from anoxic conditions using experimentally determined threshold values, but does not record progressive oxygenation. It has the unique ability to distinguish anoxic and ferruginous states from the more extreme anoxic and sulfidic state. Fe-speciation responds to regional water column conditions, unlike some other redox proxies (e.g. Mo isotopes) that provide a globally integrated signal. However, Fe (oxyhydr)oxide enrichments can also occur under oxic conditions, where Fe(II) is transported in anoxic waters into an oxic setting. This may occur during upwelling of anoxic deep waters onto the shallow shelf or where hydrothermal vents input reduced Fe directly into oxic waters. In this case, enrichments in Fe (oxyhydr)oxides imply that the adjacent deeper water column was anoxic, rather than the water column directly overlying the site of Fe enrichment. These 'false anoxic' signals should be identifiable through careful consideration of the geological context and a closer look at the distribution of FeHR phases extracted (Clarkson et al., 2014).

Fe-speciation includes a sequential chemical extraction technique that considers three iron pools: highly reactive Fe, poorly reactive Fe and total Fe. Highly reactive iron (FeHR) includes carbonate-associated Fe (Fecarb; e.g., ankerite and siderite), ferric (oxyhydr)oxides (Feox; e.g., goethite and hematite), magnetite Fe (Femag), separated using a chemical extraction technique, as well as Fe sulfide minerals (Fepy; e.g. pyrite) and acid volatile sulfur (AVS; e.g. mackinawite), separated using distillation techniques (Canfield et al., 1986). Together, these iron minerals form an iron pool that is considered biogeochemically available, or highly reactive towards biological and abiological reduction under anoxic conditions. The total iron pool (FeT) additionally includes a largely unreactive silicate iron pool, originating from detrital weathering fluxes. The proportion of total iron that is highly reactive (FeHR/FeT) is the basis of the Fe-speciation method and can be used to define thresholds for anoxic and oxic conditions (figure 1.10).

Sediments may be enriched in FeHR under anoxic marine conditions due to either the export of remobilized Fe(aq) from the oxic shelf (Raiswell and Anderson, 2005; Severmann et al., 2010; Duan et al., 2010) or under more widespread anoxia, due to upwelling of deep water Fe(aq) (Poulton and Canfield, 2011). Precipitation of this mobilized water column Fe is then potentially

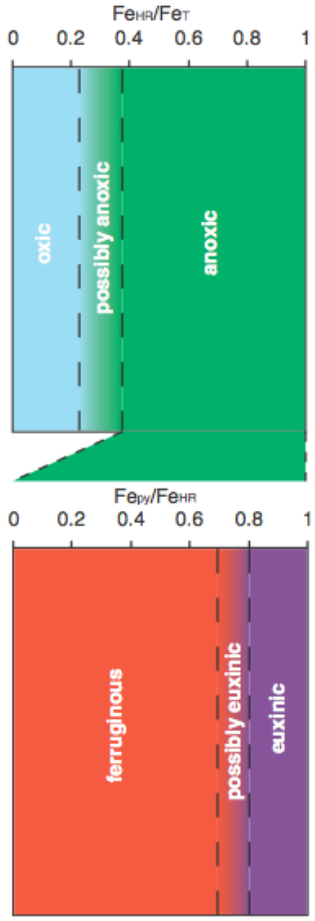

Figure 1.10: Threshold values for determining anoxic vs oxic (top) and ferruginous vs euxinic (bottom) conditions in sediments. Oxic conditions are identified by sediments with an FeHR/FeT ratio below 0.22, with an equivocal zone between 0.22 and 0.38. Anoxia is identified by sediments with a FeHR/FeT ratio greater than 0.38. Within anoxic sediments, an Fepy/FeHR ratio greater than 0.8 indicates euxinic conditions, with ratios below 0.7 indicating ferruginous conditions. From Poulton and Canfield (2011).

induced through a variety of processes, for example through Fe sulfide (pyrite) formation if the Fe encounters water column sulfide, or through Fe (oxyhydr)oxide precipitation due to oxidation at the oxycline (Canfield et al., 1996; Raiswell and Canfield, 1998; Crowe et al., 2008; Zegeye et al., 2014). These processes have the consequence that FeHR/FeT ratios provide a particularly sensitive means to determine whether a depositional setting was oxic or anoxic. Calibration in modern and ancient marine environments suggests that FeHR/FeT $<$0.22 provides a robust indication of oxic conditions, while FeHR/FeT $>$0.38 suggests deposition from an anoxic water column (Poulton and Canfield, 2011; Raiswell and Canfield, 1998; Poulton and Raiswell, 2002). Values between 0.22-0.38, however, are somewhat equivocal, and care needs to be taken to determine if such values are a consequence of masking of the additional anoxic water column

flux of FeHR, either due to rapid sedimentation (Raiswell and Canfield, 1998; Poulton et al., 2004) or due to post-depositional transformation of unsulfidized FeHR minerals to less reactive sheet silicate minerals (Poulton et al., 2004, 2010).

In the presence of sulfide, Fe(II) will be titrated from the water column to form pyrite. Examining of the Fe speciation Fepy/FeHR has the unique advantage in that it allows the separation of anoxic settings into euxinic (sulfidic) environments (Fepy/FeHR >0.7-0.8) and non-sulfidic (Fe-rich; ferruginous) environments (Fepy/FeHR <0.7) (Poulton and Canfield, 2011). Here, we use Fe-speciation on carbonates and siliciclastics from Zebra River, Nama Group, to explore oxygenation of the Nama Basin and its relation to fossil distribution.

Calibration in carbonates

The Fe-speciation proxy was originally calibrated in iron rich fine-grained shales, normally deposited in deeper water settings, but recently Clarkson et al. (2014) have demonstrated the utility of Fe-speciation in carbonates. The primary concerns for the application of Fe-speciation in carbonates are related to the decreased detrital components, and hence low FeHR and FeT. This can increase the sensitivity of the proxy to additional FeHR inputs. The impact of this process is significant at FeT values <0.5 wt% (Clarkson et al., 2014). At FeT >0.5wt% it has been demonstrated that carbonates behave consistently to siliciclastics and that Fe-speciation data can be applied to accurately identify anoxic depositional settings in limestones, albeit with different threshold values.

Clarkson et al. (2014) explore the role of late stage dolomitization on Fe-speciation data. Comparison between contemporaneous limestones and dolomites demonstrate a general increase in FeT within the dolomites, predominantly present as Fecarb and consistent with the idea of late stage alteration due to a through-flowing Fe-rich dolomitizing fluid. This process, however, is laterally heterogeneous creating highly variable results. Thus there is good evidence to avoid sampling late stage dolomites.

Deposition of carbonate-rich samples under oxic water column conditions leads to FeHR/FeT ratios <0.38 at any concentration of organic carbon (providing FeT>0.5wt%). Carbonate-rich sediments deposited under anoxic water column conditions give FeHR/FeT ratios >0.38 for any FeT concentrations (providing organic carbon content >0.5wt %). The equivocal zone, 0.22-0.38, defined for shales is not applicable to carbonates, with a single straight cut-off at 0.38. The

inclusion of TOC data alongside Fe-speciation can strengthen the use of the proxy in carbonates, and provide additional supporting redox information (see section 1.4.1).

Under oxygenated conditions there is no Fe enrichment mechanism and limestone therefore records primary low FeT values. Clarkson et al. (2014) suggest that carbonate-rich rocks containing <0.5wt% FeT and <0.5wt% TOC may indicate oxic depositional conditions, particularly when both are very low (<0.1wt%). These constraints appear valid as long as the sediments are from calci-turbidites (where rapid sedimentation could dilute the Fe supply) and have not undergone demonstrable Fe addition during deep burial dolomitization.

FeT/Al ratios

The FeT/Al proxy provides a bulk measurement of the enrichment of Fe over redox insensitive Al that can be applied to both siliciclastic and carbonate rich sediments (Lyons et al., 2003; Lyons and Severmann, 2006; Raiswell et al., 2008). FeT/Al ratios are expected to fall close to 0.53 ± 0.11 in normal marine siliciclastic as well as carbonate sediments, and as such this value acts as a baseline to identify oxic conditions. Sediments deposited from an anoxic water column show enrichments above this value (FeT/Al>0.64) (Clarkson et al., 2014; Raiswell et al., 2008). The FeT/Al ratio is unlikely to exceed 2, except where Al<0.5% (Raiswell et al., 2011). Both FeT and Al reduce with increasing $\%CaCO_3$, highlighting the anticipated dilution of major elements by carbonate. In very pure carbonates both FeT and Al contents are very low. Despite this dependence of Fe and Al concentrations on carbonate content, FeT/Al ratios are consistent across the full range of $\%CaCO_3$ contents, and so the proxy behaves consistently even in pure carbonates with low FeT. Although anomalous Al concentrations at the low end of the scale may result in false indications of anoxia, oxic signals at low FeT and Al should be robust. This means that FeT/Al can provide some useful redox information in carbonate rich samples that contain insufficient iron for Fe-speciation (Clarkson, personal communication).

An advantage of the FeT/Al proxy is that it does not suffer from post-depositional transformation of unsulfidised iron minerals from highly reactive phases to unreactive forms that may affect FeHR/FeT ratios. The FeT/Al ratio should also be unaffected by deep burial dolomitisation or metamorphism. However, the FeT/Al ratio cannot distinguish euxinic from ferruginous anoxic conditions. FeT/Al combined with Fe-speciation provides a particularly powerful means to evaluate redox conditions with respect the reduction potential of Fe. Here, we have measured FeT/Al ratios for Zebra River, alongside Fe-speciation and TOC data.

1.4.4 Sulfur isotopes

Sulfate is the second most abundant anion in the oceans and has a modern residence time of 10-20 million years, which far exceeds the mixing time of the ocean (Paytan et al., 2004). As a result, its sulfur isotope composition should provide a globally integrated archive of sulfur cycle dynamics over long timescales at modern sulfate concentrations, but this is increasingly less likely as sulfate concentrations decrease. Sulfur can reside in multiple oxidation states, and is critical for maintaining the alkalinity balance of the oceans. Sulfate is respired during dissimilatory sulfate reduction by sulfate reducing microbes in anoxic environments (Jørgensen, 1982). Two key fluxes regulating [SO_4] are riverine sulfate derived from pyrite oxidation, and marine reduction of sulfate to sulfide. Because these fluxes both depend directly on oxygen concentrations, increased [SO_4] probably correlates with increased oxygen availability. Pyrite burial represents an important source of oxygen to the atmosphere over long timescales.

The ratio of the two most common stable isotopes of sulfur, ^{32}S and ^{34}S, can be used to trace changes in the biogeochemical cycling of sulfur through time. The lighter sulfur isotope is preferentially partitioned into reduced sulfur by sulfate reducing bacteria. This lighter sulfur can be removed more permanently through pyrite burial (figure 1.11), leaving marine sulfate elevated in ^{34}S. Paired sulfate-pyrite sulfur isotope studies over long timescales show step changes relating to major changes in sulfur cycling in Earth history, which relate closely to redox changes (Canfield, 1998). Throughout the Precambrian and into the early Phanerozoic, the proportional pyrite burial flux dropped and there was a shift towards evaporites burial as the dominant pathway for sulfur loss from the oceans (Canfield, 2004). Marine sulfate is commonly preserved in phosphorite, barite and evaporite deposits, but in the Precambrian the most commonly available reliable archive is carbonate associated sulfate (CAS).

δ^{34}S fractionations predominantly occur via microbial metabolic processes: dissimilatory sulfate reduction and sulfide oxidation. Bacterial sulfate reduction (BSR) is the respiration of sulfate in the absence of oxygen to break down organic matter and produce hydrogen sulfide. The sulfide produced during this sulfate reduction can either be buried as pyrite and enter the geologic record or be returned to the marine sulfate pool via abiotic or biotic sulfide oxidation. Pyrite should be depleted in heavy ^{34}S compared with coeval sulfate. BSR can produce fractionations as large as 46‰ when sulfate concentrations are high (Kaplan and Rittenberg, 1964). Sulfate reducing bacteria are widely distributed in anoxic environments containing sulfate and have a broad ecological tolerance. Larger sulfur isotope fractionations are possible when the

oxidative side of the sulfur cycle is active, cycling sulfur species through the multiple oxidation states. This cycling occurs predominantly via sulfide oxidizing bacteria (SOB), but also sulfur disproportionating bacteria and other bacterial metabolisms. More recent experiments also report large sulfur isotope fractionations in natural environments where sulfate reducing bacteria alone are operating (Sim et al., 2011). During times of widespread sulfidic conditions in parts of the water column, the fractionation during BSR is maximised, the pyrite burial flux is enhanced, and the δ^{34}S of coeval sulfate increases accordingly.

'Superheavy pyrite', the phenomena whereby pyrite is isotopically enriched compared with coeval sulfate, has been reported in from isolated basins, including the Nama Basin (Ries et al., 2009). The primary explanation for this phenomena is the repeated oxidative cycling of sulfur under sulfate replete conditions. In this instance, the fractionation during BSR would be small, and may be masked by a negative fractionation upon reoxidation, generating sulfate which is isotopically lighter than the starting sulfate. The presence of superheavy pyrite is enigmatic, and may result from ocean stratification, sulfate limitation (Ries et al., 2009; Liu et al., 2006) or contamination of the sulfate isotopic signal (Peng et al., 2014).

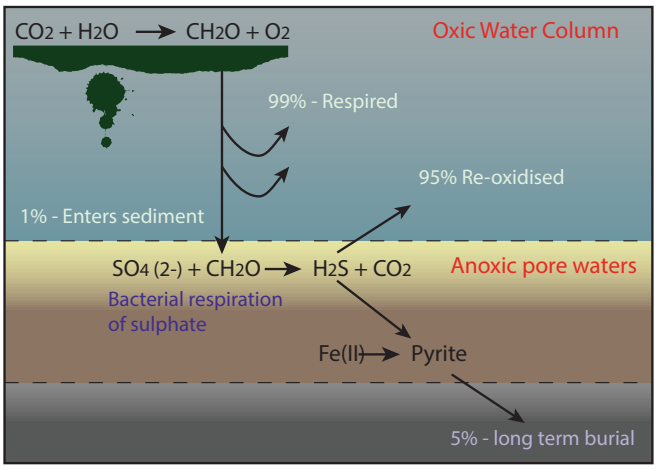

Figure 1.11: Schematic representation of organic matter breakdown through bacterial sulfate reduction in the modern ocean, including rough estimates of the magnitude of different remineralisation fluxes.

The inclusion of minor sulfur isotopes, ^{33}S and ^{36}S, can be used to provide information about the bacterial metabolisms operating in the oceans (Johnston et al., 2005; Zerkle et al., 2009), but there is a dearth of multiple sulfur isotope data in previous studies due to the time consuming analysis required to detect the less abundant isotopes (Rees, 1978). Much larger fractionations in $\Delta^{33}S$, caused by symmetry effects in the absence of an ozone, have been used to constrain an

early rise of atmospheric oxygen ~2.3 Ga (Farquhar et al., 2000).

Sulfur isotopes are often used in conjunction with other redox proxies to investigate the link between carbon, oxygen, iron and sulfur cycles. Sulfur isotopes can be used as supporting evidence for euxinic conditions, but the same S isotope signatures can result from different redox conditions through variation in sulphate concentrations, the extent of pyritisation, or the biological controls on isotope fractionation. $\delta^{34}S_{py}$ analyses are often used to support Fe-speciation data. This is important for distinguishing ferruginous from euxinic conditions, as pyrite is readily oxidised and quickly weathers to form iron oxides, altering the ratio of Fepy/FeHR.

Here, we measure multiple sulfur isotopes in modern marine sulfate to constrain the pyrite burial flux through a simple box model. We also measure sulfur isotopes in CAS and coeval pyrite from Nama Group carbonates to constrain sulfur cycle dynamics in the terminal Ediacaran.

1.4.5 Ce anomalies

The rare earth elements and yttrium (REY) are a coherent group of elements that are present in low concentrations in seawater. Experimental studies and investigations of natural environments show that REY are partitioned between solids and solution, producing distinctive REY patterns with characteristic anomalies. REY patterns may be faithfully preserved in authigenic minerals such as carbonate, phosphate and chert. Cerium (Ce) is the only REE that undergoes redox transformations under ambient ocean conditions, offering an opportunity to use REY patterns in carbonates as a palaeo-redox proxy.

The REY distribution represents the exchange equilibrium between REY (III) solution complexes (in seawater mostly mono- and di- carbonate complexes, and possibly siderophore, silicate or sulfate complexes) and REY surface complexes (hydroxide complexes such as $REYOH^{2+}$ on the surface of Fe-Mn oxides and hydroxides, clays or organic matter). Experimental work suggests this exchange equilibrium is attained fast, i.e. seconds to minutes (Byrne and Kim, 1990; Koeppenkastrop and De Carlo, 1993; Bau and Dulski, 1999). This is supported by observations in natural systems where REY flux from rivers and hydrothermal vents rapidly attain a seawater distribution pattern (German and Elderfield, 1990; Mitra et al., 1994; Sherrell et al., 1999).

The preferential removal of REY onto particles in the upper part of the water column is balanced

by their release at depth from the labile fraction of the organic and oxide coatings on detrital particles. The extent of fractionation between seawater and suspended particles is similar throughout the modern ocean, suggesting globally consistent controls on the scavenging process (Bertram and Elderfield, 1993; Sholkovitz et al., 1994). The short residence times of fast sinking particles leads to little fractionation between particles and seawater, whereas small, slow sinking particles accommodate extensive fractionation of REY (Fowler et al., 1992; Koeppenkastrop and De Carlo, 1993; Koeppenkastrop et al., 1991). The precipitation rate and size of particles, as well as overall sedimentation rates, could affect the exposure time of particles to solution, and so affect REY scavenging.

Cerium is the only REY that can undergo redox transformations under ambient marine conditions (German and Elderfield, 1990). In the presence of oxygen, Ce(III) is partially oxidised to Ce(IV) on the surface of Fe-Mn (oxyhydr)oxides, either abiotically (Bau, 1999; Koeppenkastrop and De Carlo, 1992) or via microbial mediation (Moffett, 1990), where it ceases to participate in exchange reactions between REY(III) solution and surface complexes. Hence, a certain fraction of the scavenged Ce remains as Ce(IV) on the solid surface. With time, Fe-Mn (oxyhydr)oxides preferentially accumulate Ce over the other REY, resulting in positive Ce anomalies in the solid phase, and corresponding negative Ce anomalies in solution. The fractionation of Ce relative to the other trivalent REY only occurs under oxic conditions and can be used to constrain palaeo-redox (e.g. Bodin et al. 2013; Ling et al. 2013; Meyer et al. 2012; Schroder and Grotzinger 2007).

The redox cycling of Ce is controlled primarily by its selective removal onto Fe-Mn (oxyhydr)oxides. Fe-Mn (oxhydr)oxide precipitates are categorised as hydrothermal deposits, hydrogenetic crusts, hydrogenous nodules and diagenetic nodules, based on the type of aqueous fluid from which they precipitate (Bau et al., 2014) (figure 1.12). Hydrogenous crusts and nodules precipitate from seawater initially as colloidal particles within the water column, at the surface of solid substrates such as seamounts (crusts) or by accretion around a nucleus on soft sediment (nodules). They are characterized by very slow growth rates (mm/Myr), and catalyse the oxidation of Ce under oxic conditions, resulting in large Ce enrichments. Hydrothermal Fe and Mn (oxyhydr)oxides precipitate from marine medium to low temperature hydrothermal fluids when these mix with cold seawater. Their rapid formation results in low $\sum$REY and REY patterns similar to those of seawater, but Ce continues to accumulate as long as surfaces remain exposed to seawater due to restrictive desorption of tetravalent Ce (Bau and Koschinsky, 2009). Diagenetic nodules form from metal ions in suboxic pore waters close to the sediment-

water interface, and show negative cerium anomalies, low ∑REY and Y/Ho ratios close to unity. The negative Ce anomalies of diagenetic nodules suggests that in contrast to redox insensitive REY(III), Ce is not quantitatively mobilised as pore waters are not able to reduce or transport Ce^{4+}.

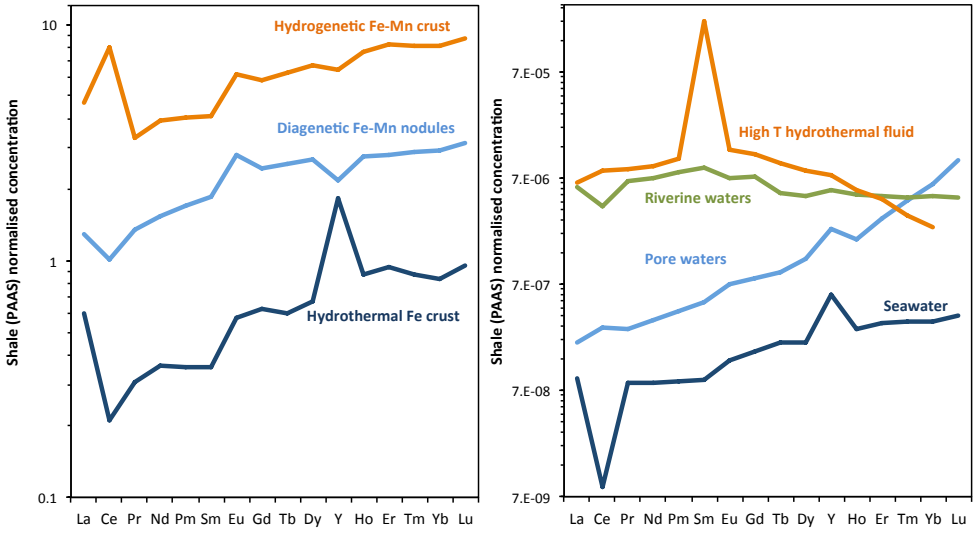

Figure 1.12: Examples of typical REY distribution patterns for different fluxes and mineral phases in marine environments, adapted from Bau et al. (2014).
Left: Marine hydrogenetic Fe-Mn crusts (Bau and Dulski, 1996), diagenetic Fe-Mn nodules and hydrothermal Fe crusts, (Bau et al., 2014).
Right: high-temperature hydrothermal (black-smoker) fluids Bau and Dulski (1996), seawater (James et al., 1995) and marine porewater (Soyol-Erdene and Huh, 2013).

The redox cycling of Ce is widely assumed to be more closely tied to the formation of Mn than to Fe (oxyhydr)oxides. Some have suggested the Fe oxides record REY patterns of the water column from which they precipitated qualitatively, in contrast to Mn oxides that scavenge Ce and LREE preferentially, and exclude Y (Bau, 1999; De Carlo, 2000; Ohta and Kawabe, 2001). Sholkovitz et al. (1994) found that the development of Ce anomalies in the coatings of particulate matter coincides with the in-situ formation of Mn-oxide rich particles. Particles from Mn poor hydrothermal pools record a seawater pattern (Edmonds and German, 2004). However, sequential leaching of seafloor nodules has produced conflicting data, suggesting that Fe oxides play a more important role in the fractionation of REY during scavenging (Bau and Koschinsky, 2009). It is not clear if the close relationship between Ce and Mn arises due to oxidation of Ce on Mn oxides or because the distribution of both elements are controlled by common processes.

The redox sensitive fractionation of Ce should impart a positive Ce anomaly onto detrital particles and a negative Ce anomaly in residual seawater REY. In general, oxygenated modern

marine settings display a strong negative Ce anomaly due to scavenging onto particles, while suboxic and anoxic waters lack negative Ce anomalies due to reductive dissolution of settling particles (figure 1.13) (Byrne et al., 1996; German et al., 1991). The release of Ce can occur via reductive dissolution of metal oxides, and the release of all REY including Ce, or via the reductive dissolution and release of cerium oxides and hydroxides from the particle surface. The reduction potential of cerium is intermediate between Mn and Fe.

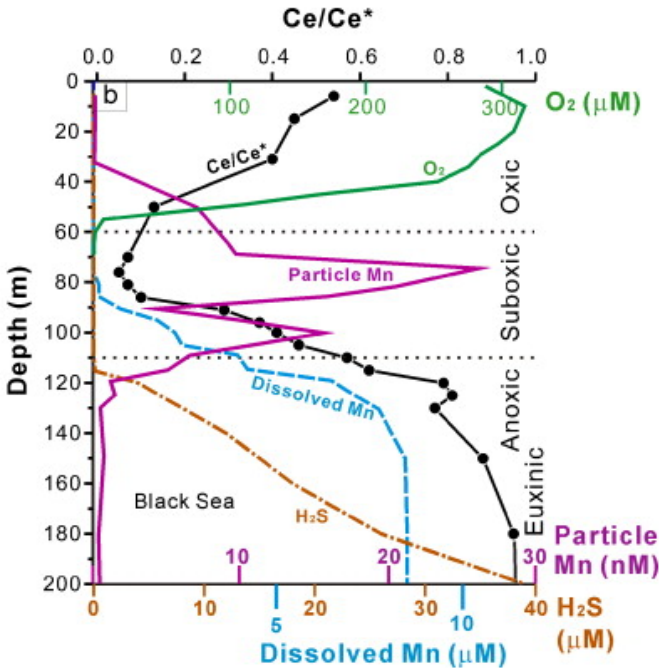

Figure 1.13: Depth profiles of Ce anomaly and concentrations of oxygen, sulfide, dissolved- and particulate-Mn, for the Black Sea BS3-6 station, emulated after Slack et al. (2007) and from Ling et al. (2013). Data sources: Ce/Ce* values from German et al. (1991), concentrations of dissolved Mn and particulate Mn from Lewis and Landing (1991), and concentrations of O_2 and sulfide from Luther III et al. (1991).

The magnitude of the negative Ce anomaly in seawater should develop progressively with depth, and may offer the potential to quantify the extent of oxygenation and the depth of the oxic surface waters. The Ce anomaly develops along with increases in the concentration of particulate Mn(IV)O_2 and returns to unity as Mn is reduced and the excess Ce is released into the water column. These processes become important between 100 and 200m depth in the modern ocean, in concert with the in-situ oxidation of dissolved Mn(II) to particulate Mn(IV) oxides (Sholkovitz et al., 1994). This pattern is also observed in the redox stratified Black sea, where negative Ce anomaly in the water column peaks at 75m water depth, coincident with the depletion of dissolved oxygen (figure 1.13). Ce anomalies then returns to values close to unity by 150m. The

Ce anomaly is eroded most rapidly in the 'suboxic' zone, where Mn reduction is occurring, but before the onset of Fe reduction. In many redox stratified basins the Ce anomaly, along with the HREE/LREE ratio and Y/Ho ratio returns to shale composite values beneath the Mn and Fe redox boundaries. In some basins, however, positive Ce anomalies and LREE enrichment develop in anoxic and suboxic zones of the water column, linked directly to Mn cycling in the suboxic zone (Bau et al., 1997; De Baar et al., 1988; De Carlo and Green, 2002; German et al., 1991).

Ce frequently displays concentration maxima in surface waters, in contrast to the other trivalent lanthanides and many other trace elements (Moffett, 1990). Aeolian deposition cannot account for the maxima as Ce is not enriched in continentally derived dust. The unique maxima for Ce must involve its redox chemistry. Microbial Mn-oxidation is photo-inhibited (Sunda and Huntsman, 1988), and this may also be the case for Ce. Lower oxidation rates in the upper photic zone would lead to longer residence times, possibly resulting in a surface maxima. Photoreduction of Ce(IV) may also be a factor.

Ce anomalies provide a spatially and temporally sensitive means to trace redox cycling in natural environments. To be of use as a palaeo-redox proxy, Ce anomalies must be faithfully preserved in authigenic minerals. Non-biogenic carbonates are thought to provide a reliable archive of seawater REY that should be largely unaffected by diagenesis or even dolomitisation (Webb et al., 2009; Banner et al., 1988). The methods used to extract a pristine seawater REY signal from carbonate phases are poorly defined and can give ambiguous results. The development of the carbonate leaching method forms a major part of this thesis, discussed in chapter 3.

1.5 The Nama Group

This study focuses on carbonate samples from the Nama Group, southern Namibia. The Nama Group preserves key changes in the terminal Ediacaran fossil record, including the introduction of biominerals and the beginnings of bioturbation, as well as preserving the Ediacaran biota. The Nama Group is unmetamorphosed, well exposed and covers large geographical areas - making it an ideal place to study temporal and spatial variation in redox at high resolution. The sedimentology and stratigraphy are well described from previous work (e.g. Saylor et al. 1998). Samples from nine shelf to basin sections have been collected as part of this study, as well as on previous field trips.

1.5.1 Geological Setting

The Nama Group is a major lithostratigraphic unit that crops out in southern Namibia and NW South Africa, and is one of the world's best preserved terminal Proterozoic carbonate and siliciclastic sequences (Germs, 1983). The Nama group was deposited approximately 550 to 543 Ma in the foreland basin of the Kalahari craton, which developed during the assembly of Gondwanaland (Germs, 1983, 1974; Stanistreet et al., 1991). The lower Nama Group (Omkyk and Hoogland members mainly) is coincident with the appearance of early biomineralizing Metazoa, such as *Cloudina*, *Namacalathus* and *Namapoikia*.

The Group was deposited in two sub-basins – the Zaris sub-basin in the north and the Witputs sub-basin in the south – which were separated by a palaeohigh, the Osis Arch (figure 1.14 and 1.15). The Kuibis Subgroup is thickest near the Damara and Gariep fold belts and thins until the Subgroup completely disappears over the Osis Ridge (Germs, 1983, 1995). The Kuibis and Schwarzrand Subgroups were deposited in settings ranging from upper shoreline/tidal flats to below-wave-base lower shoreface (Germs, 1995; Grotzinger and Miller, 2008; Saylor et al., 1995, 1998).

The age of the upper Nama Group is relatively well-constrained from the U-Pb dating of three ash beds within the group, including one at 548.8 $\pm$ 1 Ma in the Hoogland Member (Grotzinger et al., 1995) revised to 547.32 $\pm$ 0.31 Ma by Narbonne et al. (2012) (Kuibis Subgroup, Zaris sub-basin). The age of the base of the Nama Group is around 550 Ma (Ries et al., 2009). The Proterozoic-Cambrian boundary is represented by a regionally extensive erosional unconformity

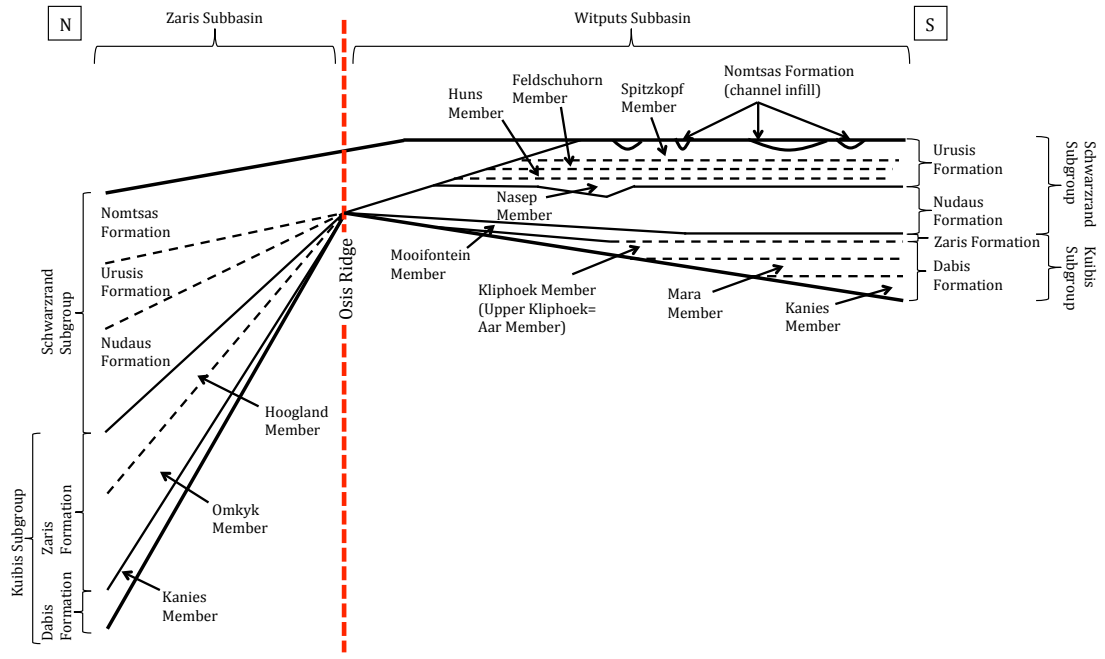

Figure 1.14: A cross section through the two sub-basins of the Nama Group, adapted from Germs (1983) by James Lyne and Fred Bowyer.

near the top of the Schwarzrand Subgroup in the southern sub-basin (Germs, 1983; Saylor et al., 1995; Narbonne et al., 2012; Grotzinger et al., 1995), which is overlain by incised-valley fill dated (U-Pb on an ashbed) at 539 $\pm$ 1 Ma (Grotzinger et al., 1995). Therefore, the Nama Group section spans at least 10 Myr and extends to within 1 Myr of the Proterozoic-Cambrian transition (Saylor et al., 1998; Ries et al., 2009).

The Nama Group contains of a series of shallowing upwards cycles, influenced by oscillations in sea levels superimposed on local basement deepening. Cycles contain facies changes from distal, medial and inner ramp conditions, occasionally reaching peritidal (Saylor et al., 1998). Distal ramp facies are characterised by interbedded shales, marls, fine sandstones, limestone laminites and rare thin beds of calcarenites, often associated with rythmites, suggesting deposition in an offshore, low energy environment. The transition to slope environments is indicated by thin-bedded limestones, with occasional breccia flows and turbidites. Medial ramp facies contain calcisiltite, heterolithic interbeds and thin-bedded limestones with thrombolite or stromatolite columns. Hummocky cross-stratification, intraclast conglomerates and coarse-grained ripples are common. The tops of the cycles are dominated by cross-stratified grainstones and irregularly laminated fine dolostone, deposited in shallow shelf environments. Isolated bioherms or laterally extensive biostromes are common with skeletal and micrite debris fill. Several shoaling cycles

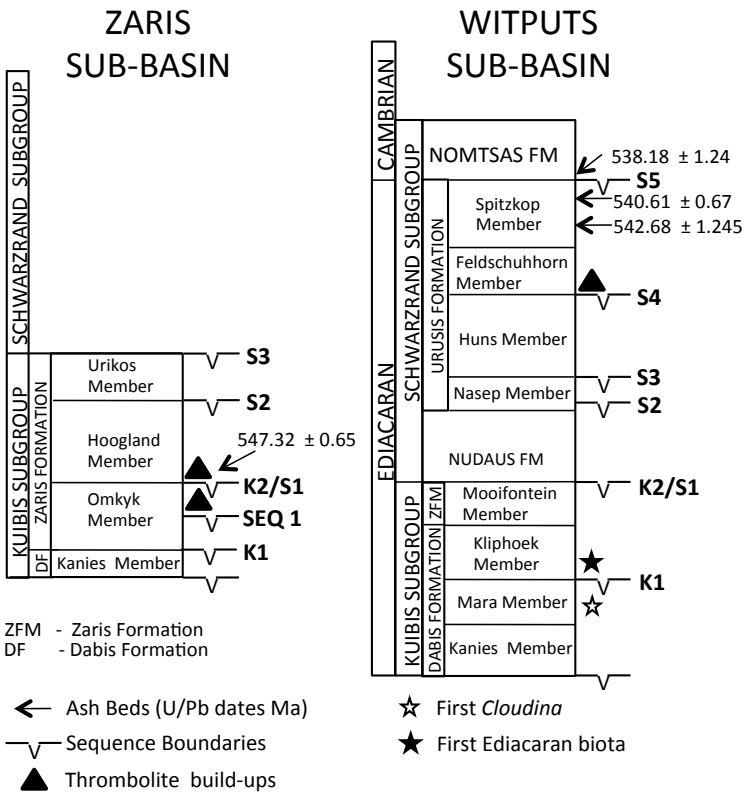

Figure 1.15: Stratigraphy, sequence boundaries, and dated ash beds of the Zaris and Witputs sub-Basins Nama Group, Namibia. Labels K1, K2, S1, S2, S3, S4 and S5 represent sequence boundaries that can be traced across both sub-basins. (from Wood et al. 2015, modified after Grotzinger and Miller 2008; Hall et al. 2013; Saylor et al. 1995, 1998).

contain evidence for deposition in supra- to intra- tidal conditions, subjected to exposure and evaporation. These are characterised by breccia beds, microbially laminated structures, planar and ripple lamination, desiccation cracks and intraclasts.

1.5.2 Ecological setting

The terminal ten million years of the Ediacaran Period witnessed a remarkable pulse in animal evolution, with the beginnings of predation and biomineralisation (Bengtson and Morris, 1992; Hua et al., 2003; Germs, 1972). The Nama Group hosts skeletal biota, Ediacaran biota and towards the upper Nama, evidence for bioturbation. Well developed thrombolite-stromatolite reefs also occur throughout the lower Nama group. The assessment of ecological changes throughout the Nama Basin is necessary to test the hypothesis that redox controlled later Ediacaran ecosystems. The distribution of biological evidence within the sampled sections has

been recorded to accompany geochemical data.

Microbialites

Microbes are the workhorses in most biogeochemical cycles. Microbial mats are efficient at element cycling and once developed only require light to function. As a result, they may form in a diverse range of settings throughout the water column and sediment pile, including anoxic environments. Although microbial mats are rare on the seafloor today, they were widespread in the Precambrian. Microbial communities are often composed of many species that recycle each others waste chemicals, including six key functional groups of microbes:

1. Oxygenic phototrophs (cyanobacteria) couple light energy to CO_2 fixation
2. Anoxygenic phototrophs (purple and green bacteria) use HS^- as an electron donor for photosynthesis
3. Aerobic heterotrophs gain energy from respiration of O_2 and organic carbon
4. Fermenters use organic carbon or sulphur as the electron donor and acceptor.
5. Anaerobic heterotrophs (sulfate reducers) respire organic carbon with SO_4^{2-}, producing HS^- .
6. Chemolithoautotrophs (sulfide oxidising bacteria and methanotrophic bacteria) that oxidise reduced sulphur with O_2 while fixing CO_2 .

Algal and bacterial processes can promote the precipitation of $CaCO_3$ minerals and trap sedimentary particles, resulting in microbial carbonates that are common in the rock record (Dupraz and Visscher, 2005). Some microbialites incorporate sediment with sticky mucus, others form by altering the alkalinity of their microenvironment and inducing the direct precipitation of calcium carbonate (usually aragonite). Sulfate reducing bacteria could play a critical role in the formation of $CaCO_3$ in lithifying microbial mats through numerous mechanisms: altering the local pH, increasing the availability of free calcium ions through the removal of carboxylic acids that bind calcium, removing sulfate (an important kinetic inhibitor for dolomite formation) and providing heterogeneous nucleation sites due to their large cell size (Braissant et al., 2007). Sulfate reducing bacteria also produce EPS, the sticky substance that binds together calcium carbonate, and that may account for the incorporation of metals into carbonate minerals (Braissant et al., 2007). Microbialites may preserve a distinct, and in some

cases more pristine, geochemistry compared with coeval abiotic carbonates (Ries et al., 2008; Webb and Kamber, 2000).

In the Precambrian, before the advent of Metazoan biomineralisation, microbialites formed a significant proportion of global carbonate precipitation. The abundance of microbialites has declined since a peak 500Myr ago, but they are still present throughout the Phanerozoic and in some modern environments (e.g. Lake Wallyungup) (Burns et al., 2004; Mcnamara, 1992). Microbial mats may have provided a food resource for the Ediacaran biota, and the decline of microbialites, and as a consequence the Ediacaran biota, may be linked to the rise of benthic filter feeders in the later Cambrian.

Thrombolite and stromatolite reefs occur at several levels within the terminal Proterozoic Nama group, on scales from 1m-1km, and as an integral facies within the transgressive systems tracts (TST). Reefs nucleate during times of increased accommodation space, forming isolated patch and pinnacle bioherms, transitioning to more sheet-like biostromes as accommodation space decreases. Microbial reefs form over a wide range of length scales. Single reef build ups, such as 'Driedoornvlagte', can reach 7Km long and 200m high within transgressive systems tracts. Driedoornvlagte reef grew vertically upwards, perhaps nucleating off a topographic high on the seafloor, and kept pace with rising relative sea level. Reef growth was eventually terminated through drowning. Reefs at other localities, such as Zebra River, formed in more restricted accommodation space. Bioherm reefs nucleate in the transgressive systems tract, often showing mushroom growth morphology from a nucleation point at the base. Reef growth is terminated by grainstone layers as accommodation space decreased. In places, the subsequent reef horizon nucleates onto palaeo-highs left by the horizon below. Higher up within Zebra River section, where accommodation space is more limited, reefs form sheet like biostromes with thinner, more stromatolitic columns.

Thrombolites have a distinct clotted fabric, and are often considered to represent a complex, mixed microbial-Metazoan ecosystem (Kennard and James, 1986). In the Nama Group, thrombolites form closely spaced stacked columns separated by inter-column fills that contain dolomitized mudstones and cross-bedded *Cloudina* - *Namacalathus* grainstones (figure 1.16). Stromatolites comprise layers of detrital particles that were trapped and bound by microbial communities, forming simple crenulated structures. Compared with thrombolites, stromatolites are better developed in conditions of relatively low accommodation under higher current velocity and sediment influx. In the Nama Group, thrombolite heads are often surrounded

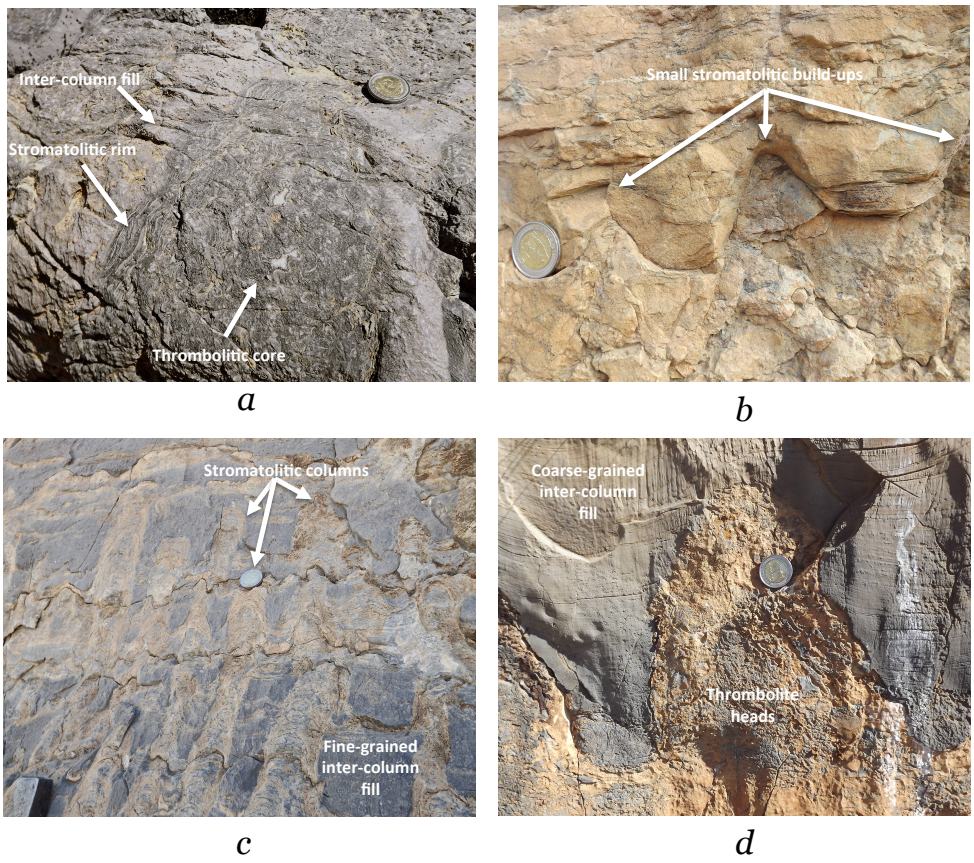

Figure 1.16: Photos of typical microbialite textures at Zebra River. Coin for scale.
a - Planar cross-sectional view of a thrombolite column with stromatolitic rim from OS2
b - Small individual stromatolite build-ups within the upper Hoogland member
c - Narrow stromatolite columns with fine-grained inter-column fill, from the base of the Hoogland member
d - Wide thrombolite heads with coarse-grained cross-bedded inter-column fill, from OS2

by a stromatolitic rim (figure 1.16 a). Microbialite column width, spacing and height vary systematically with the type of sediment being deposited; columns are generally wider and more closely spaced during carbonate deposition and narrow and widely spaced during shale deposition (Figure 1.16 c and d) (Johnson and Grotzinger, 2006). Both types of microbialites are intimately associated with the first calcifying Metazoan organisms, which may have attached themselves to the sediment surface or lived in sheltered depressions within the rough topography created by ecologically complex mats (figure 1.18).

Skeletal biota

Skeletal Metazoa appear globally and with apparent synchronicity in the rock record ~550 Ma. Metazoan hard-parts from late Ediacaran strata are represented by mineralized and non-mineralized tubes (Grant, 1990), possible siliceous microfossils (Gehling and Rigby, 1996; Kontorovich et al., 2008), and supportive calcareous skeletons (Grant, 1992; Grotzinger et al., 2000a; Wood et al., 2002). Calcified taxa include *Cloudina* (Germs, 1972), *Namacalathus* (Grotzinger et al., 2000b), *Namapoikia* (Wood et al., 2002) and some minor taxa (Zhuravlev et al., 2012). These calcified taxa are of uncertain affinity, but were probably stem group Eumetazoa, Cnidaria and Bilateria, or Cnidaria (Kruse et al., 1995; Bengtson and Morris, 1992). All were sessile benthos and grew in equatorial, shallow marine carbonate settings. The shells are weakly and some were possibly only passively mineralised. The forms exhibit remarkable evolutionary stasis throughout their ten million year history before undergoing extinction at the Precambrian/Cambrian boundary (Amthor et al., 2003).

All calcified Metazoans occur in carbonate facies, either along bedding planes of mudstones or dolostones, in thin to thickly-bedded packstones and grainstones, or associated with thrombolite reefs. These taxa have been described globally, from localities in Siberia, China, Oman, Brazil, Spain, Paraguay and Namibia (Grant, 1990; Grotzinger et al., 2000a; Hua et al., 2005; Morris et al., 1990; Wood et al., 2002; Warren et al., 2011; Zhuravlev et al., 2012). The Nama Group hosts some of the best preserved specimens of early biomineralising Metazoa, including *Cloudina*, *Namacalathus* and *Namapoikia* (Grotzinger et al., 2000a; Wood et al., 2002). Their size and distribution varies systematically across the basin (see Penny et al. in review).

With the exception of *Namapoikia*, which is found within fissures in microbialite reefs (Wood et al., 2002), Ediacaran skeletal forms have only generally constrained ecological preferences (Grant, 1990; Grotzinger et al., 2000a; Kruse et al., 1995; Germs, 1972). *Cloudina* was aggregating and gregarious. An aggregating habit in solitary organisms assists the acquisition of favorable substrate for growth to maturity; affords protection from currents or high-energy events; and reduces susceptibility to overgrowth from competitors, larval invasion and infestation, and attack by predators (Jackson, 1983). The aggregating habit has also been noted in the Ediacaran skeletal *Namacalathus* (Wood, 2011). Ecological preferences across the Nama group vary between sites, with some sections hosting larger, thicker shells in high-density beds, and others thin shells in flaggy beds.

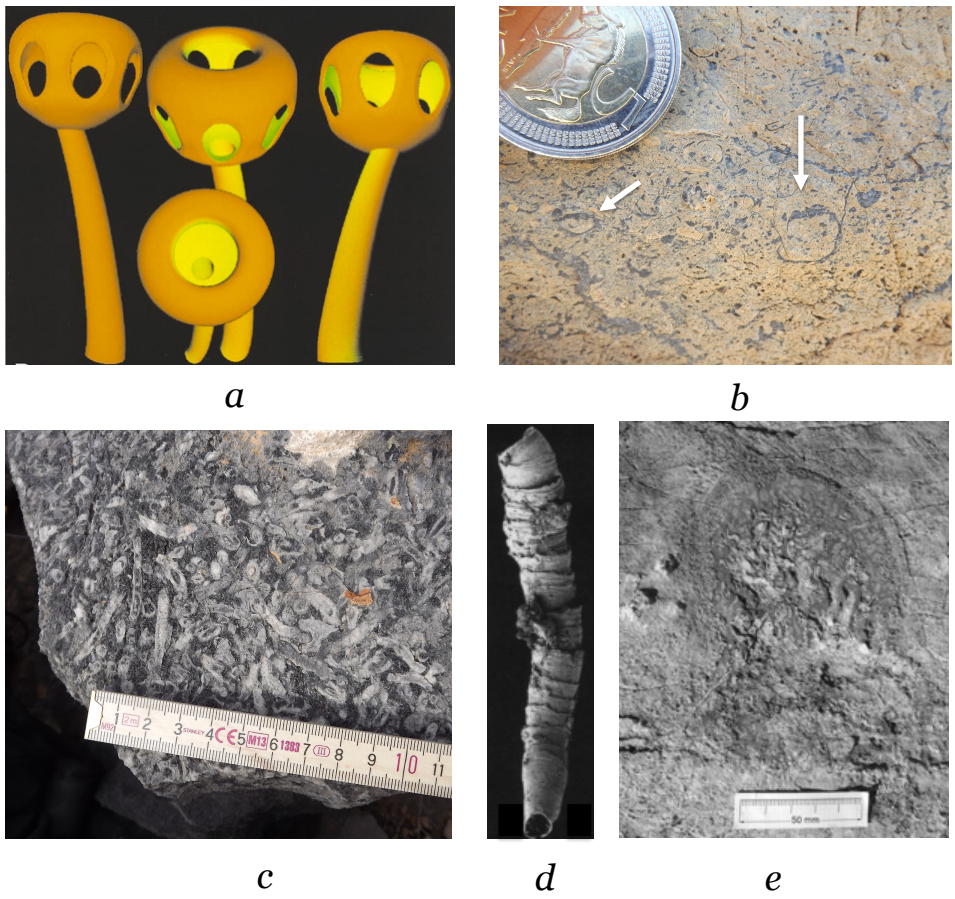

Figure 1.17: Biomineralising metazoa of the Nama Group.
A - Morphological reconstruction of *Namacalathus*, from Grotzinger et al. (2000b)
B - *Namacalathus* photographed in situ at Zebra River, Nama Group.
C - Large *Cloudina* photographed in situ at Driedoornvlagte reef complex
D - Reconstruction of *Cloudina* morphology, from Hua et al. (2003)
E - Namapoikia, photographed at Driedoornvlagte reef complex, from Wood et al. (2002).

Namacalathus, interpreted as a stem-group Eumetazoan, has a goblet-like shape, consisting of a hollow stem that flares to form a 'cup'. The cup has 6 or 7 openings in the side walls, and a larger opening in the top whose edges curl inwards towards a central space (Grotzinger et al., 2000b). Examples from the Nama Group range from 2 mm to 35 mm (Grotzinger et al., 2000b; Wood, 2011). Individuals with the smallest cup diameters are found in high energy inner ramp settings, with intermediate cup diameters in lagoonal settings (Penny et al., in review). The largest individuals are found in mid-depth reef localities, with the largest forms (>35 mm) attached to thrombolite heads (Wood, 2011). Stalks are up to ten times as long in lagoonal than inner ramp settings (30 mm compared with 3 mm). *Namacalathus* growth is isometric (Penny et al., in review), where growth size is proportional to either individual longevity or rate

of growth and growth was restricted by the longevity of favourable conditions. The largest, and so possibly most long-lived *Namacalathus* individuals occur in mid-ramp settings, and these settings also show the greatest diversity of growth habits. The small sizes and small aggregations of clonal forms found in high energy inner-ramp settings may indicate these communities were short lived and opportunistic.

Cloudina, a genus characterized by stacked funnel-shaped elements which form a distinctive cone-in-cone exoskeleton, was first described from the Nama Group (Grant, 1990; Cortijo et al., 2010), and has subsequently been reported globally from late Ediacaran carbonates (Grant, 1990). The oldest reported *Cloudina* is from the carbonate-dominated Mara Member in the Witputs Basin (Germs, 1983), and occurs throughout the Kuibis and Schwarzrand Subgroups. *Cloudina* may belong to a group of polychaete worm tubes, serpulid polychaetes or cribricyathids, or it may not even be a Metazoa (Germs, 1995). Differential preservation (dolomitic in Oman and Namibia, calcitic in Brazil, phosphatic in Spain and China) supports claims that the original mineralogy was metastable, most likely aragonitic. This is consistent with Porter (2007)'s suggestion that biomineralising Metazoa adopt a mineralogy to match the coeval seawater stable state. Late Ediacaran seawater is poorly constrained from geochemical evidence, such as ooids, but is projected to be aragonitic (Hardie, 2003).

Evidence of reef-building activity by *Cloudina*, described for the first time in Penny et al. (2014) (see appendix A), is illustrated in figure 1.18. We observed multiple examples of reef-building *Cloudina* in the mid-ramp Driedoornvlage reef complex. These *Cloudina* reefs formed open frameworks without a microbial component but with mutual attachment and cementation between individuals. Reef-building in Metazoans represents an important ecological innovation whereby individuals collectively enhance feeding efficiency and gain protection from competitors and predation, suggesting that biomineralisation in *Cloudina* may have been a response to rising predation pressures. These observations push the advent of Metazoan reef building back by twenty million years (Kruse et al., 1995), and indicate that complex ecological pressures were in force before the Cambrian explosion. Ediacaran reefs had been thought to be ecologically simple and of low biodiversity (Grotzinger et al., 2000a; Wood and Woodward, 1999) but the presence of reef-building *Cloudina*, as well as thrombolite-associated *Cloudina* and *Namacalathus* and fissure-dwelling Namapoikia, suggests a differentiation of Metazoans into the distinct open surface and cryptic biotas that characterize Phanerozoic and modern reefs.

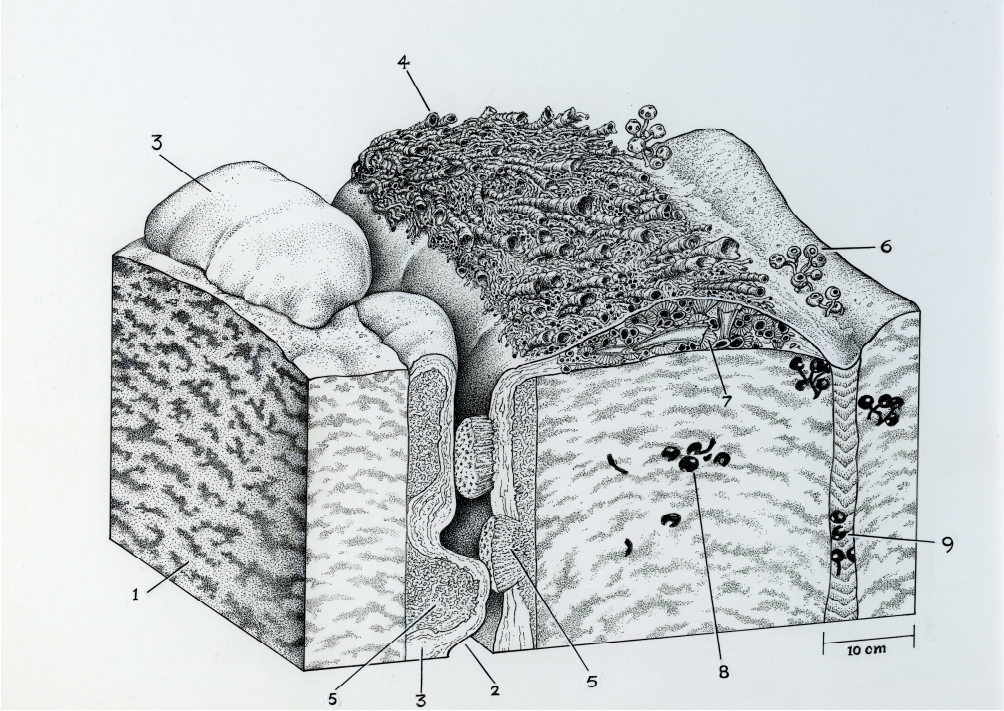

Figure 1.18: Reconstruction of a late Ediacaran reef system. 1. Thrombolite, 2. Neptunian dyke, 3. *Stromatolite*, 4. *Cloudina*, 5. *Namapoikia*, 6. *Namacalathus*, 7. Cement botryoids, 8. trapped *Namacalathus*, 9. Sediment. Copyright: J. Sibbick, produced for Penny et al. (2014).

Ediacaran biota

The Ediacaran biota are first recorded following the Gaskiers glaciation. Typical late Ediacaran fossils, such as *Ernietta*, *Pteridinium*, *Swartpuntia*, *Rangea* (e.g. Narbonne et al. 1997), and *vendotaenids* (Germs et al., 1986) have been described from both the Zaris and Witputs basins. The oldest Ediacara-type fossils occur in the Mara Member of the Kuibis Subgroup in the Witputs basin (Saylor et al., 1995), and the youngest, including *Swartpuntia*, are found 60m below the Ediacaran – Cambrian unconformity in the more southerly portion of the Witputs basin (Narbonne et al., 1997).

The Ediacaran trace fossil record is sparse, consisting mostly of small, bed-parallel burrows (Jensen et al., 2006). Small, individual burrows are described from the base of the Schwarzrand Subgroup, with more complex trace fossils appearing closer to the Cambrian boundary (figure 1.25). Trace fossils reported recently in Macdonald et al. (2014) from the Nama Group (sandstone lenses within the upper Omkyk Member, close to Zebra River) show evidence for sediment displacement in the form of U-shaped spreiten, from which Macdonald et al. (2014) infer that a bilaterian responsible for the trace exhibited a specialized and complex behavior

normally not seen until the Cambrian Period. Along with other recently reported forms (Chen et al., 2013; Liu et al., 2010; Rogov et al., 2012), these trace fossils indicate that complex behaviour, including motility and predation, may have been more widespread in the Ediacaran.

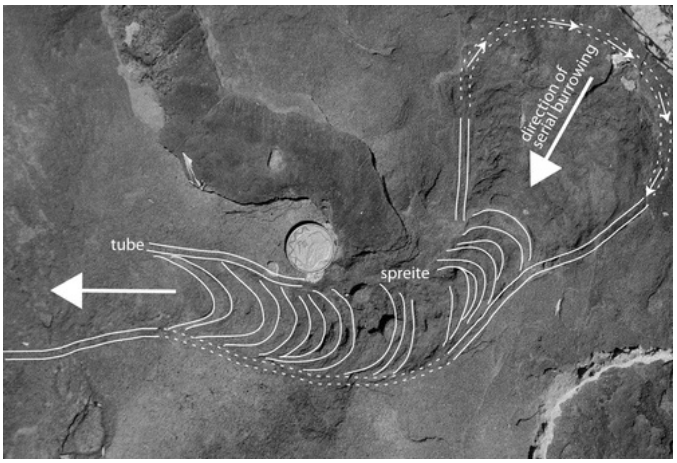

Figure 1.19: Example of a spreite trace fossil from the Omkyk member, from Macdonald et al. (2014). Image of specimen is overlain by a schematic representation of the creation of a single trace fossil. Small arrows show the direction of movement of the trace-maker to form one spreite. Large arrow shows the serial progression of the trace-maker.

The Ediacaran biota disappeared at the Cambrian boundary, along with Ediacaran skeletal forms, and their extinction was complete although not abrupt. More advanced early Cambrian fauna replaced the Ediacaran biota due to increasing predator pressure as well as environmental pressure, because vendobionts depended on declining microbial films.

1.6 Sample Sites

A total of nine localities within both the Zaris and Witputs sub-basins have been sampled for carbonates and shales (figure 1.20), along with detailed logs that note the presence of microbial fabrics and bioclasts. These sites cover inner, mid and outer ramp sections from the Kuibis Subgroup, as well as two sites from the Schwarzrand Subgroup (figure 1.21). This high resolution sampling has enabled us to explore the relationship between redox conditions and local ecology.

In the Zaris Basin, Zwartmodder (Omkyk to lower Hoogland Members) and Omkyk (Omkyk Member) represent dominantly inner ramp settings; Zebra River (Omkyk and Hoogland members) and Driedornvlagte (Upper Omkyk) are mid-ramp, and Brak (Kanies to Lower Omkyk Members) is outer ramp. In the Witputs Basin, Arasab (Kanies to Mooifontein Members) and Grens (Kanies to Aar Member) represent inner ramp, restricted settings. The Pinnacle Reefs are mid-ramp (Feldshuhhorn to lower Spitzkopf Member), and Swartpunt is inner ramp (Spitzkopf Member).

Table 1.1 gives the latitude and longitude of all sample sites. Mixed carbonate and shale samples were taken over three field seasons (detailed below). Sampling was a collaborative effort between geochemists, field geologists and palaeontologists, and some of the site descriptions below are from the supplementary information of Wood et al. (2015). Fine grained, pristine looking samples from a range of carbonate lithologies were collected at 1-10m intervals, noting lithology and cyclic stratigraphy. Samples were trimmed of weathered edges and powdered to flour grade using a Tema or micromill for geochemical analysis. Samples from Zebra River were also drilled from thin section counterparts.

- **Field trip 1** (June, 2010) Rachel Wood, Charlie Hoffman and Tony Prave collected carbonates from Brak, Omkyk, Zwartmodder, Grens, Arasab and Swartpunt.
- **Field trip 2** (December 2011) Rachel Wood and Andrew Curtis collected siliciclastics from Brak, Omkyk and Zwartmodder.
- **Field trip 3** (June 2012) Rosalie Tostevin spent 2 weeks in Zebra River canyon and Driedoornvlagte sampling and describing reef morphology. Field assistance from Gerd Winterleitner (Royal Holloway)
- **Field trip 4** (December 2013) Rachel Wood, Rosalie Tostevin, Fred Bowyer, Amelia

Penny and Andrew Curtis spent two weeks in Zaris and Witputs sub-basins. Collected carbonates from Driedoornvlagte and pinnacle reefs, ecological samples, as well as siliciclastic samples from Zebra River, Arasab and Swartpunt.

Table 1.1: Latitude and longitude of sample sites in the Nama Basin

Section	*Latitude*	*Longitude*	*location*
Zaris sub-basin			
Brak	23°58'17.00"S	16°8'6.50"E	outer ramp
Driedoornvlagte	23°52'43.58"S	16°36'35.87"E	mid ramp pinnacle reef
Zebra River	24°31'9.54"S	16°15'8.08"E	mid ramp
Omkyk	24°48'19.00"S	16°13'45.00"E	mid to inner ramp
Zwartmodder	24°53'38.13"S	16°19'30.97"E	inner ramp
Witputs sub-basin			
Grens	27°10'34.48"S	16°21'58.51"E	inner ramp
Arasab	26°53'16.93"S	16°24'47.36"E	inner ramp
Pinnacle Reefs	27°27'35.46"S	16°34'16.96"E	mid ramp pinnacle reef
Swartpunt	27° 28'29.00"S	16°41'33.00"E	inner ramp

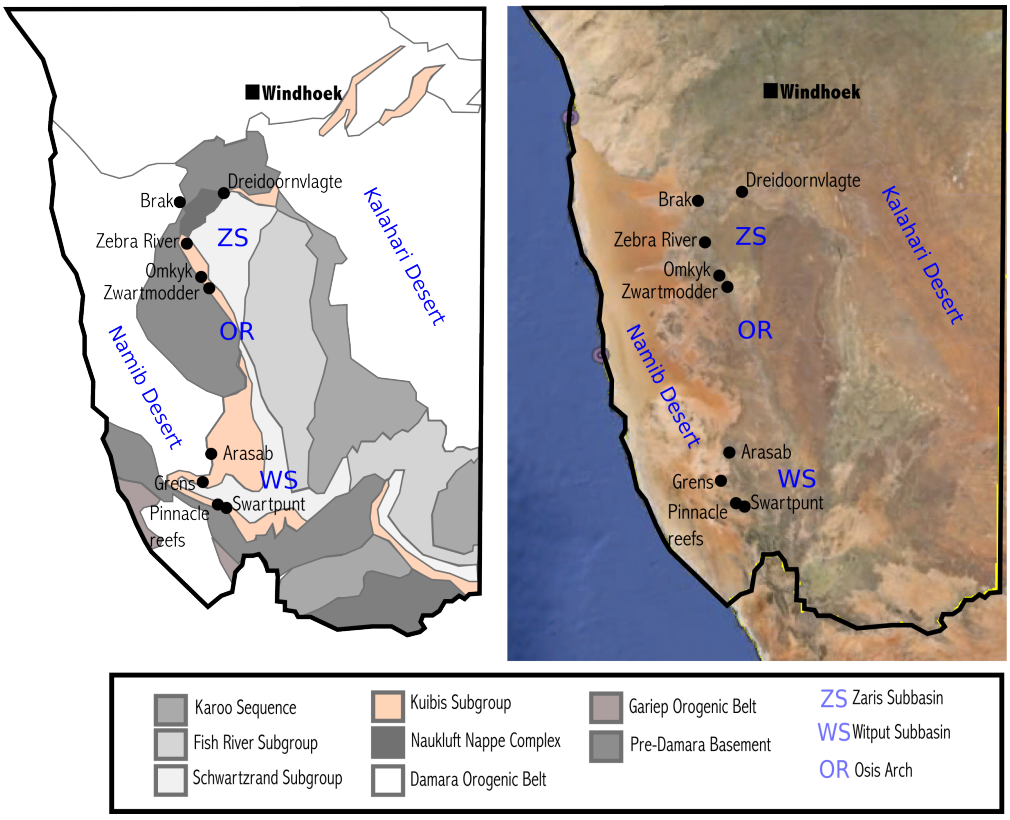

Figure 1.20: Location of sample sites in Nama Basin, against a geological sketch map adapted from Blanco et al. (2011) (left-hand side). Right-hand picture shows the same sample locations against an aerial photograph, taken from Google Earth. The major geological units dominate the landscape over large scales, bounded by the Kalahari desert to the east and the Namib desert to the west. Black outline is political border of Namibia.

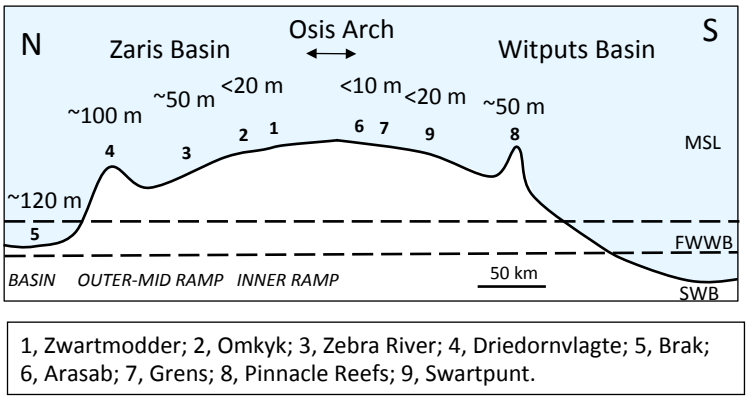

Figure 1.21: Relative position on shelf to basin transect of different sampling sites, from Wood et al. (2015). MSL = mean sea level, FWWB = fair weather wave base, SWB = storm wave base

1.6.1 The Zaris sub-basin

The Kuibis Subgroup, at the base of the Nama Group, was deposited between 550-546.9 Ma (Ries et al., 2009). Carbonate units in the Kuibis Subgroup are mostly contained within the lower and upper Omkyk member (OS1 and OS2, respectively) and the Hoogland member and are recognised across the northern Zaris sub-basin (Saylor et al., 1995, 1998; Germs, 1995).

The Omkyk Member consist of 10-20 meter-scale upward-coarsening, mid-inner ramp to shoreface cycles. The upper Omkyk member, OS2, contains a series of microbial reef systems terminating in grainstone dominated highstand sequence boundaries, representing sequential shallowing up cycles (Adams et al., 2005; Grotzinger et al., 2005).

The Hoogland member consists primarily of heterolithic interbeds that record transgressive-regressive depositional successions in mostly mid-inner ramp to middle shoreface settings, on a storm dominated carbonate ramp. The ramp displays facies gradients involving up-dip grainstones that pass down depositional dip into broad tracts of microbial laminites and finely laminated mudstones from both above and below the storm wave base (Dibenedetto and Grotzinger, 2005). The Hoogland member marks the final episode of significant carbonate deposition within the northern Nama Basin as growth was terminated due to a high influx of orogeny-derived clastics.

The Kuibis Subgroup was sampled at five localities from inner ramp to outer shelf in the Zaris sub-basin, detailed below. The Schwarzrand Subgroup in the Zaris sub-basin contains coarse-grained siliciclastics, and has not been sampled here.

1: Zwartmodder

Zwartmodder was deposited predominantly in shallow, proximal ramp settings. The section is dominated by dolomites at the base, shallowing to mainly limestone laminates, packstones and grainstones towards the top of the section. There are horizons of abundant calcified Metazoans, including small representatives of *Cloudina riemkeae* and *Namacalathus*, in the Upper Omkyk Member highstand systems tracts (HST) and lower Hoogland Member transgressive systems tracts (TST), and minor thrombolites in the Upper Omkyk Member HST.

2: Omkyk

Omkyk records a shallowing-up succession from outer-, to mid- to inner-ramp. At Omkyk, the lower part of the succession is dominated by slope turbidites, slumps and storm-beds and then shallows in the upper part to limestone grainstones showing tidal influence, together with limited thrombolites and abundant calcified Metazoans, including small representatives of *Cloudina riemkeae* and *Namacalathus*. Of note also is that large (up to 30 cm) horizontal burrow systems with spreite have been found in clastic TST in the Omkyk Member (Macdonald et al., 2014), suggesting formation by bilaterian organisms. Some shoaling cycles contain evidence for deposition in supra- to inter- tidal conditions, which may have been subjected to exposure and evaporitic conditions. There are horizons of abundant calcified Metazoans in the Upper Omkyk Member late TST only.

3: Zebra River

Zebra River was deposited in a mid-ramp setting. At Zebra River the Kanies member is a meter-scale package of coarse grained, cross-bedded sandstones and quartzites. OS1 is dominated by grainstones. In the TST of the upper Omkyk member thrombolite-stromatolite reefs nucleate, forming well defined and laterally continuous biostrome layers that can be traced for kilometers (figure 1.22). *Cloudina* and *Namacalathus* up to a centimeter in diameter can be found within thrombolite heads and lag beds within inter-reef shales. Localised clusters of larger *Namacalathus*, $<$35 mm, are found associated with thrombolites in the top half of the upper Omkyk member. Towards the top of the upper Omkyk the section shallows into grainstone dominated facies with subordinate shale horizons, containing thinner, discontinuous biostrome microbial reef systems. Shales flank individual bioherm reefs, forming inter-reef deposits, as well as lateral subordinate shales between grainstone horizons in highstand systems tracts. The Hoogland member contains storm dominated laminites and heterolithics, shallowing towards grainstone-dominated facies. Carbonate filled neptunian dykes indicate early cementation. Rip-up clasts, trough and hummocky cross-stratification, and association with inner shoreface facies (grainstones) suggest high-energy, storm dominated conditions.

Figure 1.22: Photo of typical section of OS1 and OS2 at Zebra River. Vertical scale is 160 m
1 - Laterally extensive orangy-brown microbial biostrome containing individual reef mounds, separated by inter-reef shales and marls.
2 - Termination of reef growth and a sequence of grainstones and subordinate shales
3 - Grainstone horizons become more closely spaced towards top of OS2
4 - A dolomitised Metazoan-packstone marking the Omkyk to Hoogland member transition

4: Driedoornvlagte

Driedornvlagte pinnacle reef build-up accumulated in a mid-ramp setting, during the TST of OS2. As the basement deepened the reef aggraded upwards to keep pace with relative sea level rise, and eventually drowneded and was enveloped by shales. The reef is underlain by shelf facies of Omkyk Sequence 1 (OS1), and consists of a lower unit dominated by stromatolitic reefs, overlain by a capping unit of mostly thrombolitic reef. Stratigraphically younger shales of the Urikos Member (Kuibis Subgroup) form the poorly-exposed plain south of the reef (figure 1.23 A). The buildup is 7km wide and 200m high. This thickness reflects the incised accommodation space associated with the deeper water setting compared to Zebra River reefs. The buildup is composed predominantly of thrombolitic limestones and grainstones, with minor dolomitisation. Calcified Metazoan fossils are abundant, particularly towards the top of the section where *Cloudina* and *Namapoikia* are found associated with thrombolites (figure 1.23 C). Large *Namacalathus* (up to 3cm in diameter) are also abundant lower in the section (figure 1.23 B). Fissure-inhabiting *Namapoikia*, first described from this section in Wood et al. (2002), are found towards the top of the section. Reef-building *Cloudina* (up to 8 mm diameter) are described for the first time in Penny et al. (2014) (appendix A).

5: Brak

Brak represents a distal, deep ramp setting that shallowed-up through time. The Brak section is dominated by fine-grained dolostones inter-bedded with thin sandstones, shales and quartzites indicative of deeper, outer ramp conditions, with shallow subtidal grainstones present only

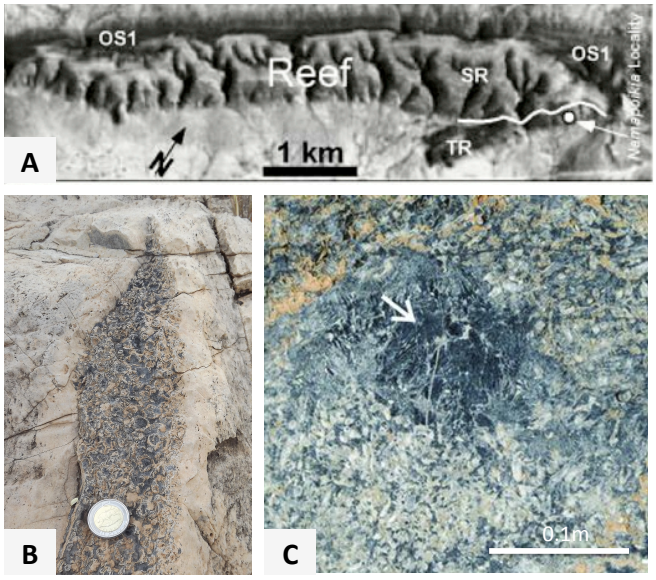

Figure 1.23: Morphology and ecology of Driedoornvlagte pinnacle reef
A - Landsat image showing outcrop expression of Driedoornvlagte reef complex. Outcrop dips 40 degrees to the south. Reef is underlain by shelf facies of Omkyk Sequence 1 (OS1), and consists of a lower unit dominated by stromatolitic reefs (SR), overlain by a capping unit of mostly thrombolitic reef (TR). Stratigraphically younger shales of the Urikos Member (Kuibis Subgroup) form the poorly-exposed plain south of the reef. The *Namapoikia* locality from Wood et al. (2002) is marked. Figure from Penny et al. (2014)
B - Large *Namacalathus* in lenses on S face of reef
C - *Cloudina* forming coalescing thickets enclosing a primary reef cavity, from Penny et al. (2014).

towards the very top of the section. There are no Metazoans or thrombolites present, but some stromatolites in the Kanies Member.

1.6.2 The Witputs sub-basin

In the Witputs sub-basin, the Kanies Member is overlain by the carbonate-dominated Mara Member. The upper Kuibis Subgroup is represented by siliciclastics of the Kliphoek Member and the overlying carbonate Mooifontein Member of the Zaris Formation. The sandstones were interpreted by Saylor et al. (1995) as upper-shoreface, delta- or tide-influenced deposits that prograded across the underlying carbonate platform during sealevel lowstand and were trapped during regional transgression of the craton. The upper part of the Kuibis Subgroup forms an extensive carbonate platform that maintains a relatively constant thickness (30–40 m) over the Witputs sub-basin, pinching out near the Osis Ridge. Saylor et al. (1998) commented that

little change in the thickness of these facies suggests deposition across a broad region of low relief during flooding of the craton. The Mooifontein Member is a a thin-bedded limestone interpreted as storm reworking. South of the Osis Ridge, the Kuibis Subgroup is truncated by an unconformity with deep canyon cutting into the Mooifontein Member and filled with conglomerate.

The overlying Schwarzrand Subgroup of the Witputs sub-basin reaches a maximum thickness of 1000m, and consists of clastic and carbonate in the lower part (Nudaus and overlying Nasep Member of the Urusis Formation), a carbonate-dominated middle-part (comprising the Huns, Feldschuhhorn and Spitzkopf Members) and an upper conglomeratic unit that infills incised valleys (Nomtsas Formation). The top of the Huns member is a flooding surface, which may also be coincident with a sequence boundary (Saylor et al., 1995), on which pinnacle reefs initiated on distal parts of the platform. The reefs are enveloped within siltstones of the Feldschuhhorn Member. Distal parts of the Spitzkopf Member are truncated and incised by valleys infilled with the Nomtsas Formation.

The Kuibis Subgroup has been sampled at two localities in the Witputs sub-basin (Arasab and Grens). The upper carbonate-dominated part of the Schwarzrand Subgroup has been sampled at two further localities (Swartpunt and Pinnacle Reefs), detailed below.

6: Arasab

Arasab was deposited in shallow, proximal ramp settings. The base of the section is predominantly composed of limestone units (often displaying evaporitic fabrics) punctuated by thin shale interbeds, transitioning to thick quartzite beds of the lower Kliphoek Member, followed by interbedded shale and limestone of the upper Kliphoek (/Aar) Member (figure 1.24 A). The section is capped by a thick limestone unit of the Mooifontein Member containing distinct oolite bands in the lower reaches. Though the lower Kliphoek quartzite and Aar Member units are known to contain abundant soft-bodied Metazoan fossils in other localities, none have been noted in the Arasab section.

7: Grens

Grens includes all members of the Dabies Formation of the Kuibis Subgroup. Conglomerates, sandstones and shales dominate the lowermost 20m, defining the Kanies Member at Grens, with

overlying facies of the Mara Member predominantly composed of limestone with shale interbeds clearly defining patterns of shoaling cyclicity (further evidence from evaporitic fabrics). The Mara Member is markedly thicker at Grens than Arasab, indicative of increasing accommodation space with distance south. Finally the Kliphoek Member is composed of limestone with small layers of quartzite, and the capping Aar Member consists of shale, limestone, and dolo-cemented quartzite. In-situ assemblages of the Ediacaran fossil *Nemiana* are abundant.

8: Pinnacle Reefs

The Pinnacle Reefs at Swartkloofberg Farm, southern Namibia, were deposited in a mid-ramp setting. They initiated on the flooded surface of the Huns Platform. At the base the reef carbonate interfingers with siltstones and shales, but the reefs then grew up to 40 m topographic relief above the sea floor (figure 1.24 C). Thrombolites are associated with abundant in-situ *Namacalathus*. After termination of reef growth, they were enveloped by the shales of the Feldschuhorn Member, of which they now form a part.

9: Swartpunt

Swartpunt was deposited in an inner ramp setting within the Schwarzrand Subgroup, and shallows up section (figure 1.24 B). The base of the section is dominated by laminated limestone containing *Namacalathus* and other bioclastic material, as well as microbialites, some of which have a 'leopardskin' texture. Distal turbidites contain intermittent and small burrows. Broken fossil lags and rip-up clasts suggest an outer ramp setting above storm wave base. Two ash beds also lie at this level within the succession. Overlying the limestones are beds of shale and quartzite, containing burrows and soft-bodied fossils (Figure 1.25). These in turn give way to more laminated limestones containing small ($<$5 mm) *Cloudina* and *Namacalathus*.

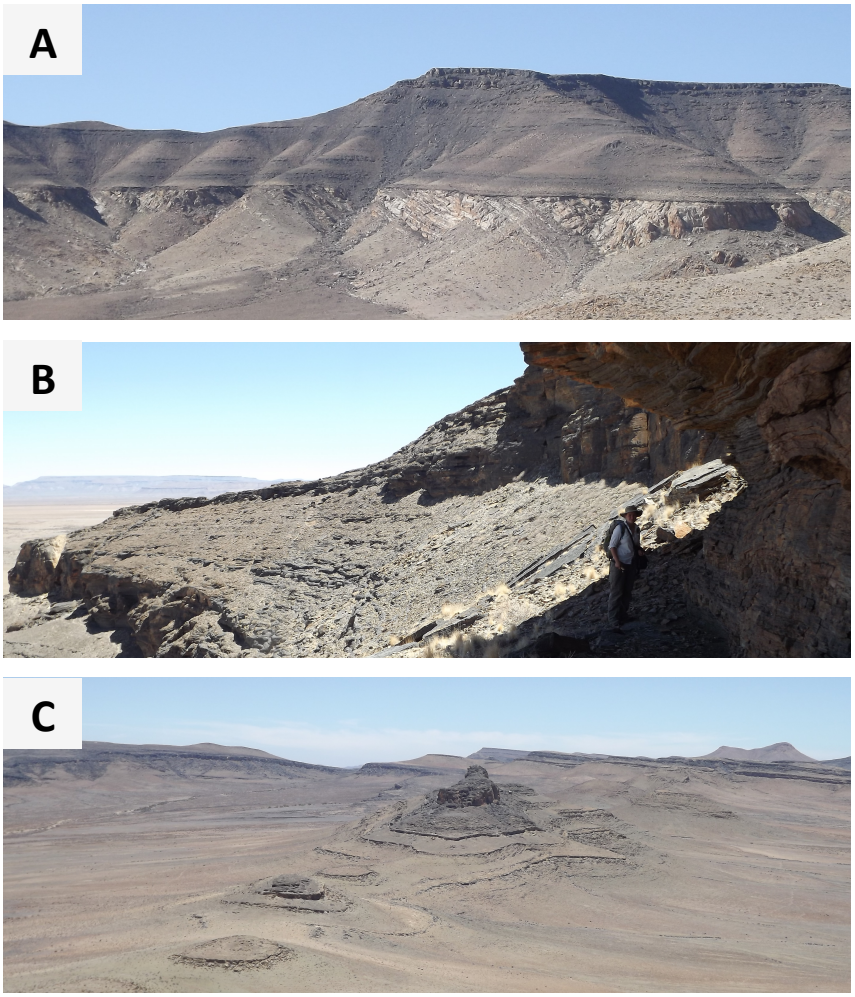

Figure 1.24: Outcrops from the Witputs sub-basin.
A Arasab section, part of the Kuibis sub-group.
B Swartpunt, part of the Schwartzrand Subgroup, taken from half way up outcrop looking NE. Amelia for scale.
C Pinnacle Reefs of the Schwartzrand Subgroup. Taken from Swartpunt looking northwest.

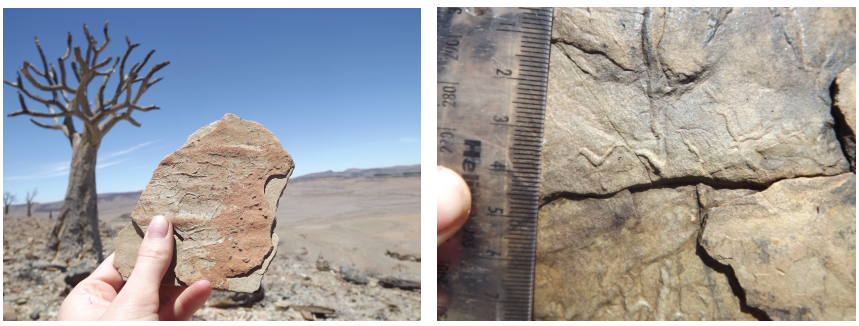

Figure 1.25: Evidence for bioturbation at Swartpunt. Right hand photo shows complex trace fossils from Treptichnus family

1.7 Contributions

The sample collection described in section 1.6 and the Fe-speciation, TOC, carbon isotope data presented within chapter 2 were collected as part of a wide collaborative effort led by Rachel Wood. Data presented in chapter 2 focuses on Zebra River, as the sample collection and analyses were all undertaken as part of this thesis. However, Zebra River can only be fully interpreted in the context of the field observations and data from across the Nama Basin, and this was collected partly for this study, but contains many contributions from others, listed below in table 1.2.

The method development work in chapter 3 was undertaken as part of this thesis. Samples used for leaching experiments came partly from the Nama Basin, collected by those listed in 1.2, with additional modern samples from Matthew Clarkson (see Clarkson et al. 2014 for details), and from Dalian in North China, collected by Steven Robinson and Graham Shields.

The rare earth element data presented in chapter 4 was collected as part of this thesis, but using samples from across the Nama Basin, collected by those listed in table 1.2, and the interpretation relies on the accompanying Fe-speciation data that was also collected as part of a collaboration with others.

The model and discussion in chapter 5 was developed as part of this thesis. However, the model relies in part on previously unpublished multiple sulfur isotope data from modern marine sulfate. The seawater samples were donated by Karen Casciotti and Jim K Bishop, and the analyses were made, but not interpreted, during a 2010 Master's thesis by R Tostevin at the University of Cambridge.

The data in 6 was collected as part of this thesis. Samples used are from Zebra River and were also collected as part of this thesis. The method used was developed by Tianchen He.

Relevant support, supervision and helpful conversations, as well as the above information, are noted at the start of each chapter to clarify contributions. Images or text taken from the work of others are acknowledged where appropriate.

Table 1.2: Author contributions to datasets presented in chapters 2 and 3

Sample site	Collection	Crushing	TOC	$\delta^{13}C$	Fe spec	Fe/Al	Major elements & REE
Zaris sub-basin							
Brak	FT1&2	JL	RW&FB	JL	MC	RG	RT
Driedoornvlagte	FT4	AP	RT	N/A	RT&FB	RG	RT
Zebra River	FT3	RT	RT	RT	RT&FB	RT	RT
Omkyk	FT1&2	JL	RT	JL	JL	RG	RT
Zwartmodder	FT1&2	JL	RT	JL	MC	RG	RT
Witputs sub-basin							
Grens	FT1	JL	RT	JL	FB&RT	RG	RT
Arasab	FT1&4	FB&JL	RT	JL	MC&FB&RT	RG	RT
Pinnacle Reef	FT4	AP	RT	AP	FB&RT	RG	
Swartpunt	FT1&4	AP&JL	RT	JL	MC&RT&FB	RG	RT

MC - Matthew Clarkson (Edinburgh University)
RW - Rachel Wood (Edinburgh University)
JL - James Lyne (Edinburghmetal University)
AP - Amelia Penny (Edinburgh University)
RT - Rosalie Tostevin
RG - Romain Guilbaud
FB - Fred Bowyer (Edinburgh Univeristy)
FT1 - Field trip 1 (June 2010) RW, Anthony Prave, Charlie Hoffman
FT2 - Field trip 2 (December 2011) RW and Andrew Curtis
FT3 - Field trip 2 (June 2012) Rosalie Tostevin
FT4 - Field trip 3 (December 2013) RW, AP, RT, FB and Andrew Curtis
All Fe-speciation data collected in collaboration with Romain Guilbaud and Simon Poulton at the University of Leeds.

1.8 Thesis Aims

The aim of this thesis is to enhance our understanding of geochemical proxies through method improvements, constraining major fluxes in modern geochemical cycles and inter-proxy calibrations, and then to combine these proxies to reconstruct redox conditions in the terminal Ediacaran during the emergence of complex animal life.

- Constrain the gross burial flux of pyrite in modern marine sediments worldwide.

- Improve the leaching method for extracting rare earth elements preserved in carbonates, a proxy that has the potential to preserve high-resolution redox information in shallow marine carbonate settings.

- Revisit reports of 'superheavy pyrite' in the Nama Group

- Compare and calibrate two distinct redox proxies, Fe-speciation and Ce anomalies, in carbonate settings.

- Reconstruct redox conditions across nine sites of different water depths in the terminal Ediacaran Nama Group using a multi-proxy high resolution approach, alongside biological logs, to evaluate the hypothesis that redox exerted a control on late Precambrian ecosystems.

1.9 Thesis outline

The results within this thesis are presented as a series of chapters, some of which have been submitted, or are due to be submitted, as publications.

Chapter 2 presents carbon isotope, total organic carbon and Fe-speciation data for carbonate and shale samples from Zebra River, the Nama Group. The data from Zebra River is interpreted in wider context alongside similar data from 8 other sections across the Nama Group, to present a detailed temporal and spatial reconstruction of redox for the Nama Basin. Through the use of traditional redox proxies we lay the ground work for understanding redox in this critical time period of Earth history.

Forms part of an article published in Precambrian research: *Wood, R. A., Poulton, S.W., Prave, A.R., Hoffmann, K-H., Clarkson, M.O., Guilbaud, R., Lyne, J.W., Tostevin, R., Bowyer, F., Penny, A.M., Curtis, A., and Kasemann, S.A., Dynamic redox conditions control late Ediacaran ecosystems in the Nama Group, Namibia*

Chapter 3 tests the utility of cerium anomalies as a redox proxy in carbonates, through the refinement of leaching procedures and calibration in modern samples. This investigation recommends an optimal leaching procedure to be used for obtaining a pure seawater signal in carbonates, and as such acts as the groundwork for chapter 4.

To submit as: *Tostevin, R., Shields-Zhou, G. A., Tarbuck, G. M., He, T., and Clarkson, M.O Effective use of Ce anomalies as a redox proxy in carbonate settings*

Chapter 4 applies the method developed in chapter 3 to the Nama Group, to assess redox across nine sites in the Nama Basin. We combine Ce anomaly and Fe-speciation data in carbonates for the first time, and identify a progressive spectrum of redox environments across two sub-basins.

To submit as: *Tostevin, R., Wood R. A., Shields-Zhou G. A., Poulton, S.W., Guilbaud, R., Bowyer, F., Penny, A.M., He, T., Curtis, A., Prave. A. R., Hoffmann, K-H., and Clarkson, M.O. Manganous oceanic conditions limited the distribution of early animal life.*

Chapter 5 uses sulfur isotope data from modern marine sulfate to explore the fraction of pyrite

burial in modern sediments with a box-model.

Published in Earth and Planetary Science Letters as: *Tostevin, R., Turchyn, A. V., Farquhar, J., Johnston D. T., Eldridge, D. L., Bishop, J. K. B., McIlvin, M., Multiple sulfur isotope constraints on the modern sulfur cycle*

Chapter 6 uses sulfur isotope data from paired sulfate-pyrite to explore the sulfate concentration and sulfur cycling in the Nama Basin, and compare with redox information from chapters 2 and 4.

To submit to as: *Tostevin, R., He, T., Shields-Zhou, G., Turchyn, A. V., Antler, G., The sulfur cycle in the terminal Neoproterozoic - new insights from the Nama Group, Namibia*

Chapter 7 is the synthesis of these individual investigations, and seeks to highlight the questions raised in this thesis. Conclusions and concepts for further work are also included in this chapter.

References

Adams, E. W., Grotzinger, J. P., Watters, W. A., Schroder, S., McCormick, D. S., Al-Siyabi, H. A., 2005. Digital characterization of thrombolite-stromatolite reef distribution in a carbonate ramp system (terminal proterozoic, nama group, namibia). AAPG Bulletin 89 (10), 1293–1318.

Aller, R., 1990. Bioturbation and manganese cycling in hemipelagic sediments. Philosophical Transactions of the Royal Society of London. Series A, Mathematical and Physical Sciences 331 (1616), 51–68.

Aller, R. C., 1994. Bioturbation and remineralization of sedimentary organic matter: effects of redox oscillation. Chemical Geology 114 (3), 331–345.

Amthor, J. E., Grotzinger, J. P., Schroder, S., Bowring, S. A., Ramezani, J., Martin, M. W., Matter, A., May 2003. Extinction of Cloudina and Namacalathus at the Precambrian-Cambrian boundary in oman. Geology 31, 431.

Anbar, A. D., Knoll, A. H., Aug. 2002. Proterozoic ocean chemistry and evolution: A bioinorganic bridge? Science 297, 1137–1143.

Banner, J. L., Hanson, G. N., Meyers, W. J., 1988. Rare earth element and Nd isotopic variations in regionally extensive dolomites from the Burlington-Keokuk formation (Mississippian): Implications for REE mobility during carbonate diagenesis. Journal of Sedimentary Research 58 (3).

Bau, M., 1999. Scavenging of dissolved yttrium and rare earths by precipitating iron oxyhydroxide: experimental evidence for Ce oxidation, Y-Ho fractionation, and lanthanide tetrad effect. Geochimica et Cosmochimica Acta 63 (1), 67–77.

Bau, M., Dulski, P., 1996. Distribution of yttrium and rare-earth elements in the Penge and Kuruman iron-formations, Transvaal Supergroup, South Africa. Precambrian Research 79 (1), 37–55.

Bau, M., Dulski, P., 1999. Comparing yttrium and rare earths in hydrothermal fluids from the mid-atlantic ridge: implications for Y and REE behaviour during near-vent mixing and for the Y/Ho ratio of proterozoic seawater. Chemical Geology 155 (1), 77–90.

Bau, M., Koschinsky, A., 2009. Oxidative scavenging of cerium on hydrous Fe oxide: evidence from the distribution of rare earth elements and yttrium between Fe oxides and Mn oxides in hydrogenetic ferromanganese crusts. Geochemical Journal 43 (1), 37–47.

Bau, M., Moller, P., Dulski, P., Feb. 1997. Yttrium and lanthanides in eastern Mediterranean seawater and their fractionation during redox-cycling. Marine Chemistry 56 (12), 123–131.

Bau, M., Schmidt, K., Koschinsky, A., Hein, J., Kuhn, T., Usui, A., 2014. Discriminating between different genetic types of marine ferro-manganese crusts and nodules based on rare earth elements and yttrium. Chemical Geology 381, 1–9.

Bekker, A., Holland, H., Wang, P.-L., Rumble, D., Stein, H., Hannah, J., Coetzee, L., Beukes, N., 2004. Dating the rise of atmospheric oxygen. Nature 427 (6970), 117–120.

Bengston, S., 2004. Early skeletal fossils. Paleontological Society Papers 10 (10), 67–77.

Bengtson, S., Morris, S. C., 1992. Early radiation of biomineralizing phyla. In: Origin and early evolution of the Metazoa. Springer, pp. 447–481.

Bergman, N. M., Lenton, T. M., Watson, A. J., 2004. COPSE: a new model of biogeochemical cycling over Phanerozoic time. American Journal of Science 304 (5), 397–437.

Berner, R. A., Mar. 1987. Models for carbon and sulfur cycles and atmospheric oxygen; application to paleozoic geologic history. American Journal of Science 287 (3), 177–196.

Berner, R. A., Canfield, D. E., Apr. 1989. A new model for atmospheric oxygen over Phanerozoic time. American Journal of Science 289 (4), 333–361, PMID: 11539776.

Berry, W. B., Wilde, P., 1978. Progressive ventilation of the oceans; an explanation for the distribution of the lower Paleozoic black shales. American Journal of Science 278 (3), 257–275.

Bertram, C., Elderfield, H., 1993. The geochemical balance of the rare earth elements and neodymium isotopes in the oceans. Geochimica et Cosmochimica Acta 57 (9), 1957–1986.

Bishop, J. K., 2009. Autonomous observations of the ocean biological carbon pump. Lawrence Berkeley National Laboratory.

Bjerrum, C. J., Canfield, D. E., Apr. 2011. Towards a quantitative understanding of the late Neoproterozoic carbon cycle. Proceedings of the National Academy of Sciences 108 (14), 5542 –5547.

Blanco, G., Germs, G., Rajesh, H., Chemale Jr., F., Dussin, I., Justino, D., May 2011. Provenance and paleogeography of the Nama Group (Ediacaran to early Palaeozoic, Namibia): Petrography, geochemistry and U-Pb detrital zircon geochronology. Precambrian Research 187 (12), 15–32.

Bodin, S., Godet, A., Westermann, S., Follmi, K. B., Jul. 2013. Secular change in northwestern Tethyan water-mass oxygenation during the late Hauterivian-early Aptian. Earth and Planetary Science Letters 374, 121–131.

Bottomley, D. J., Veizer, J., Nielsen, H., Moczydlowska, M., 1992. Isotopic composition of disseminated sulfur in precambrian sedimentary rocks. Geochimica et Cosmochimica Acta 56 (8), 3311–3322.

Botz, R., Pokojski, H.-D., Schmitt, M., Thomm, M., 1996. Carbon isotope fractionation during bacterial methanogenesis by CO_2 reduction. Organic Geochemistry 25 (3), 255–262.

Boyle, R., Dahl, T. W., Dale, A. W., Shields-Zhou, G., Zhu, M.-y., Brasier, M., Canfield, D. E., Lenton, T., 2014. Stabilization of the coupled oxygen and phosphorus cycles by the evolution of bioturbation. Nature Geoscience 7 (9), 671–676.

REFERENCES

Boyle, R. A., Lenton, T. M., Williams, H. T., 2007. Neoproterozoic 'snowball Earth' glaciations and the evolution of altruism. Geobiology 5 (4), 337–349.

Braissant, O., Decho, a. W., Dupraz, C., Glunk, C., Przekop, K. M., Visscher, P. T., Dec. 2007. Exopolymeric substances of sulfatereducing bacteria: Interactions with calcium at alkaline pH and implication for formation of carbonate minerals. Geobiology 5 (4), 401–411.

Bristow, T. F., Kennedy, M. J., 2008. Carbon isotope excursions and the oxidant budget of the Ediacaran atmosphere and ocean. Geology 36 (11), 863–866.

Budd, G. E., 2008. The earliest fossil record of the animals and its significance. Philosophical Transactions of the Royal Society B: Biological Sciences 363 (1496), 1425–1434.

Buick, R., Dunlop, J., Groves, D., 1981. Stromatolite recognition in ancient rocks: an appraisal of irregularly laminated structures in an early archaean chert-barite unit from north pole, western australia. Alcheringa 5 (3), 161–181.

Burns, B. P., Goh, F., Allen, M., Neilan, B. A., Oct. 2004. Microbial diversity of extant stromatolites in the hypersaline marine environment of shark bay, australia. Environmental Microbiology 6 (10), 1096–1101.

Burns, S. J., Matter, A., 1993. Carbon isotopic record of the latest Proterozoic from Oman. Eclogae Geologicae Helvetiae.

Butterfield, N. J., 2000. Bangiomorpha pubescens n. gen., n. sp.: implications for the evolution of sex, multicellularity, and the mesoproterozoic/neoproterozoic radiation of eukaryotes. Paleobiology 26 (3), 386–404.

Butterfield, N. J., jan 2009. Oxygen, animals and oceanic ventilation: an alternative view. Geobiology 7 (1), 1–7.

Byrne, R. H., Kim, K.-H., Oct. 1990. Rare earth element scavenging in seawater. Geochimica et Cosmochimica Acta 54 (10), 2645–2656.

Byrne, R. H., Liu, X., Schijf, J., sep 1996. The influence of phosphate coprecipitation on rare earth distributions in natural waters. Geochimica et Cosmochimica Acta 60 (17), 3341–3346.

Calver, C. R., 2000. Isotope stratigraphy of the Ediacarian (Neoproterozoic iii) of the Adelaide Rift Complex, Australia, and the overprint of water column stratification. Precambrian Research 100 (1), 121–150.

Canfield, D., Thamdrup, B., 2009. Towards a consistent classification scheme for geochemical environments, or, why we wish the term suboxicwould go away. Geobiology 7 (4), 385–392.

Canfield, D. E., 1994. Factors influencing organic carbon preservation in marine sediments. Chemical Geology 114 (3), 315–329.

Canfield, D. E., Dec. 1998. A new model for Proterozoic ocean chemistry. Nature 396 (6710), 450–453.

Canfield, D. E., 2004. The evolution of the earth surface sulfur reservoir. American Journal of Science 304 (10), 839–861.

Canfield, D. E., May 2013. Sulfur isotopes in coal constrain the evolution of the phanerozoic sulfur cycle. Proceedings of the National Academy of Sciences of the United States of America 110 (21), 8443–8446, PMID: 23650346.

Canfield, D. E., Farquhar, J., may 2009. Animal evolution, bioturbation, and the sulfate concentration of the oceans. Proceedings of the National Academy of Sciences of the United States of America 106 (20), 8123–8127, PMID: 19451639 PMCID: PMC2688866.

Canfield, D. E., Lyons, T. W., Raiswell, R., 1996. A model for iron deposition to euxinic Black Sea sediments. American Journal of Science 296 (7), 818–834.

Canfield, D. E., Poulton, S. W., Knoll, A. H., Narbonne, G. M., Ross, G., Goldberg, T., Strauss, H., 2008. Ferruginous conditions dominated later Neoproterozoic deep-water chemistry. Science 321 (5891), 949 –952.

Canfield, D. E., Poulton, S. W., Narbonne, G. M., Jan. 2007. Late-Neoproterozoic deep-ocean oxygenation and the rise of animal life. Science 315 (5808), 92 –95.

Canfield, D. E., Raiswell, R., Westrich, J. T., Reaves, C. M., Berner, R. A., 1986. The use of chromium reduction in the analysis of reduced inorganic sulfur in sediments and shales. Chemical Geology 54 (1), 149–155.

Canfield, D. E., Stewart, F. J., Thamdrup, B., Brabandere, L. D., Dalsgaard, T., Delong, E. F., Revsbech, N. P., Ulloa, O., Dec. 2010. A cryptic sulfur cycle in oxygen minimum zone waters off the Chilean coast. Science 330 (6009), 1375–1378.

Carbone, C., Narbonne, G. M., 2014. When life got smart: the evolution of behavioral complexity through the Ediacaran and early Cambrian of NW canada. Journal of Paleontology 88 (2), 309–330.

Catling, D. C., Zahnle, K. J., McKay, C. P., 2001. Biogenic methane, hydrogen escape, and the irreversible oxidation of early Earth. Science 293 (5531), 839–843.

Chambers, L., Trudinger, P., 1979. Microbiological fractionation of stable sulfur isotopes: a review and critique. Geomicrobiology Journal 1 (3), 249–293.

Chen, Z., Zhou, C., Meyer, M., Xiang, K., Schiffbauer, J. D., Yuan, X., Xiao, S., 2013. Trace fossil evidence for Ediacaran bilaterian animals with complex behaviors. Precambrian Research 224, 690–701.

Chen, Z., Zhou, C., Xiao, S., Wang, W., Guan, C., Hua, H., Yuan, X., 2014. New ediacara fossils preserved in marine limestone and their ecological implications. Scientific reports 4.

Clarkson, M. O., Poulton, S. W., Guilbaud, R., Wood, R. A., 2014. Assessing the utility of Fe/Al and Fe-speciation to record water column redox conditions in carbonate-rich sediments. Chemical Geology.

Cohen, B. L., Aug. 2005. Not armour, but biomechanics, ecological opportunity and increased fecundity as keys to the origin and expansion of the mineralized benthic metazoan fauna. Biological Journal of the Linnean Society 85 (4), 483–490.

Condon, D., Zhu, M., Bowring, S., Wang, W., Yang, A., Jin, Y., 2005. U-Pb ages from the Neoproterozoic Doushantuo Formation, China. Science 308 (5718), 95–98.

Cortijo, I., Marti Mus, M., Jensen, S., Palacios, T., 2010. A new species of Cloudina from the terminal Ediacaran of Spain. Precambrian Research 176 (1), 1–10.

Crowe, S. A., Døssing, L. N., Beukes, N. J., Bau, M., Kruger, S. J., Frei, R., Canfield, D. E., 2013. Atmospheric oxygenation three billion years ago. Nature 501 (7468), 535–538.

REFERENCES

Crowe, S. A., Jones, C., Katsev, S., Magen, C., O'Neill, A. H., Sturm, A., Canfield, D. E., Haffner, G. D., Mucci, A., Sundby, B., et al., 2008. Photoferrotrophs thrive in an Archean Ocean analogue. Proceedings of the National Academy of Sciences 105 (41), 15938–15943.

Dahl, T. W., Canfield, D. E., Rosing, M. T., Frei, R. E., Gordon, G. W., Knoll, A. H., Anbar, A. D., 2011. Molybdenum evidence for expansive sulfidic water masses in 750Ma oceans. Earth and Planetary Science Letters 311 (3), 264–274.

Dahl, T. W., Hammarlund, E. U., Anbar, A. D., Bond, D. P., Gill, B. C., Gordon, G. W., Knoll, A. H., Nielsen, A. T., Schovsbo, N. H., Canfield, D. E., 2010. Devonian rise in atmospheric oxygen correlated to the radiations of terrestrial plants and large predatory fish. Proceedings of the National Academy of Sciences 107 (42), 17911–17915.

Daly, R. A., 1907. The limeless ocean of pre-cambrian time. American Journal of Science 134, 93–115.

Danovaro, R., Dell'Anno, A., Pusceddu, A., Gambi, C., Heiner, I., Kristensen, R. M., 2010. The first metazoa living in permanently anoxic conditions. BMC biology 8 (1), 30.

Darwin, C., 1859. On the origins of species by means of natural selection. London: Murray.

De Baar, H. J., German, C. R., Elderfield, H., van Gaans, P., May 1988. Rare earth element distributions in anoxic waters of the Cariaco Trench. Geochimica et Cosmochimica Acta 52 (5), 1203–1219.

De Carlo, E. H., Green, W. J., Apr. 2002. Rare earth elements in the water column of Lake Vanda, McMurdo Dry Valleys, Antarctica. Geochimica et Cosmochimica Acta 66 (8), 1323–1333.

De Carlo, E. R., 2000. Rare earth element fractionation in hydrogenetic Fe-Mn crusts: The influence of carbonate complexation and phosphatization on Sm/Yb ratios. Society for Sedimentary Geology.

Degens, E., 1969. Biogeochemistry of stable carbon isotopes. In: Organic geochemistry. Springer, pp. 304–329.

Degens, F. T., Kazmierczak, J., Ittekkot, V., 1985. Cellular response to Ca^{2+} stress and its geological implications. Palaeontologica 30, 115–135.

den Camp, O., Kartal, B., Guven, D., Van Niftrik, L., Haaijer, S., Van Der Star, W., Van De Pas-Schoonen, K., Cabezas, A., Ying, Z., Schmid, M., et al., 2006. Global impact and application of the anaerobic ammonium-oxidizing(anammox) bacteria. Biochemical Society Transactions 34 (1), 174–178.

Derry, L. A., 2010. A burial diagenesis origin for the Ediacaran Shuram-Wonoka carbon isotope anomaly. Earth and Planetary Science Letters 294 (1), 152–162.

Derry, L. A., Kaufman, A. J., Jacobsen, S. B., 1992. Sedimentary cycling and environmental change in the Late Proterozoic: evidence from stable and radiogenic isotopes. Geochimica et Cosmochimica Acta 56 (3), 1317–1329.

Detmers, J., Bruchert, V., Habicht, K. S., Kuever, J., 2001. Diversity of sulfur isotope fractionations by sulfate-reducing prokaryotes. Applied and Environmental Microbiology 67 (2), 888–894.

Dibenedetto, S., Grotzinger, J., 2005. Geomorphic evolution of a storm-dominated carbonate ramp (c. 549 ma), Nama Group, Namibia. Geological Magazine 142 (5), 583 –604.

Dobson, D. P., Brodholt, J. P., 2005. Subducted banded iron formations as a source of ultralow-velocity zones at the core–mantle boundary. Nature 434 (7031), 371–374.

Droser, M. L., Jensen, S., Gehling, J. G., 2002. Trace fossils and substrates of the terminal Proterozoic–Cambrian transition: implications for the record of early bilaterians and sediment mixing. Proceedings of the National Academy of Sciences 99 (20), 12572–12576.

Duan, Y., Severmann, S., Anbar, A. D., Lyons, T. W., Gordon, G. W., Sageman, B. B., 2010. Isotopic evidence for Fe cycling and repartitioning in ancient oxygen-deficient settings: Examples from black shales of the mid-to-late Devonian Appalachian basin. Earth and Planetary Science Letters 290 (3), 244–253.

Dupraz, C., Visscher, P. T., Sep. 2005. Microbial lithification in marine stromatolites and hypersaline mats. Trends in Microbiology 13 (9), 429–438.

Edmonds, H. N., German, C. R., 2004. Particle geochemistry in the rainbow hydrothermal plume, mid-atlantic ridge. Geochimica et Cosmochimica Acta 68 (4), 759–772.

El Albani, A., Bengtson, S., Canfield, D. E., Bekker, A., Macchiarelli, R., Mazurier, A., Hammarlund, E. U., Boulvais, P., Dupuy, J.-J., Fontaine, C., et al., 2010. Large colonial organisms with coordinated growth in oxygenated environments 2.1 Gyr ago. Nature 466 (7302), 100–104.

Erwin, D. H., Laflamme, M., Tweedt, S. M., Sperling, E. A., Pisani, D., Peterson, K. J., Nov. 2011. The Cambrian conundrum: Early divergence and later ecological success in the early history of animals. Science 334 (6059), 1091–1097, PMID: 22116879.

Farquhar, J., Bao, H., Thiemens, M., 2000. Atmospheric influence of earth's earliest sulfur cycle. Science 289 (5480), 756 –758.

Fike, D. A., Grotzinger, J. P., Pratt, L. M., Summons, R. E., Dec. 2006. Oxidation of the Ediacaran Ocean. Nature 444 (7120), 744–747.

Fowler, S., Hamilton, T., Peinert, R., La Rosa, J., Teyssie, J., 1992. The vertical flux of rare earth elements in the northwestern Mediterranean. In: EROS 2000 (European River Ocean System): Proceedings of the Third Workshop on the North-West Mediterranean Sea. pp. 401–412.

Frei, R., Gaucher, C., Dssing, L. N., Sial, A. N., Dec. 2011. Chromium isotopes in carbonates – A tracer for climate change and for reconstructing the redox state of ancient seawater. Earth and Planetary Science Letters 312 (12), 114–125.

Garrels, R. M., Lerman, A., Nov. 1984. Coupling of the sedimentary sulfur and carbon cycles; an improved model. American Journal of Science 284 (9), 989–1007.

Gehling, J. G., Feb. 1999. Microbial mats in terminal Proterozoic siliciclastics; Ediacaran death masks. PALAIOS 14 (1), 40 –57.

Gehling, J. G., Narbonne, G. M., Anderson, M. M., 2000. The first named Ediacaran body fossil, Aspidella terranovica. Palaeontology 43 (3), 427–456.

Gehling, J. G., Rigby, J. K., 1996. Long expected sponges from the Neoproterozoic Ediacara fauna of South Australia. Journal of Paleontology, 185–195.

German, C. R., Elderfield, H., 1990. Application of the Ce anomaly as a paleoredox indicator: The ground rules. Paleoceanography 5 (5), P. 823.

REFERENCES

German, C. R., Holliday, B. P., Elderfield, H., Dec. 1991. Redox cycling of rare earth elements in the suboxic zone of the Black Sea. Geochimica et Cosmochimica Acta 55 (12), 3553–3558.

Germs, G., 1983. Implications of a sedimentary facies and depositional environmental analysis of the Nama Group in South West Africa/Namibia. Geological Society of South Africa Special Publication II, 89–114.

Germs, G. J., Knoll, A. H., Vidal, G., 1986. Latest Proterozoic microfossils from the Nama Group, Namibia (South West Africa). Precambrian Research 32 (1), 45–62.

Germs, G. J. B., Oct. 1972. New shelly fossils from Nama Group, South West Africa. American Journal of Science 272 (8), 752–761.

Germs, G. J. B., may 1974. The Nama Group in South West Africa and its relationship to the pan-african geosyncline. The Journal of Geology 82 (3), 301–317.

Germs, G. J. B., May 1995. The neoproterozoic of southwestern Africa, with emphasis on platform stratigraphy and paleontology. Precambrian Research 73 (14), 137–151.

Gibson, R., Atkinson, R., 2003. Oxygen minimum zone benthos: adaptation and community response to hypoxia. Oceanography and Marine Biology: An Annual Review 41, 1–45.

Gill, B. C., Lyons, T. W., Young, S. A., Kump, L. R., Knoll, A. H., Saltzman, M. R., 2011. Geochemical evidence for widespread euxinia in the Later Cambrian ocean. Nature 469 (7328), 80–83.

Gradstein, F. M., Ogg, J. G., Smith, A. G., Bleeker, W., Lourens, L. J., 2004. A new geologic time scale, with special reference to Precambrian and Neogene. Episodes 27 (2), 83–100.

Grant, S. W., 1990. Shell structure and distribution of Cloudina, a potential index fossil for the terminal Proterozoic. American Journal of Science 290-A, 261–294, PMID: 11538690.

Grant, S. W., Mar. 1992. Carbon isotopic vital effect and organic diagenesis, Lower Cambrian Forteau Formation, northwest Newfoundland: Implications for δ^{13}C chemostratigraphy. Geology 20 (3), 243–246.

Grazhdankin, D., 2004. Patterns of distribution in the Ediacaran biotas: facies versus biogeography and evolution. Paleobiology 30 (2), 203 –221.

Grotzinger, J., Miller, R., 2008. The Nama Group. Vol. 2. Geological Society of Namibia.

Grotzinger, J. P., Adams, E. W., Schroder, S., 2005. Microbial–metazoan reefs of the terminal Proterozoic Nama Group (c. 550–543 Ma), Namibia. Geological Magazine 142, 499–517.

Grotzinger, J. P., Bowring, S. A., Saylor, B. Z., Kaufman, A. J., Oct. 1995. Biostratigraphic and geochronologic constraints on early animal evolution. Science 270 (5236), 598 –604.

Grotzinger, J. P., Fike, D. A., Fischer, W. W., 2011. Enigmatic origin of the largest-known carbon isotope excursion in Earth's history. Nature Geoscience 4 (5), 285–292.

Grotzinger, J. P., Watters, W. A., Knoll, A. H., 2000a. Calcified metazoans in thrombolite-stromatolite reefs of the terminal Proterozoic Nama Group, Namibia. Paleobiology 26 (3), 334 –359.

Grotzinger, J. P., Watters, W. A., Knoll, A. H., 2000b. Calcified metazoans in thrombolite-stromatolite reefs of the terminal proterozoic nama group, namibia. Paleobiology 26 (3), 334–359.

Halevy, I., Peters, S. E., Fischer, W. W., Jul. 2012. Sulfate burial constraints on the Phanerozoic sulfur cycle. Science 337 (6092), 331–334.

Hall, M., Kaufman, A. J., Vickers-Rich, P., Ivantsov, A., Trusler, P., Linnemann, U., Hofmann, M., Elliott, D., Cui, H., Fedonkin, M., et al., 2013. Stratigraphy, palaeontology and geochemistry of the late Neoproterozoic Aar Member, southwest Namibia: Reflecting environmental controls on Ediacara fossil preservation during the terminal Proterozoic in African Gondwana. Precambrian Research 238, 214–232.

Halverson, G. P., Hoffman, P. F., Schrag, D. P., Maloof, A. C., Rice, A. H. N., 2005. Toward a Neoproterozoic composite carbon-isotope record. Geological Society of America Bulletin 117 (9-10), 1181–1207.

Hardie, L. A., Sep. 2003. Secular variations in Precambrian seawater chemistry and the timing of Precambrian aragonite seas and calcite seas. Geology 31 (9), 785 –788.

Higgins, J., Fischer, W., Schrag, D., Jun. 2009. Oxygenation of the ocean and sediments: Consequences for the seafloor carbonate factory. Earth and Planetary Science Letters 284 (12), 25–33.

Hoffman, P. F., Kaufman, A. J., Halverson, G. P., Schrag, D. P., 1998. A Neoproterozoic snowball earth. Science 281 (5381), 1342 –1346.

Hoffman, P. F., Schrag, D. P., 2002. The snowball earth hypothesis: testing the limits of global change. Terra nova 14 (3), 129–155.

Holland, H. D., 2002. Volcanic gases, black smokers, and the Great Oxidation Event. Geochimica et Cosmochimica Acta 66 (21), 3811–3826.

Holland, H. D., 2006. The oxygenation of the atmosphere and oceans. Philosophical Transactions of the Royal Society B: Biological Sciences 361 (1470), 903–915.

Hood, A. V., Wallace, M. W., 2014. Marine cements reveal the structure of an anoxic, ferruginous neoproterozoic ocean. Journal of the Geological Society, 2013–099.

Hua, H., Chen, Z., Yuan, X., Zhang, L., Xiao, S., Apr. 2005. Skeletogenesis and asexual reproduction in the earliest biomineralizing animal cloudina. Geology 33 (4), 277 –280.

Hua, H., Pratt, B. R., Zhang, L., Oct. 2003. Borings in Cloudina shells: Complex predator-prey dynamics in the Terminal Neoproterozoic. PALAIOS 18 (4-5), 454 –459.

Jackson, J. B. C., 1983. Biological determinants of present and past sessile animal distributions. Biotic Interactions in recent and fossil benthic communities. Plenum Press, New York, 39–120.

James, R., Elderfield, H., Palmer, M., 1995. The chemistry of hydrothermal fluids from the Broken Spur site, 29 N Mid-Atlantic Ridge. Geochimica et Cosmochimica Acta 59 (4), 651–659.

Javaux, E., Beghin, J., Houzay, J., Blanpied, C., 2013. The boring billion: An exciting time for early eukaryotes! Goldschmidt 2013 abstracts.

Jenkyns, H. C., 2010. Geochemistry of oceanic anoxic events. Geochemistry, Geophysics, Geosystems 11 (3).

REFERENCES

Jensen, S., Droser, M. L., Gehling, J. G., 2006. A critical look at the Ediacaran trace fossil record. In: Neoproterozoic geobiology and paleobiology. Springer, pp. 115–157.

Jensen, S., Gehling, J. G., Droser, M. L., 1998. Ediacara-type fossils in Cambrian sediments. Nature 393 (6685), 567–569.

Johnson, J., Grotzinger, J. P., 2006. Affect of sedimentation on stromatolite reef growth and morphology, Ediacaran Omkyk member (Nama Group), Namibia. South African journal of geology 109 (1-2), 87–96.

Johnston, D., Gill, B., Masterson, A., Beirne, E., Casciotti, K., Knapp, A., Berelson, W., 2014. Placing an upper limit on cryptic marine sulphur cycling. Nature.

Johnston, D. T., Farquhar, J., Wing, B. A., Kaufman, A. J., Canfield, D. E., Habicht, K. S., Jun. 2005. Multiple sulfur isotope fractionations in biological systems: A case study with sulfate reducers and sulfur disproportionators. American Journal of Science 305 (6-8), 645–660.

Johnston, D. T., Wolfe-Simon, F., Pearson, A., Knoll, A. H., 2009. Anoxygenic photosynthesis modulated proterozoic oxygen and sustained earth's middle age. Proceedings of the National Academy of Sciences 106 (40), 16925–16929.

Jørgensen, B. B., Apr. 1982. Mineralization of organic matter in the sea bed – the role of sulphate reduction. Nature 296 (5858), 643–645.

Kamber, B. S., Webb, G. E., 2001. The geochemistry of late Archaean microbial carbonate: implications for ocean chemistry and continental erosion history. Geochimica et Cosmochimica Acta 65 (15), 2509–2525.

Kamber, B. S., Webb, G. E., 2007. Transition metal abundances in microbial carbonate: a pilot study based on in situ LA–ICP–MS analysis. Geobiology 5 (4), 375–389.

Kaplan, I. R., Rittenberg, S. C., Feb. 1964. Microbiological fractionation of sulphur isotopes. Journal of General Microbiology 34 (2), 195–212, PMID: 14135528.

Kasemann, S. A., Prave, A. R., Fallick, A. E., Hawkesworth, C. J., Hoffman, K.-H., 2010. Neoproterozoic ice ages, boron isotopes, and ocean acidification: Implications for a snowball earth. Geology 8 (9), 775–778.

Kashefi, K., Lovley, D. R., 2003. Extending the upper temperature limit for life. Science 301 (5635), 934–934.

Kasting, J. F., Ono, S., 2006. Palaeoclimates: the first two billion years. Philosophical Transactions of the Royal Society B: Biological Sciences 361 (1470), 917–929.

Kaufman, A. J., Hayes, J., Knoll, A. H., Germs, G. J., 1991. Isotopic compositions of carbonates and organic carbon from upper Proterozoic successions in Namibia: stratigraphic variation and the effects of diagenesis and metamorphism. Precambrian Research 49 (3), 301–327.

Kennard, J. M., James, N. P., Oct. 1986. Thrombolites and stromatolites: Two distinct types of microbial structures. PALAIOS 1 (5), 492–503, ArticleType: research-article / Full publication date: Oct., 1986 / Copyright 1986 SEPM Society for Sedimentary Geology.

Kennedy, M., Droser, M., Mayer, L. M., Pevear, D., Mrofka, D., 2006. Late Precambrian oxygenation; inception of the clay mineral factory. Science 311 (5766), 1446–1449.

Kimura, H., Watanabe, Y., 2001. Oceanic anoxia at the Precambrian-Cambrian boundary. Geology 29 (11), 995–998.

Kirschvink, J. L., Hagadorn, J. W., 2000. A grand unified theory of biomineralization. The biomineralisation of Nano- and Micro-structures, 139–150.

Kirschvink, J. L., Kopp, R. E., 2008. Palaeoproterozoic ice houses and the evolution of oxygen-mediating enzymes: the case for a late origin of photosystem ii. Philosophical Transactions of the Royal Society B: Biological Sciences 363 (1504), 2755–2765.

Klok, C. J., Harrison, J. F., 2009. Atmospheric hypoxia limits selection for large body size in insects. PLoS One 4 (1), e3876.

Knauth, L. P., Kennedy, M. J., 2009. The late precambrian greening of the earth. Nature 460 (7256), 728–732.

Knoll, A. H., 1992. The early evolution of eukaryotes: a geological perspective. Science 256 (5057), 622–627.

Knoll, A. H., Jan. 2003a. Biomineralization and evolutionary history. Reviews in Mineralogy and Geochemistry 54, 329–356.

Knoll, A. H., 2003b. The geological consequences of evolution. Geobiology 1 (1), 3–14.

Knoll, A. H., Javaux, E. J., Hewitt, D., Cohen, P., 2006. Eukaryotic organisms in Proterozoic oceans. Philosophical Transactions of the Royal Society B: Biological Sciences 361 (1470), 1023–1038.

Knoll, A. H., Sperling, E. A., 2014. Oxygen and animals in earth history. Proceedings of the National Academy of Sciences 111 (11), 3907–3908.

Koeppenkastrop, D., De Carlo, E. H., 1992. Sorption of rare-earth elements from seawater onto synthetic mineral particles: An experimental approach. Chemical Geology 95 (3), 251–263.

Koeppenkastrop, D., De Carlo, E. H., 1993. Uptake of rare earth elements from solution by metal oxides. Environmental science & technology 27 (9), 1796–1802.

Koeppenkastrop, D., Decarlo, E., Roth, M., 1991. A method to investigate the interaction of rare earth elements in aqueous solution with metal oxides. Journal of radioanalytical and nuclear chemistry 152 (2), 337–346.

Kontorovich, A., Varlamov, A., Grazhdankin, D., Karlova, G., Klets, A., Kontorovich, V., Saraev, S., Terleev, A., Belyaev, S. Y., Varaksina, I., et al., 2008. A section of Vendian in the east of West Siberian Plate. Russian Geology and Geophysics 49 (12), 932–939.

Kopp, R. E., Kirschvink, J. L., Hilburn, I. A., Nash, C. Z., 2005. The Paleoproterozoic snowball earth: a climate disaster triggered by the evolution of oxygenic photosynthesis. Proceedings of the National Academy of Sciences of the United States of America 102 (32), 11131–11136.

Kruse, P. D., Zhuravlev, A. Y., James, N. P., 1995. Primordial metazoan-calcimicrobial reefs: Tommotian (early Cambrian) of the Siberian platform. Palaios, 291–321.

Le Guerroué, E., Mar. 2010. Duration and synchroneity of the largest negative carbon isotope excursion on earth: The Shuram/Wonoka anomaly. Comptes Rendus Geoscience 342 (3), 204–214.

Leckie, R. M., Bralower, T. J., Cashman, R., 2002. Oceanic anoxic events and plankton evolution: Biotic response to tectonic forcing during the mid-Cretaceous. Paleoceanography 17 (3), 13–1.

Lenton, T. M., Boyle, R. A., Poulton, S. W., Shields-Zhou, G. A., Butterfield, N. J., 2014. Co-evolution of eukaryotes and ocean oxygenation in the Neoproterozoic era. Nature Geoscience.

Lenton, T. M., Crouch, M., Johnson, M., Pires, N., Dolan, L., Feb. 2012. First plants cooled the Ordovician. Nature Geoscience 5, 86–89.

Lenton, T. M., Watson, A. J., 2004. Biotic enhancement of weathering, atmospheric oxygen and carbon dioxide in the Neoproterozoic. Geophysical research letters 31 (5).

Levin, S., Whitfield, M., 1994. Patchiness in marine and terrestrial systems: From individuals to populations [and discussion]. Philosophical Transactions of the Royal Society of London. Series B: Biological Sciences 343 (1303), 99–103.

Lewis, B., Landing, W., 1991. The biogeochemistry of manganese and iron in the Black Sea. Deep Sea Research Part A. Oceanographic Research Papers 38, S773–S803.

Li, C., Love, G. D., Lyons, T. W., Fike, D. A., Sessions, A. L., Chu, X., Apr. 2010. A stratified redox model for the Ediacaran ocean. Science (New York, N.Y.) 328 (5974), 80–83, PMID: 20150442.

Ling, H.-F., Chen, X., Li, D., Wang, D., Shields-Zhou, G. A., Zhu, M., 2013. Cerium anomaly variations in Ediacaran to earliest Cambrian carbonates from the Yangtze Gorges area, South China: Implications for oxygenation of coeval shallow seawater. Precambrian Research 225 (0).

Liu, A. G., Mcllroy, D., Brasier, M. D., 2010. First evidence for locomotion in the Ediacara biota from the 565 ma Mistaken Point Formation, Newfoundland. Geology 38 (2), 123–126.

Liu, T.-B., Maynard, J. B., Alten, J., 2006. Superheavy S isotopes from glacier-associated sediments of the Neoproterozoic of south China: Oceanic anoxia or sulfate limitation? Geological Society of America Memoirs 198, 205–222.

Logan, G. A., Hayes, J., Hieshima, G. B., Summons, R. E., 1995. Terminal Proterozoic reorganization of biogeochemical cycles. Nature 376 (6535), 53–56.

Love, G. D., Grosjean, E., Stalvies, C., Fike, D. A., Grotzinger, J. P., Bradley, A. S., Kelly, A. E., Bhatia, M., Meredith, W., Snape, C. E., et al., 2009. Fossil steroids record the appearance of Demospongiae during the Cryogenian period. Nature 457 (7230), 718–721.

Luther III, G. W., Church, T. M., Powell, D., 1991. Sulfur speciation and sulfide oxidation in the water column of the Black Sea. Deep Sea Research Part A. Oceanographic Research Papers 38, S1121–S1137.

Lyons, T. W., Reinhard, C. T., Planavsky, N. J., 2014. The rise of oxygen in earth's early ocean and atmosphere. Nature 506 (7488), 307–315.

Lyons, T. W., Severmann, S., 2006. A critical look at iron paleoredox proxies: New insights from modern euxinic marine basins. Geochimica et Cosmochimica Acta 70 (23), 5698–5722.

Lyons, T. W., Werne, J. P., Hollander, D. J., Murray, R., 2003. Contrasting sulfur geochemistry and Fe/Al and Mo/Al ratios across the last oxic-to-anoxic transition in the Cariaco Basin, Venezuela. Chemical Geology 195 (1), 131–157.

Macdonald, F. A., Pruss, S. B., Strauss, J. V., 2014. Trace fossils with spreiten from the late Ediacaran Nama Group,Namibia: complex feeding patterns five million years before the Precambrian–Cambrian boundary. Journal of Paleontology 88 (2), 299–308.

Maloof, A. C., Porter, S. M., Moore, J. L., Dudas, F. O., Bowring, S. A., Higgins, J. A., Fike, D. A., Eddy, M. P., Nov. 2010. The earliest cambrian record of animals and ocean geochemical change. Geological Society of America Bulletin 122 (11-12), 1731–1774.

Mángano, M. G., Buatois, L. A., 2014. Decoupling of body-plan diversification and ecological structuring during the Ediacaran–Cambrian transition: evolutionary and geobiological feedbacks. Proceedings of the Royal Society B: Biological Sciences 281 (1780), 20140038.

Marin, F., Smith, M., Isa, Y., Muyzer, G., Westbroek, P., feb 1996. Skeletal matrices, muci, and the origin of invertebrate calcification. Proceedings of the National Academy of Sciences of the United States of America 93 (4), 1554–1559, PMID: 11607630 PMCID: PMC39979.

Martin, J. H., Knauer, G. A., Karl, D. M., Broenkow, W. W., 1987. Vertex: carbon cycling in the northeast Pacific. Deep Sea Research Part A. Oceanographic Research Papers 34 (2), 267–285.

Martin, M., Grazhdankin, D., Bowring, S., Evans, D. A. D., Fedonkin, M., Kirschvink, J., 2000. Age of Neoproterozoic bilatarian body and trace fossils, White Sea, Russia: Implications for metazoan evolution. Science 288 (5467), 841–845.

McFadden, K. A., Huang, J., Chu, X., Jiang, G., Kaufman, A. J., Zhou, C., Yuan, X., Xiao, S., 2008. Pulsed oxidation and biological evolution in the Ediacaran Doushantuo Formation. Proceedings of the National Academy of Sciences 105 (9), 3197–3202.

McIlroy, D., Logan, G. A., 1999. The impact of bioturbation on infaunal ecology and evolution during the Proterozoic–Cambrian transition. Palaios 14 (1), 58–72.

Mcnamara, K. J., 1992. Stromatolites - A key to understanding the early evolution of life. Western Australia Museum.

Meyer, E. E., Quicksall, A. N., Landis, J. D., Link, P. K., Bostick, B. C., Jan. 2012. Trace and rare earth elemental investigation of a Sturtian cap carbonate, Pocatello, Idaho: Evidence for ocean redox conditions before and during carbonate deposition. Precambrian Research 192195, 89–106.

Meyer, K., Kump, L., Ridgwell, A., 2008. Biogeochemical controls on photic-zone euxinia during the end-Permian mass extinction. Geology 36 (9), 747–750.

Meysman, F. J., Middelburg, J. J., Heip, C. H., 2006. Bioturbation: a fresh look at Darwin's last idea. Trends in Ecology & Evolution 21 (12), 688–695.

Mills, D. B., Ward, L. M., Jones, C., Sweeten, B., Forth, M., Treusch, A. H., Canfield, D. E., 2014. Oxygen requirements of the earliest animals. Proceedings of the National Academy of Sciences 111 (11), 4168–4172.

Mitra, A., Elderfield, H., Greaves, M., 1994. Rare earth elements in submarine hydrothermal fluids and plumes from the Mid-Atlantic ridge. Marine Chemistry 46 (3), 217–235.

Moffett, J. W., May 1990. Microbially mediated cerium oxidation in sea water. Nature 345 (6274), 421–423.

REFERENCES

Morris, S. C., Mattes, B., Chen, M., 1990. The early skeletal organism Cloudina: new occurrences from Oman and possibly China. American Journal of Science, 245–260.

Müller, M., Mentel, M., van Hellemond, J. J., Henze, K., Woehle, C., Gould, S. B., Yu, R.-Y., van der Giezen, M., Tielens, A. G., Martin, W. F., 2012. Biochemistry and evolution of anaerobic energy metabolism in eukaryotes. Microbiology and Molecular Biology Reviews 76 (2), 444–495.

Narbonne, G., Xiao, S., Shields, G., Gradstein, F., Ogg, J., Ogg, G., 2012. The Ediacaran Period. The Geologic Time Scale, 413–435.

Narbonne, G. M., 2005. The Ediacara biota: Neoproterozoic origin of animals and their ecosystems. Annu. Rev. Earth Planet. Sci. 33, 421–442.

Narbonne, G. M., Gehling, J. G., 2003. Life after snowball: the oldest complex Ediacaran fossils. Geology 31 (1), 27–30.

Narbonne, G. M., Kaufman, A. J., Knoll, A. H., 1994. Integrated chemostratigraphy and biostratigraphy of the Windermere Supergroup, northwestern Canada: Implications for Neoproterozoic correlations and the early evolution of animals. Geological Society of America Bulletin 106 (10), 1281–1292.

Narbonne, G. M., Myrow, P. M., Landing, E., Anderson, M. M., 1987. A candidate stratotype for the Precambrian-Cambrian boundary, Fortune Head, Burin Peninsula, southeastern Newfoundland. Canadian Journal of Earth Sciences 24 (7), 1277–1293.

Narbonne, G. M., Saylor, B. Z., Grotzinger, J. P., 1997. The youngest Ediacaran fossils from southern Africa. Journal of Paleontology, 953–967.

Nothdurft, L. D., Webb, G. E., Kamber, B. S., Jan. 2004. Rare earth element geochemistry of Late Devonian reefal carbonates, Canning Basin, Western Australia: confirmation of a seawater REE proxy in ancient limestones. Geochimica et Cosmochimica Acta 68 (2), 263–283.

Nursall, J., 1959. Oxygen as a prerequisite to the origin of the metazoa. Nature 183, 1170–1172.

Och, L. M., Shields-Zhou, G. A., 2012. The Neoproterozoic oxygenation event: environmental perturbations and biogeochemical cycling. Earth-Science Reviews 110 (1), 26–57.

Och, M., Shields-Zhou, G. A., Poulton, S. W., Manning, C., Thirlwall, M. F., Li, D., Chen, X., Ling, H., Osborn, T., Cremonese, L., 2011. Redox changes in early cambrian black shales at Xiaotan section, Yunnan Province, South China. Precambrian Research 225 (0).

Ohta, A., Kawabe, I., 2001. REE (iii) adsorption onto mn dioxide (mno_2) and fe oxyhydroxide: Ce (III) oxidation by mno_2. Geochimica et Cosmochimica Acta 65 (5), 695–703.

Orgel, L. E., 1998. The origin of life - a review of facts and speculations. Trends in biochemical sciences 23 (12), 491–495.

Palmer, A. R., Feb. 1992. Calcification in marine molluscs: how costly is it? Proceedings of the National Academy of Sciences 89 (4), 1379 –1382.

Parfrey, L. W., Lahr, D. J., Knoll, A. H., Katz, L. A., 2011. Estimating the timing of early eukaryotic diversification with multigene molecular clocks. Proceedings of the National Academy of Sciences 108 (33), 13624–13629.

Payne, J. L., McClain, C. R., Boyer, A. G., Brown, J. H., Finnegan, S., Kowalewski, M., Krause Jr, R. A., Lyons, S. K., McShea, D. W., Novack-Gottshall, P. M., et al., 2011. The evolutionary consequences of oxygenic photosynthesis: a body size perspective. Photosynthesis research 107 (1), 37–57.

Paytan, A., Kastner, M., Campbell, D., Thiemens, M. H., Jun. 2004. Seawater sulfur isotope fluctuations in the Cretaceous. Science 304 (5677), 1663–1665.

Peng, Y., Bao, H., Pratt, L. M., Kaufman, A. J., Jiang, G., Boyd, D., Wang, Q., Zhou, C., Yuan, X., Xiao, S., Loyd, S., 2014. Widespread contamination of carbonate-associated sulfate by present-day secondary atmospheric sulfate: Evidence from triple oxygen isotopes. Geology 42 (9), 815–818.

Penny, A., Wood, R., Curtis, A., Bowyer, F., Tostevin, R., Hoffman, K.-H., 2014. Ediacaran metazoan reefs from the Nama Group, Namibia. science 344 (6191), 1504–1506.

Penny, A., Wood, R. A., Bowyer, F., Curtis, A., Tostevin, R., in review. Phenotypic plasticity and intraspecific niche partitioning in the earliest skeletal metazoans: *Namacalathus* from the Ediacaran Nama Group, Namibia. Geology - (-), –.

Piper, D., Calvert, S., 2009. A marine biogeochemical perspective on black shale deposition. Earth-Science Reviews 95 (1), 63–96.

Planavsky, N., Bekker, A., Rouxel, O. J., Kamber, B., Hofmann, A., Knudsen, A., Lyons, T. W., Nov. 2010a. Rare Earth Element and yttrium compositions of Archean and Paleoproterozoic Fe formations revisited: New perspectives on the significance and mechanisms of deposition. Geochimica et Cosmochimica Acta 74 (22), 6387–6405.

Planavsky, N. J., Asael, D., Hofmann, A., Reinhard, C. T., Lalonde, S. V., Knudsen, A., Wang, X., Ossa Ossa, F., Pecoits, E., Smith, A. J. B., Beukes, N. J., Bekker, A., Johnson, T. M., Konhauser, K. O., Lyons, T. W., Rouxel, O. J., apr 2014a. Evidence for oxygenic photosynthesis half a billion years before the Great Oxidation Event. Nature Geoscience 7 (4), 283–286.

Planavsky, N. J., Bekker, A., Hofmann, A., Owens, J. D., Lyons, T. W., Nov. 2012. Sulfur record of rising and falling marine oxygen and sulfate levels during the lomagundi event. Proceedings of the National Academy of Sciences 109 (45), 18300–18305, PMID: 23090989.

Planavsky, N. J., Reinhard, C. T., Wang, X., Thomson, D., McGoldrick, P., Rainbird, R. H., Johnson, T., Fischer, W. W., Lyons, T. W., 2014b. Low Mid-Proterozoic atmospheric oxygen levels and the delayed rise of animals. Science 346 (6209), 635–638.

Planavsky, N. J., Rouxel, O. J., Bekker, A., Lalonde, S. V., Konhauser, K. O., Reinhard, C. T., Lyons, T. W., 2010b. The evolution of the marine phosphate reservoir. Nature 467 (7319), 1088–1090.

Platt, T., Harrison, W. G., 1985. Biogenic fluxes of carbon and oxygen in the ocean. Nature 318 (6041), 55–58.

Porter, S. M., Jun. 2007. Seawater chemistry and early carbonate biomineralization. Science 316 (5829), 1302.

Poulton, S., Raiswell, R., 2002. The low-temperature geochemical cycle of iron: from continental fluxes to marine sediment deposition. American Journal of Science 302 (9), 774–805.

Poulton, S. W., Canfield, D. E., 2005. Development of a sequential extraction procedure for iron: implications for iron partitioning in continentally derived particulates. Chemical Geology 214 (3), 209–221.

Poulton, S. W., Canfield, D. E., 2011. Ferruginous conditions: a dominant feature of the ocean through Earth's history. Elements 7 (2), 107–112.

Poulton, S. W., Fralick, P. W., Canfield, D. E., 2004. The transition to a sulphidic ocean 1.84 billion years ago. Nature 431 (7005), 173–177.

Poulton, S. W., Fralick, P. W., Canfield, D. E., 2010. Spatial variability in oceanic redox structure 1.8 billion years ago. Nature Geoscience 3 (7), 486–490.

Raiswell, R., Anderson, T., 2005. Reactive iron enrichment in sediments deposited beneath euxinic bottom waters: constraints on supply by shelf recycling. Geological Society, London, Special Publications 248 (1), 179–194.

Raiswell, R., Buckley, F., Berner, R. A., Anderson, T., 1988. Degree of pyritization of iron as a paleoenvironmental indicator of bottom-water oxygenation. Journal of Sedimentary Research 58 (5).

Raiswell, R., Canfield, D. E., 1998. Sources of iron for pyrite formation in marine sediments. American Journal of Science 298 (3), 219–245.

Raiswell, R., Canfield, D. E., 2012. The iron biogeochemical cycle past and present. Geochemical Perspectives 1 (1), 1–2.

Raiswell, R., Newton, R., Bottrell, S. H., Coburn, P. M., Briggs, D. E., Bond, D. P., Poulton, S. W., 2008. Turbidite depositional influences on the diagenesis of Beecher's Trilobite Bed and the Hunsrück Slate; sites of soft tissue pyritization. American Journal of Science 308 (2), 105–129.

Raiswell, R., Reinhard, C. T., Derkowski, A., Owens, J., Bottrell, S. H., Anbar, A. D., Lyons, T. W., 2011. Formation of syngenetic and early diagenetic iron minerals in the late Archean Mt. McRae Shale, Hamersley Basin, Australia: new insights on the patterns, controls and paleoenvironmental implications of authigenic mineral formation. Geochimica et Cosmochimica Acta 75 (4), 1072–1087.

Rees, C. E., Apr. 1978. Sulphur isotope measurements using SO_2 and SF_6. Geochimica et Cosmochimica Acta 42 (4), 383–389.

Reinhard, C. T., Planavsky, N. J., Lyons, T. W., 2013. Long-term sedimentary recycling of rare sulphur isotope anomalies. Nature 497 (7447), 100–103.

Richards, F. A., Redfield, A. C., 1954. A correlation between the oxygen content of sea water and the organic content of marine sediments. Deep Sea Research (1953) 1 (4), 279–281.

Riding, R., Fralick, P., Liang, L., 2014. Identification of an Archean marine oxygen oasis. Precambrian Research 251, 232–237.

Ries, J. B., Anderson, M. A., Hill, R. T., Mar. 2008. Seawater Mg/Ca controls polymorph mineralogy of microbial $CaCO_3$: a potential proxy for calcite-aragonite seas in Precambrian time. Geobiology 6 (2), 106–119, PMID: 18380873.

Ries, J. B., Fike, D. A., Pratt, L. M., Lyons, T. W., Grotzinger, J. P., 2009. Superheavy pyrite in the terminal Proterozoic Nama Group, southern Namibia: A consequence of low seawater sulfate at the dawn of animal life. Geology 37 (8), 743 –746.

Rogov, V., Marusin, V., Bykova, N., Goy, Y., Nagovitsin, K., Kochnev, B., Karlova, G., Grazhdankin, D., 2012. The oldest evidence of bioturbation on Earth. Geology 40 (5), 395–398.

Romankevich, E. A., 1984. Geochemistry of organic matter in the ocean. Springer-Verlag Berlin.

Rosing, M. T., Frei, R., 2004. U-rich Archaean sea-floor sediments from Greenland – indications of >3700 ma oxygenic photosynthesis. Earth and Planetary Science Letters 217 (3), 237–244.

Rothman, D. H., Hayes, J. M., Summons, R. E., Jul. 2003. Dynamics of the Neoproterozoic carbon cycle. Proceedings of the National Academy of Sciences 100 (14), 8124–8129.

Runnegar, B., 1991. Precambrian oxygen levels estimated from the biochemistry and physiology of early eukaryotes. Global and Planetary Change 5 (1), 97–111.

Sahoo, S. K., Planavsky, N. J., Kendall, B., Wang, X., Shi, X., Scott, C., Anbar, A. D., Lyons, T. W., Jiang, G., sep 2012. Ocean oxygenation in the wake of the Marinoan glaciation. Nature 489 (7417), 546–549.

Sarnthein, M., Winn, K., Zahn, R., 1987. Paleoproductivity of oceanic upwelling and the effect on atmospheric $C0_2$ and climatic change during deglaciation times. In: Abrupt climatic change. Springer, pp. 311–337.

Saylor, B. Z., Grotzinger, J. P., Germs, G. J., may 1995. Sequence stratigraphy and sedimentology of the Neoproterozoic Kuibis and Schwarzrand Subgroups (Nama Group), southwestern Namibia. Precambrian Research 73 (14), 153–171.

Saylor, B. Z., Kaufman, A. J., Grotzinger, J. P., Urban, F., 1998. A composite reference section for terminal Proterozoic strata of Southern Namibia. SEPM Journal of Sedimentary Research Vol. 68 (1998),.

Schidlowski, M., 1988. A 3,800-million-year isotopic record of life from carbon in sedimentary rocks. Nature 333 (6171), 313–318.

Schrag, D. P., Higgins, J. A., Macdonald, F. A., Johnston, D. T., 2013. Authigenic carbonate and the history of the global carbon cycle. science 339 (6119), 540–543.

Schroder, S., Grotzinger, J., Jan. 2007. Evidence for anoxia at the Ediacaran-Cambrian boundary: the record of redox-sensitive trace elements and rare earth elements in Oman. Journal of the Geological Society 164 (1), 175–187.

Schunck, H., Lavik, G., Desai, D. K., Großkopf, T., Kalvelage, T., Löscher, C. R., Paulmier, A., Contreras, S., Siegel, H., Holtappels, M., et al., 2013. Giant hydrogen sulfide plume in the oxygen minimum zone off Peru supports chemolithoautotrophy. PloS one 8 (8), e68661.

Scott, C., Lyons, T. W., Bekker, A., Shen, Y., Poulton, S. W., Chu, X., Anbar, A. D., mar 2008. Tracing the stepwise oxygenation of the Proterozoic ocean. Nature 452 (7186), 456–459.

Seilacher, A., 2007. The nature of vendobionts. Geological Society, London, Special Publications 286 (1), 387–397.

Severmann, S., McManus, J., Berelson, W. M., Hammond, D. E., 2010. The continental shelf benthic iron flux and its isotope composition. Geochimica et Cosmochimica Acta 74 (14), 3984–4004.

Sherrell, R. M., Field, M. P., Ravizza, G., 1999. Uptake and fractionation of rare earth elements on hydrothermal plume particles at 9 45°N, East Pacific Rise. Geochimica et Cosmochimica Acta 63 (11), 1709–1722.

Shields-Zhou, G., Och, L., Mar. 2011. The case for a Neoproterozoic Oxygenation Event: Geochemical evidence and biological consequences. GSA Today 21, 4–11.

Shixing, Z., Huineng, C., 1995. Megascopic multicellular organisms from the 1700-million-year-old Tuanshanzi Formation in the Jixian area, North China. Science 270 (5236), 620–622.

Sholkovitz, E. R., Landing, W. M., Lewis, B. L., Mar. 1994. Ocean particle chemistry: The fractionation of rare earth elements between suspended particles and seawater. Geochimica et Cosmochimica Acta 58 (6), 1567–1579.

Sim, M. S., Bosak, T., Ono, S., Jul. 2011. Large sulfur isotope fractionation does not require disproportionation. Science 333 (6038), 74–77, PMID: 21719675.

Simkiss, K., Dec. 1977. Biomineralization and detoxification. Calcified Tissue Research 24 (1), 199–200.

Slack, J., Grenne, T., Bekker, A., Rouxel, O., Lindberg, P., 2007. Suboxic deep seawater in the late Paleoproterozoic: evidence from hematitic chert and iron formation related to seafloor-hydrothermal sulfide deposits, central Arizona, USA. Earth and Planetary Science Letters 255 (1), 243–256.

Soyol-Erdene, T.-O., Huh, Y., Nov. 2013. Rare earth element cycling in the pore waters of the bering sea slope (IODP exp. 323). Chemical Geology 358, 75–89.

Stanistreet, I. G., Kukla, P. A., Henry, G., 1991. Sedimentary basinal responses to a Late Precambrian Wilson Cycle: the Damara Orogen and Nama Foreland, Namibia. Journal of African Earth Sciences (and the Middle East) 13 (1), 141–156.

Strauss, H., Bengtson, S., Myrow, P. M., Vidal, G., 1992. Stable isotope geochemistry and palynology of the late Precambrian to Early Cambrian sequence in Newfoundland. Canadian Journal of Earth Sciences 29 (8), 1662–1673.

Sunda, W. G., Huntsman, S. A., 1988. Effect of sunlight on redox cycles of manganese in the southwestern Sargasso Sea. Deep Sea Research Part A. Oceanographic Research Papers 35 (8), 1297–1317.

Tarhan, L. G., Droser, M. L., 2014. Widespread delayed mixing in early to middle Cambrian marine shelfal settings. Palaeogeography, Palaeoclimatology, Palaeoecology 399, 310–322.

Tostevin, R., Turchyn, A. V., Farquhar, J., Johnston, D. T., Eldridge, D. L., Bishop, J. K., McIlvin, M., 2014. Multiple sulfur isotope constraints on the modern sulfur cycle. Earth and planetary science letters 396, 14–21.

Warren, L. V., Fairchild, T. R., Gaucher, C., Boggiani, P. C., Poire, D. G., Anelli, L. E., Inchausti, J. C., 2011. Corumbella and in situ Cloudina in association with thrombolites in the Ediacaran Itapucumi group, Paraguay. Terra Nova 23 (6), 382–389.

Webb, G. E., Kamber, B. S., May 2000. Rare earth elements in Holocene reefal microbialites: a new shallow seawater proxy. Geochimica et Cosmochimica Acta 64 (9), 1557–1565.

Webb, G. E., Nothdurft, L. D., Kamber, B. S., Kloprogge, J. T., Zhao, J.-X., 2009. Rare earth element geochemistry of scleractinian coral skeleton during meteoric diagenesis: a sequence through neomorphism of aragonite to calcite. Sedimentology 56 (5), 14331463.

Wood, Rachel, A., May 2011. Paleoecology of the earliest skeletal metazoan communities: Implications for early biomineralization. Earth-Science Reviews 106 (1-2), 184–190.

Wood, R., Poulton, S., Prave, A., Hoffmann, K.-H., Clarkson, M., Guilbaud, R., Lyne, J., Tostevin, R., Bowyer, F., Penny, A., et al., 2015. Dynamic redox conditions control late Ediacaran metazoan ecosystems in the Nama Group, Namibia. Precambrian Research 261, 252–271.

Wood, R., Woodward, R., 1999. Reef evolution. Vol. 414. Oxford University Press Oxford.

Wood, R. A., Grotzinger, J. P., Dickson, J. A. D., Jun. 2002. Proterozoic modular biomineralized metazoan from the Nama Group, Namibia. Science 296 (5577), 2383 –2386.

Xiao, S., Laflamme, M., 2009. On the eve of animal radiation: phylogeny, ecology and evolution of the Ediacara biota. Trends in Ecology & Evolution 24 (1), 31–40.

Yin, L., Zhu, M., Knoll, A. H., Yuan, X., Zhang, J., Hu, J., 2007. Doushantuo embryos preserved inside diapause egg cysts. Nature 446 (7136), 661–663.

Zegeye, A., Bonneville, S., Benning, L. G., Sturm, A., Fowle, D. A., Jones, C., Canfield, D. E., Ruby, C., MacLean, L. C., Nomosatryo, S., et al., 2012. Green rust formation controls nutrient availability in a ferruginous water column. Geology 40 (7), 599–602.

Zegeye, A., Etique, M., Carteret, C., Ruby, C., Schaaf, P., Francius, G., 2014. Origin of the differential nanoscale reactivity of biologically and chemically formed green rust crystals investigated by chemical force spectroscopy. The Journal of Physical Chemistry C 118 (11), 5978–5987.

Zerkle, A. L., Farquhar, J., Johnston, D. T., Cox, R. P., Canfield, D. E., Jan. 2009. Fractionation of multiple sulfur isotopes during phototrophic oxidation of sulfide and elemental sulfur by a green sulfur bacterium. Geochimica et Cosmochimica Acta 73 (2), 291–306.

Zhuravlev, A. Y., Liñán, E., Vintaned, J. A. G., Debrenne, F., Fedorov, A. B., 2012. New finds of skeletal fossils in the terminal neoproterozoic of the siberian platform and spain. Acta Palaeontologica Polonica 57 (1), 205–224.